COHESIVE PROPERTIES OF WHEAT FLOUR AND THEIR EFFECT ON THE SIZE-BASED SEPARATION PROCESS

by

KALIRAMESH SILIVERU

B.Tech., Acharya N. G Ranga Agricultural University, 2010
M.Tech., Annamalai University, 2012

AN ABSTRACT OF A DISSERTATION

submitted in partial fulfillment of the requirements for the degree

DOCTOR OF PHILOSOPHY

Department of Grain Science and Industry
College of Agriculture

KANSAS STATE UNIVERSITY
Manhattan, Kansas

2016

Abstract

Wheat flour processing involves gradual size reduction and size-based fractionation of milled components. The size-based separation efficiency of wheat flour particles, with minimum bran contamination, is an important flour mill operational parameter. The flour particles often behave as imperfect solids with discontinuous flow and agglomerates during the separation process due to their differences in physical and chemical characteristics. Noticeable loss in throughput has been observed during sieving of soft wheat flour compared to that of hard wheat flour due to differences in inter-particle cohesion. However, there is limited understanding on the factors that influence the inter-particulate forces. Direct and indirect methods were applied to investigate the effects of moisture content, particle size, sifter load, and chemical composition on the cohesion behavior of flours from different wheat classes.

Image analysis approach was used to quantify the particle characteristics such as surface lipid content, roughness, and morphology with respect to particle size to better understand the differences between hard and soft wheat flours. Surface lipid content and roughness values showed that the soft wheat flours are more cohesive than hard wheat flours. The morphology values revealed the irregularity in flour particles, irrespective of wheat class and particle size, due to nonuniform fragmentation of endosperm particles. The chemical composition significantly contributes to the differences in cohesion and flowability of wheat flours. Based on the particle parameters, a granular bond number (GBN) model was developed to predict the dynamic flow of wheat flour. In order to further understand the wheat flour flow behavior during size-based separation, a correlation was developed using the discrete element method (DEM). The error of predictions demonstrated that this correlation can be used to estimate the sieving performance and sieve blinding phenomenon of wheat flour.

The experimental results from this dissertation work and the numerical model could eventually be instrumental to improve the efficiency of size-based separation of flour from various wheat classes. In addition, the models developed in this study will contribute significantly to understand the inter-particle cohesion as influenced by chemical composition.

COHESIVE PROPERTIES OF WHEAT FLOUR AND THEIR EFFECT ON THE SIZE-BASED SEPARATION PROCESS

by

KALIRAMESH SILIVERU

B.Tech., Acharya N. G Ranga Agricultural University, 2010
M.Tech., Annamalai University, 2012

A DISSERTATION

submitted in partial fulfillment of the requirements for the degree

DOCTOR OF PHILOSOPHY

Department of Grain Science and Industry
College of Agriculture

KANSAS STATE UNIVERSITY
Manhattan, Kansas

2016

Approved by:

Co-Major Professor
R. P. Kingsly Ambrose

Approved by:

Co-Major Professor
Praveen V. Vadlani

Copyright

Abstract

Wheat flour processing involves gradual size reduction and size-based fractionation of milled components. The size-based separation efficiency of wheat flour particles, with minimum bran contamination, is an important flour mill operational parameter. The flour particles often behave as imperfect solids with discontinuous flow and agglomerates during the separation process due to their differences in physical and chemical characteristics. Noticeable loss in throughput has been observed during sieving of soft wheat flour compared to that of hard wheat flour due to differences in inter-particle cohesion. However, there is limited understanding on the factors that influence the inter-particulate forces. Direct and indirect methods were applied to investigate the effects of moisture content, particle size, sifter load, and chemical composition on the cohesion behavior of flours from different wheat classes.

Image analysis approach was used to quantify the particle characteristics such as surface lipid content, roughness, and morphology with respect to particle size to better understand the differences between hard and soft wheat flours. Surface lipid content and roughness values showed that the soft wheat flours are more cohesive than hard wheat flours. The morphology values revealed the irregularity in flour particles, irrespective of wheat class and particle size, due to nonuniform fragmentation of endosperm particles. The chemical composition significantly contributes to the differences in cohesion and flowability of wheat flours. Based on the particle parameters, a granular bond number (GBN) model was developed to predict the dynamic flow of wheat flour. In order to further understand the wheat flour flow behavior during size-based separation, a correlation was developed using the discrete element method (DEM). The error of predictions demonstrated that this correlation can be used to estimate the sieving performance and sieve blinding phenomenon of wheat flour.

The experimental results from this dissertation work and the numerical model could eventually be instrumental to improve the efficiency of size-based separation of flour from various wheat classes. In addition, the models developed in this study will contribute significantly to understand the inter-particle cohesion as influenced by chemical composition.

Table of Contents

List of Figures

List of Tables

List of Abbreviations

AFM	Atomic Force Microscope
AIF	Angle of Internal Friction
BTEM	Band Target Entropy Minimization
DEM	Discrete Element Method
FD	Fractal Dimension
FF	Flow Function
GBN	Granular Bond Number
HRS	Hard Red Spring wheat
HRW	Hard Red Winter wheat
HWW	Hard White Winter wheat
JKR	Johnson-Kendall-Roberts
m.c	Moisture content
r.h	Relative humidity
SEM	Scanning Electron Microscope
SEP	Standard Error of Prediction
SRW	Soft Red Winter wheat
SWW	Soft White Winter wheat
vdW	van der Waals force
w.b.	Wet basis

Acknowledgements

First and foremost, with profound indebtedness, I owe a great many thanks to my major advisor, Dr. Kingsly Ambrose, for his excellent guidance, supervision, encouragement, and support throughout the period of my doctoral study. As a supervisor, he has always been available, patient, motivating, and supporting in all aspects. I owe my deepest gratitude for creating number of opportunities to travel to conferences, networking with research groups, and chances to collaborate with them. His company, positive attitude, moral support, and brotherly treatment will be remembered lifelong. I express my sincere gratitude and convey my heartfelt thanks to my co-major advisor, Dr. Praveen Vadlani, for accepting to be my mentor when Dr. Kingsly moved to Purdue University. I am extremely grateful to Dr. Vadlani, for his support in creating lab space for carrying out my experiments and also indefinite number of hours of discussion which boosted my research skills and moral values. He has always been very kind and has been concerned about progress of my research and welfare of my family.

It is an honor to express my sincere gratitude to Dr. Mark Casada, Dr. Dirk Maier, Dr. P. V. Reddy, and Dr. Ronaldo Maghirang for serving on my thesis committee. I am extremely grateful to Dr. Casada for his constructive advice during DEM modeling and allowing me to use the relative humidity chamber for the bulk cohesion experiments and giving access to the computer to run my simulations. I feel honored that Dr. Maier showed keen interest in my work since the very beginning. I owe great many thanks to him for taking time during his visits to K-State and giving constructive comments on my research. I am very thankful to Dr. Reddy for digging into age old research articles, which were not available through library sources and lending me the study materials on the wheat flour surface starch and protein concepts. Thanks

are due to Dr. Maghirang for his constant motivation during my research and his guidance for turning out the documents in timely fashion.

I have thoroughly enjoyed every bit of discussion and sharing the knowledge and experimental data on different topics related to microscopy and morphology measurement techniques with all my research collaborators – Dr. Jin Wang, Grace Lau, Shuying Cheng, Dr. Djanaguiraman, and Qisong Xu. I am very thankful to Edwin Brokesh for taking strenuous efforts in constructing the sifter stack geometry for the DEM modeling work. I owe a big thanks to Drs. Digvir Jayas and Alagusundaram for being my master's supervisors and for their immense support and constant encouragement in creating the opportunities for pursuing the advance level graduate degrees.

In no particular order, I am thankful to all my past and present colleagues of two research groups I worked with – *Dr. Josephine Boac, Dr. Rumela Bhadra, Abhay Patwa, Qi Bian, Achint Sanghi, Sam Cook, Yumeng, Camila, Dr. Yadhu, and Dr. Krishna*. Thanks a lot for lending your time to help in my experiments, looking into my experimental data and simulations, and answering my calls during weird timings. Noteworthy thanks to undergraduate helpers – Michael, Binghui, Jeevan, and Shiwei for helping me with the bulk cohesion experiments. I greatly appreciate the help of support staff at the Department of Grain Science for their official and personal help during my program of study. I thank the support engineers at BEOCAT cluster team of K-State, and EDEM team, DEM solutions, UK for their constant support and cooperation for running my simulations.

Raghu, Srikar, Sandeep, Dr. Mishra sir, Barath - Gowthami, Sam – Heather, Pandalaneni - Hari Priya, Pavan, Putta - Ankitha, Michael, Jennifer, Deanna, Mario, Chetan, Sudheer, Madhu, Karthik, Vybhav, Rani, Prathyusha, and Naga are my dear friends whom I could trust and rely on

at all times. You guys have always stood by me, when I was high, low, exhausted, and excited. I appreciate your constant push so as to work hard and with sincerity.

Finally, I would like to thank my family. I am obliged to my parents, Siliveru Krishna Rao and Adi Lakshmi for making me what I am today. Without your love, care, and support all this would not have been possible. I know you would have had sleepless nights thinking of me, but all your sacrifices have now finally paid off. I would like to thank my sister and brother-in-law, Drs. Swetha Deepika - Surendra Babu for their love and the belief they had in me. I truly thank both of you for stepping into my shoes and taking care of parent's health and not letting me know about any issues, so that I could focus on my research work.

I acknowledge Anderson's research grant and Research Programs of College of Agriculture, Kansas State University for providing graduate research assistantship.

Chapter 1 - Introduction

Understanding the factors that influence the inter-particle cohesion of particles during sieving process is one of the major unsolved problems, which impacts throughput and efficiency of size-based separation process. This dissertation presents a study on the effect of surface characteristics, chemical composition, particle characteristics, and sifter load on the cohesion behavior of flours from different wheat classes. The study involved experimental measurements and mathematical modeling of the dynamic flow behavior of wheat flour during sieving process. In this work, the significance of inherent particle characteristics and external conditions on the flow behavior of wheat flours were evaluated. Mathematical tools that aid in predicting the flow behavior of wheat flours and that explain the sieve blinding phenomenon were developed. The experimental results and mathematical models could help to improve the efficiency of size-based separation of particulate materials.

This chapter gives an overview of the inter-particle cohesion of wheat flour and its impact on the size-based separation process which is the primary focus of this dissertation work. In section 1.1, the factors that lead to cohesion of wheat flours and flow problems during sieving process are enumerated. The hypothesis, goals, and the objectives of this study are given in Section 1.2. The overview of this dissertation work is discussed in Section 1.3.

1.1. Problem Statement

The end product of wheat milling is classified as flour in which "not less than 98 percent of the flour passes through a cloth having openings not larger than those of woven wire cloth designated 212 μm (No. 70)" (U.S. Code of Federal Regulations CFR, 2013). Wheat flours are obtained through a series of grinding and sifting operations whereby the bran and germ are separated from the endosperm and that the maximum amount of flour can be extracted (Campbell et al., 2007). Flour particle size significantly affects the physico-chemical characteristics of the end product (Wang and Flores, 2000). To limit bran contamination in flour and to separate flour particles based on size, wheat milling industries depend on the sieving/sifting process. Thus, the mechanics of fine sieving received much attention and new generation of sieves, screen cloths, and sifter stacks have evolved (Roberts and Beddow, 1968). However, most of these developments did not account for the cohesive material handling challenges. It is proven that sieving soft wheat flour leads to loss in throughput in comparison with hard wheat flour (Neel, 1982).

Using a sieving index, Neel and Hoseney (1984a) explained that the loss in throughput while sieving soft wheat flour was largely due to the flour cohesiveness. Bulking number, and bridging threshold tests further identified that moisture content, presence or absence of fat, differences in particle size distribution, and particle surface roughness were responsible for the cohesiveness in flours. Bian et al. (2015) also reported that the soft wheat flour is more cohesive than the hard wheat flour. Higher cohesiveness in soft wheat flours could be due to the presence of surface fat, higher surface roughness, and presence of lower density particles (Neel and Hoseney, 1984b; Kuakpetoon et al., 2001). This indicates that differences in cohesion between hard and soft wheat flours are not due to a single factor but from interaction of physical,

chemical, and surface properties. Therefore, it is important to understand the fundamentals behind the cohesion phenomena in order to develop an efficient particle size separation process.

1.2. Research Hypotheses and Goals

The difference in wheat flour composition originates from their class/variety, roller milling specifications, and the size and density based fractionation process (Wang and Flores, 2000). Because of wide variability in surface properties and physico-chemical composition of wheat flours, understanding the effect of these factors on inter-particle cohesion under different breakage patterns of endosperm (particle size distribution), moisture content, and sifter load variations is important. In this dissertation work, it was hypothesized that variation in particle surface characteristics obstructs the movement of particles over the screen surface. The particle surface characteristics can affect the inter-particle cohesion of wheat flour and can affect the efficiency of size based separation process.

1.2.1. Research objectives

The overall goal of this project was to understand the flour particle properties that influence cohesion in order to improve the size based separation process. The objectives of this study are listed below:

1. Determine the surface physical and chemical characteristics of hard and soft wheat flours.
2. Determine the significance of particle size, moisture content, sifter load, and chemical composition on bulk cohesion of wheat flours.
3. Develop a correlation to predict the flow behavior of wheat flours based on the particle physical and chemical characteristics.

4. Develop and validate a discrete element method (DEM) model to describe the wheat flour sieving process.

1.3. Dissertation Outline

The dissertation is divided into six chapters excluding this chapter. Chapter 2 covers the review of literature on inter-particle cohesion of granular systems, factors that influence inter-particle cohesion, and DEM models that are used for describing inter-particulate cohesion are reviewed. In Chapter 3, the different surface physico-chemical and morphological characteristics of wheat flours are presented. Chapter 4 describes the significance of physical and chemical composition and variation in sifter load on bulk cohesion of wheat flours. In Chapter 5, the prediction model for describing the flow behavior of wheat flours during the sieving process is discussed. Chapter 6 describes the development of DEM model of the sieving process of wheat flour and the lab scale sieving procedures used for validation of the model. Further discussions are provided on the sieve blinding phenomena and sieving efficiency. The summary of the findings of this dissertation work and suggestions for future work based on the understandings gained from this research work are discussed in Chapter 7.

1.4. References

Bian, Q., Sittipod, S., Garg, A., & Ambrose, R. P. K. (2015). Bulk flow properties of hard and soft wheat flours. *Journal of Cereal Science*, 63, 88–94.

Campbell, G.M. (2007). Roller milling of wheat. *Powder Technology*, 12, 392–425.

CFR. (2013). 21 CFR 137.105: Requirements for specific standardized cereal flours and related products. Code of Federal Regulations, Washington, D.C.

Kuakpetoon, D., Flores, R. A., & Milliken, G. A. (2001). Dry mixing of wheat flours: Effect of particle properties and blending ratio. *LWT - Food Science and Technology*, 34, 183–193.

Neel, D. V. (1982). *Parameters affecting the flowability of hard wheat and soft wheat flours and their relationship to sifting.* Unpublished PhD Thesis. Kansas State University, KS, U.S.A.

Neel, D. V., & Hoseney, R. C. (1984a). Sieving characteristics of soft and hard wheat flours. *Cereal Chemistry*, 61, 259–261.

Neel, D. V., & Hoseney, R. C. (1984b). Factors affecting flowability of hard and soft wheat flours. *Cereal Chemistry*, 61, 262–266.

Roberts, T. A., & Beddow, J. K. (1968). Some effects of particle shape and size upon blinding during sieving. *Powder Technology*, 2, 121–124.

Wang, L., & Flores, R. A. (2000). Effects of flour particle size on the textural properties of flour tortillas. *Cereal Chemistry*, 31, 263–272.

Chapter 2 - Wheat Flour Sieving, Cohesion of Granular Systems and Discrete Element Method: Literature Review

In this chapter, the factors that influence the sieving process are presented. The physical, chemical, and surface characteristics that influence the inter-particle cohesion of granular systems are also presented. The section includes a review on cohesive forces and measurement techniques that are available to understand the inter-particle cohesion are discussed (Section 2.3). In Section 2.4, Discrete Element Method (DEM) working principle, model implementation, and different models developed by researchers for the calculation of inter-particle cohesion are discussed. The aim of this Chapter is to describe in detail the experimental and theoretical approaches in order to help understand the inter-particle cohesion of granular systems.

2.1. Wheat Flour Sieving

Wheat milling involves a series of grinding and sifting/sieving operations whereby bran layers and germ are separated from the endosperm to extract a maximum amount of flour (Campbell et al., 2007). Wheat flour sieving is the simplest level of particle size-based dry separation process. The sieving process has changed very little from its inception. Operative flour millers referred to this separation process as either sieving or screening. The batch process of particle separation using screens is called sieving, whereas continuous process is referred as the screening process (Neel, 1982). The particle size of wheat flour significantly affects its physico-chemical properties (Wang and Flores, 2000). Thus, the flour miller ensures efficient separation of endosperm particles based on size with minimum bran contamination (Posner and Hibbs, 2005). The most common sieving machines in the flour mill include: (1) a gyrating box sifter stack consisting of approximately 30 stacked sieves and capable of making up to eight

separations; (2) a reciprocating sieve stack capable of making two to four separations; and (3) a reel-type machine consisting of a screen cylinder that moves or rotates the material on the screen surface and is capable of making two to three separations (Posner and Hibbs, 2005). Irrespective of the type of sifter stack, the separation is achieved by the movement of particles on the screen surface, which allows the particles smaller than the screen opening to pass through by the force of gravity. Though the sieving process looks simple, it is governed by multidisciplinary principles ranging from physics to applied fluid mechanics (Liu, 2009) and the success of this process is controlled by many factors which are elucidated in the following section.

2.2. Factors Affecting the Sieving Process

The factors affecting the sieving process can broadly be classified as the machine parameters (design and operational parameters) and wheat flour characteristics (Fig. 2-1).

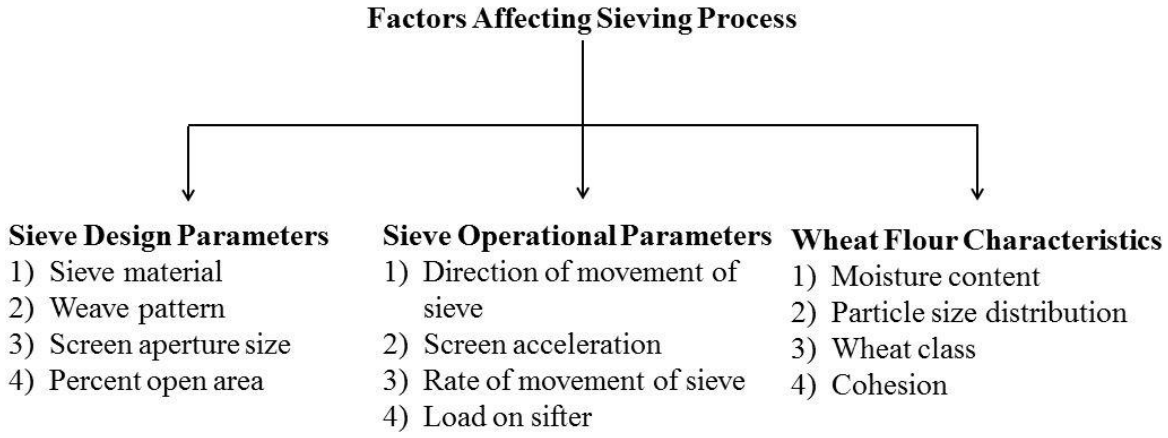

Figure 2-1: Factors affecting the sieving process.

The effect of sieve design parameters and sieve operational parameters on the sieve efficiency could be found in Whitby (1958), Roberts and Beddow (1968), and Schroeder (2000). The fundamentals in choosing an appropriate sieve material and percent open area which are

critical are explained in this section. Flour mills generally rely on screens that are made of smooth material in order to avoid drag on the particles and to assist the passage of granular materials through the sieve (Posner and Hibbs, 2005). The screens made of stainless steel material are commonly used for sieving coarse particles, whereas screens made of polyester or polyamides are used for sieving finer flour particles (Schroeder, 2000). These synthetic materials (polyester and polyamide) are preferred for sieving finer flour particles, because they are not affected by the variation in the moisture content of particles and also have the ability to provide a better shearing action on the surface of screen (Ricklefs, 2002).

Percent open area is another important factor that affects the efficiency of the sieving process. The screen with greater percent open area results in more fine material passing than the screen (same aperture size) with lesser percent open area (Posner and Hibbs, 2005). For sieving fine flour particles an optimal open area of 43% is preferred (Schroeder, 2000). Extensive research work has been done by various researchers on the mechanics of sieving fine particulate materials that helped in the evolution of industrial scale 'plant sifters' from a small scale 'gyrating sifters' (Whitby, 1958; Roberts and Beddow, 1968; Schroeder, 2000; Ricklefs, 2002). Improvements are made not only in sieve design and construction but also in the process of automation of sieving process. Though technical advancements are made on the sieve design and operational parameters, the milling industry still relies on the technical knowledge of the operators to adjust the sifter stack from time to time. Handling challenges could originate from the effect of surface, physical, and chemical characteristics of incoming wheat flour stock that influences the inter-particulate cohesion which in turn affects the sieving efficiency and throughput. The factors that affect the cohesion and flowability are described in detail in section 2.3.2.

2.3. Cohesion of Fine Granular Systems

Cohesion of fine granular systems may be defined as the strength exerted by a granular material against the shearing stress in the absence of compression forces applied perpendicularly to the direction of shearing stress (Rumpf, 1961). It is proven that, for most of the fine granular systems, cohesion increases with the addition of moisture content. However, there are some fine granular powders that are naturally cohesive with dry and stable bridges formed between these powders leading to caking or agglomeration (Neel, 1982). Cocoa, coffee, chalk, and wheat flour are good examples of this category (Baerns, 1966). Different inter-particle or cohesive forces act on fine granular system and make them cohesive and lead to formation of agglomerates (Peleg, 1977). In the following sub-section, the various inter-particle forces that induce cohesion are described.

2.3.1. Cohesive forces in powder beds

Rumpf (1961) classified and discussed the various mechanisms by which particles are attracted or interlocked. Mechanisms of inter-particle attraction have been divided into four major groups: van der Waals forces, liquid bridges, electrostatic forces, and mechanical interlocking (Rumpf, 1961).

For fine particles (average particle size ~ 100 μm or less), the inter-particle cohesive force is dominant relative to gravity, hence causes flowability issues (Castellanos, 2005). For fine, dry, and uncharged particles, van der Waals force (i.e. intermolecular force) is dominant compared to the other three forces because the van der Waals force can be orders of magnitude greater than particle weight (Castellanos, 2005).

2.3.1.1. Van der Waals forces

The induced electrostatic attractions between molecules create van der Waals interactions (vdW) (Israelachvili, 1990). The electrons in an atom can arrange themselves anywhere within their orbitals, and may group momentarily toward one side of the molecule, thus creating a temporary slight negative charge on one side and positive on the other side. The neighboring nonpolar molecule will then tend to become polar with a positive charge on the end close to the first molecule (Israelachvili, 1990). Van der Waals interactions are thus a function of the inter-particle spacing at the molecular level. When the distance increases, attraction takes place; as the distance decreases, the electron clouds associated with the molecules overlap, hence repulsion occurs. The total intermolecular pair potential is obtained by summing the attractive and repulsive potential. The van der Waals pair potential for two molecules can be represented as

$$W\,(r) = \frac{C}{S^n} \qquad (2\text{-}1)$$

where, *C* is a constant, *r* is the distance between the molecules, and *S* is the separation distance, and 'n' could be taken as '6' as suggested by London (1937). The resulting force between the molecules is:

$$F\,(S) = \frac{dW\,(S)}{dS} = \frac{Cn}{S^{n+1}} \qquad (2\text{-}2)$$

Fine granular systems are large bodies containing many such molecules. The Hamaker theory (Hamaker, 1937) assumes that the interaction energies between the isolated molecule and all the molecules in the large body are additive and non-interacting (Seville et al., 1997). Thus the net interaction energy can be found by integrating the molecular interaction over the entire body, and can result in energy/force relations that are effective over vastly larger distances (Seville et al., 1997). For example, the interaction energy between a sphere and a surface can be

$$W\ (S) = \frac{-AR}{6S} \qquad (2\text{-}3)$$

And the resulting force is

$$F\ (S) = \frac{AR}{12\ S^2} \qquad (2\text{-}4)$$

where, *A* is the Hamaker constant, *R* is the radius of the sphere and *S* is the distance between the sphere and the surface.

Inter-molecular attraction is a significant factor for agglomeration of the fine particles which are separated by short range (100 Å) (Neel, 1982). There is little information on the specific influence of such forces on the flowability of food powders. Indirect evidence of the contribution of such short-range forces in foods can be found in White et al. (1967). They showed that various food powders did not flow when their particle size was less than 120 µm. Observation by Peleg et al. (1973) showed that microcrystalline cellulose, a free flowing insoluble powder, could develop a considerable tensile strength upon exertion of relatively small pressure with very little change in bulk density. Neel (1982) reported flowability issues in wheat flour when the average particle size was less than 75 µm. These studies indicate that van der Waals forces may be a significant factor affecting the flowability of fine powders.

2.3.1.2. Liquid bridging

The second type of inter-particle cohesive force to be considered is liquid bridging, which is the result of having adsorbed water or other binding agents such as free lipids, fats, etc. on the surface (Neel, 1982). In the case of granular systems, the liquid bridges can be formed due to moisture absorption (hygroscopic materials), melting (fatty components), chemical reactions that liberate liquid (browning), excessive liquid ingredient (flavoring oils), moisture liberation during the crystallization of amorphous materials, and accidental wetting of the powder or the

equipment. Because particles with these characteristics are very common in food industries, enormous work has been dedicated towards understanding the formation of liquid bridges and their effects on bulk characteristic of powders (Moreyra and Peleg, 1981; Scoville and Peleg, 1981; Aguilera et al., 1995; Teunou and Fitzpatrick, 1999). These studies proved that the availability of excess water causes dissolution of local bridges (i.e. other types of inter-particle bridges) and leads to formation liquid bridges between powder particles. A sudden temperature change or removal of moisture (drying after wetting) from the liquid bridges converts them into solid bridges (Billings et al., 2006). The higher the adsorption/absorption ability of a particle, the higher will be the propensity of cohesion.

2.3.1.3. Electrostatic forces

Electrostatic cohesion occurs in particles with excess opposing charges formed due to friction (Rhodes, 1998). This situation may also arise when particles come in contact attributable to different contact potential values (Schubert, 1987). The electrostatic energy generated during the movement of dried food powders could result in the formation of a layer of powder on the equipment during processes like mixing, pneumatic transport, and fluidization (Bhandari et al., 2013).

2.3.1.4. Mechanical interlocking

Fibrous, bulky, and flaky particles can interlock or fold about each other resulting in "form-closed" bonds otherwise termed as "mechanical interlocking" (Pietsch, 1991). Such mechanical interlocking can be formed when temperature of the materials rises to reach a certain viscosity that causes the molecules at the interface begin to flow into each other. When the temperature decreases again, a merger can take place, which leads to the formation of

mechanical interlocking/matting/meshing between the particles (Griffith, 1991). Particles with irregular or fibrous shapes will tend to have more mechanical interlocking bridges than that of regular objects (Rumpf, 1961).

2.3.2. Factors affecting inter-particle cohesion

2.3.2.1. Moisture

Due to hygroscopic nature of cereal based powders, these powders adsorb or absorb moisture from the air if the relative humidity of ambient air is higher than the equilibrium relative humidity of the powder (Fitzpatrick et al., 2004). The moisture uptake increases the formation of liquid-bridges in turn increasing the cohesion. Baerns (1966) found that wheat flour at higher moisture was so cohesive that, it could not be fluidized using standard methods. He related that this phenomenon is due to the agglomeration and bridging between particles which was formed by inter-particle adhesive forces (liquid bridges). Increase in moisture content has been found to increase inter-particle cohesion of wheat flour (Neel and Hoseney 1984a, 1984b; Teunou and Fitzpatrick, 1999; Iqbal and Fitzpatrick, 2006). Water adsorbed onto the surface of a particle has also been supposed to tend to dissolve soluble components and form liquid bridges between particles, which lead to cohesion and flow difficulties (Landillon et al., 2008). However, due to the complex physio-chemical nature of wheat flour, there is still lack of knowledge on understanding the contribution of moisture content on the flow behavior of wheat flour during handling and processing operations. Thus, there is need for further research in identifying the moisture levels where the flow of flour changes from an easy flow to cohesive flow.

2.3.2.2. Particle size distribution

Particle size distribution has been considered as one of the most important physical properties which affect the cohesion of granular materials. Newitt and Conway-Jones (1958) found that the agglomeration of fine particulate systems depended on two principal factors: (i) average particle size and (ii) particle size distribution. Their empirical findings were validated by Peleg (1977) and Neel and Hoseney (1984a), and stated that inter-particle forces will increase or decrease according to average particle size or particle size distribution. For powders, reduction in particle size tends to increase cohesion behavior because the particle surface area per unit mass increases, creating a greater number of contact points for additional inter-particulate interactions (Neel and Hoseney, 1984a). For wheat flour a negative relationship exists among flour cohesion and mean particle size (Neel and Hoseney, 1984a, 1984b; Kuakpetoon et al., 2001).

2.3.2.3. Particle shape and surface characteristics

It has been shown by experimental and computational methods that particle shape has a significant effect on inter-particle cohesion (Roberts and Beddow, 1968; Liu and Litster, 1991; Wu and Cocks, 2006). Mechanical interlocking of irregular shaped particles could result in higher cohesion compared to that of regular shaped particles. The cohesion force also depends on surface roughness of the particles (Ata et al., 2002), as surface roughness controls the mechanical interlocking between particles on formation of van der Waals forces of attraction (Landillon, 2008). The roughness of a surface has a larger effect on the cohesion force, and change in roughness by fractions can change the van der Waals interaction by up to several orders of magnitude (Castellanos, 2005). Furthermore, Neel and Hoseney (1984a) indicated that the chemical composition (presence of fat) had a significant effect on cohesion of wheat flour. This study demonstrated that presence of lipids on the surface was a significant contributor to the

cohesiveness of flour. It is evident (Section 2.3.1) that the major cause for cohesion of dry and fine granular systems (e.g. wheat flour) are van der Waals forces and liquid bridging. While the cited studies confirm the effect of surface roughness and surface fat composition on cohesion, there is no systematic study on these surface properties for wheat flour. Evaluation of surface roughness and surface lipid composition parameters for different particle sizes will give an insight into the inter-particle cohesion and bulk flow behavior of wheat flour.

2.3.2.4. Type of wheat class

Neel and Hoseney (1984a) and Bian et al. (2015) compared the flow behavior of hard and soft wheat flours, and found that the soft wheat flour is more cohesive than the hard wheat flour. Hareland (1994) also observed that soft wheat flour does not pass freely through the sieve openings whereas hard wheat flours pass without adhering to the sieve mesh. The higher cohesiveness in soft wheat flour could be due to the differences in particle size, surface composition, surface roughness, and density (Neel and Hoseney, 1984b; Kuakpetoon et al., 2001). In these studies, the researchers had used wheat flour obtained from different facilities but, it would be useful to quantify the differences in flow behavior of wheat flours from different classes that are obtained using similar milling processes.

2.3.3. Measurement of cohesive behavior of powders

The cohesive/flow behavior of powders is greatly influenced by the different inter-particle cohesive forces as explained in the previous section. The cohesivity of the particulate system affects the particulate material ability to flow (Thakur, 2014). There are many experimental methods to evaluate the flowability of bulk solids. In this section, the common testing methods used to measure the cohesiveness are briefly described.

Mass flow test is a simple and common test used by the industry. In this test the powder is poured through a tube or conical funnel and the mass flow rate is calculated (Neel, 1982). A lower mass flow rate relates to a greater cohesive strength. For powders that have greater cohesive strength this procedure can be burdensome (Neel, 1982) because the test gives an indication of cohesion only and doesn't accurately measure the cohesive strength.

Empirical methods have also been used to assess the powder flowability such as, Hausner ratio (HR) and Compressibility index (CI) values. The Hausner ratio is the ratio of tapped bulk density to the loose bulk density and it relates to gain in cohesive strength after the compaction (Hausner, 1967). The powders with little gain in bulk density are considered to be non-cohesive (Hausner ratio < 1.25) (Eben, 2008) while a higher value indicates greater in cohesion. The limitation of this test is that it does not link the cohesive strength to the application of external stress (Thakur, 2014). Another similar empirical method is Compressibility index, which is the ratio of increase in bulk density due to tapping (Carr, 1965). Based on the CI and HR values, the powders could be classified into different flow categories (Table 2-1). While both the HR and CI can give a quick and rough measure of powder cohesion in certain circumstances, these measures are criticized in academia for not having strong theoretical basis (Thakur, 2014).

Table 2-1: Hausner ratio and compressibility index.

Flow indicator	HR	CI (%)
Excellent	1.00 –1.11	≤ 10
Good	1.12 –1.18	11–15
Fair	1.19 –1.25	16–20
Passable	1.26 – 1.34	21–25
Poor	1.35 – 1.45	26–31
Very poor	1.46 – 1.59	32–37
Cohesive	>1.60	>38

(Reference: Eben, 2008)

Flowability can also be measured by using shear testers which are backed by well-established physical theory. Direct shear testers can measure shear flow properties of powders that include angle of internal friction, effective angle of internal friction, cohesion, yield loci, and flow function. The direct shear testers provide a shear stress value for a given consolidation and normal stress.

The yield strength of the macro-scale cohesion of particulate cohesion of materials can be described Coulomb cohesion. The Mohr-Coulomb failure criterion is derived from the graphical representation of the shear conditions of the material. The material failure is represented by the linear envelope that is obtained from a plot of the material's shear stress versus the applied normal stress and is described as:

$$|\sigma_t| = \sigma_n \tan\varphi + C \qquad (2\text{-}5)$$

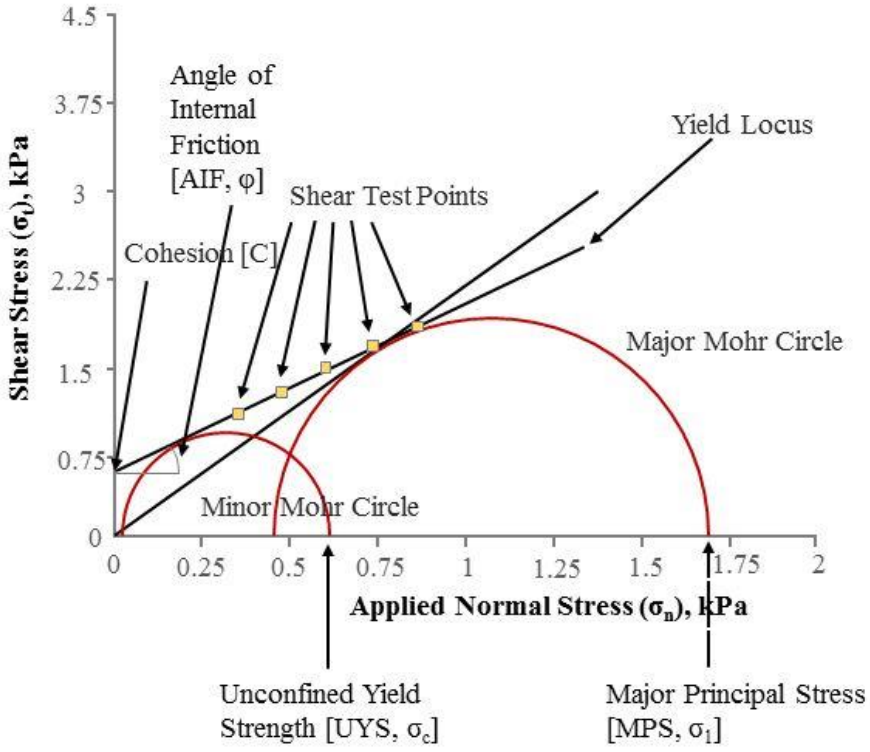

Figure 2-2: Measurement of cohesion and flow function.

Equation 2-5 divides the mechanical strength of the material into the angle of internal friction φ and the cohesion of the material C. Here, σ_n and σ_t are the normal and tangential stress in the material. At each pre-shear load the unconfined yield strength (UYS, σ_c) and major principal stress (MPS, σ_1) were calculated from the two Mohr's circles which were drawn tangent to the yield locus (Fitzpatrick et al., 2004). To characterize the flowability of granular systems, Jenike (1964) proposed the ratio of major principal stress (σ_1) and the unconfined yield strength (σ_c) called the flow function (FF):

$$FF = \frac{\sigma_1}{\sigma_C} \qquad (2\text{-}6)$$

Based on the flow function values, the powders could be classified into different flow categories (Table 2-2).

Table 2-2: Classification of powders.

Type of powder	Flow function value
Very cohesive	< 2
Cohesive	2 to 4
Easy flow	4 to 10
Free Flow	> 10

(Reference: Jenike, 1964)

The most common instrument used for flowability evaluation is the Jenike shear tester designed by Jenike (1967), which is a translational shear tester. In translational shear tester, the shear is applied by translation motion, which limits the amount of shear displacement that can be applied for shearing action. The other major limitation is sample preparation, which needs to be clarified for a meaningful interpretation of the results (Neel, 1982). Peleg (1977) noted that starch and wheat flour exhibit 'slip-stick effect' when using the Jenike shear cell. The 'slip-stick effect' (also known as stick-slip friction) is a friction phenomenon occurring in many granular systems, where particle surfaces are sliding against each other. To encounter the limitations caused by translational shear tester, a torsional shear cell (FT4 powder rheometer) will be employed in this dissertation, which was proven to be successful in characterizing the flow behavior of powders in pharmaceutical industry.

2.3.4. Prediction of flow behavior of powders

To access the flowability/flow behavior of powders, industries often rely on the measurement of different parameters like mass flow rate, Hausner ratio, Compressibility index, angle of repose, and flow function values and correlate them with the previously determined values for flow. These methods were proven to be successful for granular materials whose

particle size is greater than 100 μm (Castellanos, 2005). However, these methods are time consuming, cumbersome and practically not feasible for assessing the flow behavior of finer powder materials (~100 μm and smaller). With the increase in usage of finer powder materials in the food industry, there is need for development of alternative methods to assess the flow behavior of fine powders. Given that powder flowability is essential to formulate new products, there has been much effort devoted to this topic with most studies focused on elucidating the effect of moisture (Teunou and Fitzpatrick, 1999; Fitzpatrick et al., 2004; Landillon et al., 2008), particle size distribution (Neel and Hoseney, 1984a, 1984b; Kuakpetoon et al., 2001), and consolidated time (Kamath et al., 1994; Teunou and Fitzpatrick, 1999). However, it is important to understand the underlying mechanisms responsible for the flow behavior of dry and fine cohesive materials.

Fine, dry, and uncharged powders are dominated by the inter-particle-cohesion force known as the van der Waals (vdW) force (Castellanos, 2005). The van der Waals force can be orders of magnitude greater than particle weight, the ratio of which is known as the granular Bond number (Eq. 2-7).

$$Bo_g = \frac{F_{cohesion}}{W_g} \tag{2-7}$$

In order to account for the vdW force between two particles, many cohesive force models have been proposed that were discussed in Section 2.3.1.1. The vdW cohesive force can be formulated from a modified Rumpf cohesion model (Eq. 2-8) proposed by Chen et al. (2008). This modified model also considers the non-contact interaction between two particles separated by a distance H_0 and the contact forces between particles and asperities (Capace et al., 2015).

$$F_{cohesion} = \frac{A}{12z_0^2}\left(\frac{d_p}{2(^{H_0}/_{z_0})^2} + \frac{3d_{asp}d_p}{d_{asp}+ d_p}\right) \tag{2-8}$$

where A is Hamaker constant (J), Z_0 is the equilibrium separation distance, d_p is the particle diameter (m), H_0 is the separation distance, and d_{asp} is asperity diameter (m). The first term within the parenthesis on the right hand side of Eq. (2-8) accounts for the non-contact force between two particles separated by distance H_0, whereas the second term accounts for the contact force between the particles.

The Bond number concept is widely adapted in the pharmaceutical industry has been shown to correlate well with other bulk-scale properties such as bulk density (Yu et al., 2003; Capece et al., 2014), angle of repose (Jallo et al., 2011), and flow function coefficient (Huang et al., 2014; Capece et al., 2015). In this dissertation work, Bond number concept is used to predict the flow behavior of wheat flour during size based separation process.

In this research work, discrete element method (DEM) technique is used to correlate inter-particle cohesion with the particle size separation process of wheat flour. The DEM technique and different cohesion models are reviewed in the following section.

2.4. Discrete Element Method (DEM)

The discrete element method (DEM), developed by Cundall and Strack (1979), is a tool for analyzing quasi-static problems related to densely packed granular materials. DEM has increasingly been used in several research areas like engineering, material science, physics, geology, mineralogy, agriculture, and more (Thakur, 2014). Numerical calculation in the discrete element method employs two main equations in the calculation cycle: (i) Newton's equations of translational and rotational motion for each particle, and (ii) the forces and torques which are calculated based on contact constitutive laws (Itasca, 2003). Figure 2-3 shows a simplified calculation cycle in DEM (Itasca, 2003). The particles are modelled as rigid bodies interacting at

soft contacts. An overlap is allowed at particle contact, however, this overlap is not real but it allows modelling the deformation at the particle contact in an indirect way (Itasca, 2003). The numerical time step should be chosen such that any disturbance during a single time step only affects the immediate neighboring particles to ensure the stability of the whole system (O'Sullivan and Bray, 2004). For the success of DEM simulations, the formulation of equations indicating the motion of particles, choosing the optimum time step, and defining the particle shape are critical which are elucidated in the following section.

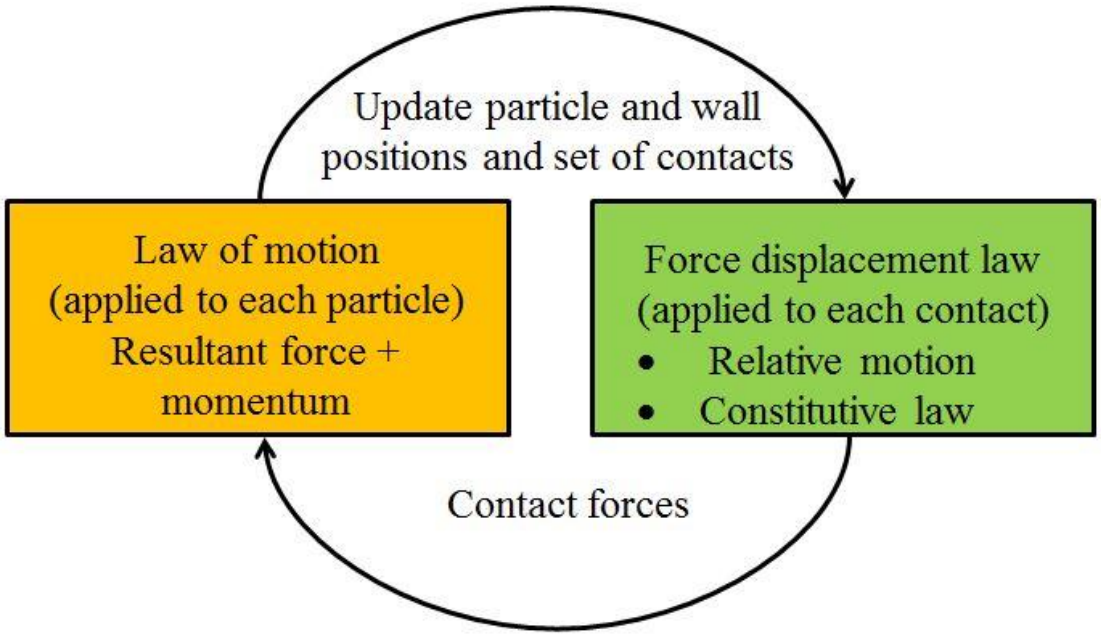

Figure 2-3: Calculation cycle in DEM.

(Source: Itasca, 2003)

2.4.1. An overview of DEM

2.4.1.1. Formulation

Particle-particle interactions are modelled using the soft contact approach where rigid particles are allowed to overlap each other at the contact point with very small overlaps, typically

less than 1% of the particle diameter at each time step. The contact force is calculated according to the contact model as a function of the overlap.

The changes in positions and velocities of the particles due to the contact and gravitational forces are calculated from the integration of Newton's motion equations. For particle 'i' the translational motion is given as (Remy et al., 2009):

$$m_i \frac{d^2}{dt^2} \boldsymbol{x_i} = \boldsymbol{f_i} + m_i \boldsymbol{g} \qquad (2\text{-}9)$$

where, m_i = mass of the particle, t = time, $\mathbf{x_i}$ = position of the particle, $\mathbf{f_i}$ = summation of all forces acting on the particle ($\boldsymbol{f_i} = \boldsymbol{\Sigma_c f_i^c}$), and $\mathbf{g}$ = acceleration due to gravity. The rotational motion equation for particle 'i' is given by (Remy et al., 2009):

$$I_i \frac{d}{dt} \boldsymbol{\omega_i} = \boldsymbol{T_i} \qquad (2\text{-}10)$$

where, I_i = moment of inertia for particle i, ω_i = angular velocity, and T_i = total torque acting on it, which is defined by equation (2-7) (Remy et al., 2009):

$$T_i = \sum_{i=1}^{N_c} l_i^c \times f_i^c \qquad (2\text{-}11)$$

where l_i^c is the vector from the center of particle i to the contact point and $\boldsymbol{f_i^c}$ is the contact force.

2.4.1.2. Determination of computational time step

The time-step in DEM simulation is time increment between two consecutive iterations. A sufficiently small integration time step is required to ensure the stability of simulation by having a sufficient number of time steps within each collision (Li et al., 2005). In a granular system assembly, force transmission between individual particles is through the Rayleigh wave that travels around the surface of elastic bodies. Computational time is a major concern in using the DEM because of the calculation of particle interactions and spatial movement at very small time steps (Boac et al., 2014). The DEM time step should be chosen such that the time step for

calculating particle information should be less than the time required for a Rayleigh wave to transverse the minimum size particle in the assembly (Li et al., 2005). The Rayleigh wave velocity (Vr) for the force transmission is given by equation (2-8) (Li et al., 2005; DEM solutions, 2013):

$$V_r = \chi . \sqrt{\frac{G}{\rho_s}} \qquad (2\text{-}12)$$

where, G = shear modulus, ρ_s = solid density of particle, and χ = parameter related to Poisson's ratio (υ) (Thornton and Randall, 1988) is defined as:

$$\chi = 0.1631\,\upsilon + 0.8766 \qquad (2\text{-}13)$$

If the particles in the granular assemblies have same properties, the critical time step (Tc) can be given as (Li et al., 2005; DEM solutions, 2013):

$$T_c = \frac{\pi r_{min}\sqrt{\frac{\rho_s}{G}}}{0.1631\upsilon + 0.8766} \qquad (2\text{-}14)$$

where, r_{min} = minimum size of particle in the granular assembly.

Particle Flow Code (PFC) by Itasca (2003) presented a simple method to calculate critical time step using equation (2-11):

$$T_c = \sqrt{\frac{m}{K_{max}}} \qquad (2\text{-}15)$$

where, m = mass of particle and k_{max} =maximum contact stiffness in the granular assembly.

In DEM simulations the actual time step is normally chosen by multiplying the critical time step by a factor of safety. A study by O'Sullivan and Bray (2004) has shown that the critical time step is a function of packing configuration and number of contacts per particle. They suggest that a critical time step of less than $0.221\sqrt{m/K_{max}}$ should be chosen for an assembly of particle for three dimensional cases if rotation is allowed. According to Itasca (2003), a time step

of 80% of T_c should be chosen for general simulations, and 25% of T_c for rapidly changing simulations. EDEM (DEM Solutions, 2013) suggests a time step of 20% of T_c (given by equation 2-10) for densely packed assemblies and 40% of T_c for loose granular systems.

2.4.1.3. Particle shape

The great majority of DEM studies in the literature were conducted using either 2D disks or 3D spheres (Thakur, 2014). Spherical particles are preferred because they facilitate the contact detection and calculation of inter-particle forces; however, spherical particles are more prone to rolling within a granular assembly than non-spherical particles due to lack of interlocking. Real particles are rarely spherical and it has been shown that particle shape significantly affects powder packing, compressibility, and flow (Deng and Davé, 2013; Johanson, 2009; Kaerger et al., 2004; Wu and Cocks, 2006; Zou and Yu, 1996). In general, the more aspherical the particle, the more difficult it is to pack, compresses, and flow. A number of numerical and experimental studies (Aoki and Suzuki, 1971; Chong et al., 1979; Li et al., 2004; Roberts and Beddow, 1968) have also shown that particle shape affects the flowability of the powder. Recent DEM studies (Chung and Ooi, 2008; Härtl and Ooi, 2008; Zhou and Ooi, 2009) have shown that particle interlocking arising from geometric interaction contributes significantly to the bulk granular friction, so it is important to introduce a degree of non-sphericity in particle shape to capture the behavior of real solids which are very rarely spherical.

Rolling friction is often used in order to simulate the effect of non-sphericity in particle shape (Wensrich and Katterfeld, 2012). They ran a series of simulations of angle of repose tests with paired particles and idealized spherical particles with rolling friction. They found some similarity; however, there is a significant discrepancy quantitatively. The reason for this

discrepancy is attributed to the fact that in some cases particle shape favors rotation, whereas in some cases it resists rotation (Thakur, 2014).

2.4.2. Working principle of DEM

Depending on the processes being modelled, approaches in DEM can be classified into soft-sphere approach and the hard-sphere approach (Boac et al., 2014). The difference between the two is that the hard-sphere approach does not account for the deformation of particles during collision while the soft-sphere approach does. In case of soft sphere, the overlap taking place between the particles at the point of contact is an indicator for the deformation of the particle. The extent of overlap is dependent on the inter-particle contact forces and the resulting motion of the particles and is determined by the use of contact models (O'Sullivan, 2011). Due to the ability to describe the bulk material physics, the soft sphere approach is the most commonly used in the grain and food processing industries (Boac et al., 2014). Thus to model the wheat flour particles, in this research work a soft sphere approach is used.

DEM involves modeling the particle motion for each particle and monitoring particle interactions at each contact (Boac et al., 2014). Depending on the process conditions, DEM models the flow of individual particles, the collisions, contacts, and interactions that the particles undergo with other particles as well as with the surrounding environment (Cleary, 2001). Collisions and contacts cause the forces acting on each particle to change their position, velocity, and characteristics. The resultant force is calculated by making use of contact models based on the force-displacement laws, and the resulting position and velocity data of the particles are calculated using Newton’s Second Law of motion. This cycle of calculation of the resulting force, position and velocity of the particles is repeated for each particle for the defined number of time steps which results in simulating the flow of particles in a particle-machine system (Quist,

2012). Therefore, the future of each particle is predicted by the cyclical repetition of an algorithm at every time step (Gonzalez-Montellano et al., 2012).

2.4.3. Contact models

The following sections describe different models that describe cohesive contact behavior that are applied as external forces in Newton's Second Law. These models use spherical particles to simulate three-dimensional systems and make the following assumptions about the contact:

- The behavior is elastic and isotropic
- The tangential component of the force does not affect the normal component
- The contact deflection is small ($\delta n << a$, the contact zone radius)

2.4.3.1. Linear cohesion model

The linear cohesion model (DEM Solutions, 2013) is a contact model implemented with DEM to simulate cohesive particles. The contact model adds an additional normal cohesive force to the Hertz-Mindlin contact model. There is no modification to the tangential force. The contact force is defined by Equation (2-16) where A is the contact area and k is the cohesion energy density (J/m^3).

$$F = k\,A \tag{2-16}$$

Linear cohesion models are generally employed to simulate the discharge of a granular material from the hoppers. In these models it was found that these models fail to capture the stress-history-dependent behavior of particles and also these models are not suitable to model the van der Waals forces between the particles.

2.4.3.2. The Bradley model

This model neglects contact deformations and considers the van der Waals forces. Bradley (1921) showed that the adhesive force for rigid spheres follows a force derived from the Lennard-Jones potential, which is a mathematical model that approximates the interactions between a pair of neutral atoms or molecules. The force of adhesion between two rigid spheres is described by:

$$f_n = \frac{8\pi R^* Y_{surf}}{3}\left[\frac{1}{4}\left(\frac{\delta_n}{\delta_o}\right)^{-8} - \left(\frac{\delta_n}{\delta_o}\right)^{-2}\right] \qquad (2\text{-}17)$$

where, δ_0 = equilibrium separation distance between the particles.

Figure 2-4 provides an example of the Bradley cohesion model and illustrates the attractive force between particles at a distance (Radjai and Dubois, 2011).

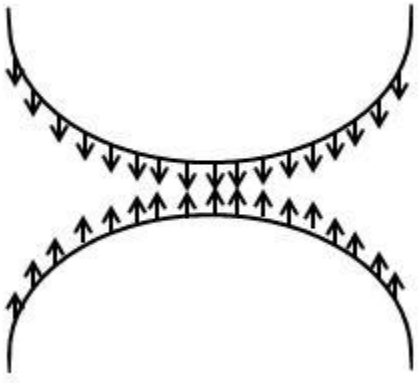

Figure 2-4: The Bradley model.
(Source: Radjai and Dubois, 2011).

The disadvantage of this model is that two particles gets separated when the forces pulling the particles reached at $\delta_0 = \delta_n$. Once the particles are separated the model assumes that there will not be any force acting between the particles, which is wrong in practical situations. The other disadvantage of this model is that, cohesive force computed between the particles is

insufficient to overcome the force of gravity and cannot generate material clumping or material adhesion to system walls.

2.4.3.3. The Derjaguin-Muller-Toporov model

A distinguishing feature of the Derjaguin-Muller-Toporov (DMT) model is the neglect of contact deflection (Muller et al., 1980). It is indirectly taken into account through the calculation of the attraction force and uses the Hertzian contact model. The attraction force between two particles is given by (Muller et al., 1980):

$$f_{DMT} = -2\pi R^{*} \Upsilon_{surf} \qquad (2\text{-}18)$$

where R^{*} is effective radius.

The DMT model is a good approximation of cohesive forces for small particles within the limit of weak cohesion. The attraction force is limited by the separation distance between two contacting particles at which the bond is broken. This limit is smaller for DMT and the particles to which it properly applies to. Figure 2-5 shows a schematic representation of the DMT contact model (Muller et al., 1980; Maugis, 1992; Radjai and Dubois, 2011). It illustrates how the contact deflection is indirectly taken into account through the attractive force between the particles.

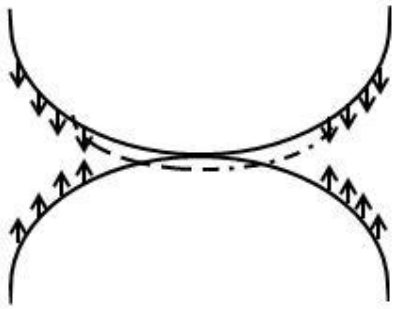

Figure 2-5: The Derjaguin-Muller-Toporov model.

(Source: Radjai and Dubois, 2011).

These models are often used in modeling the cohesion forces between the finer materials during bulk conveying systems. The major disadvantage of this model is with its implementation in DEM software, since it considers the cohesive force between the particles increases with time of contact and leads to the rupture of particles. This can be true in bulk handling/conveying systems, but in case of size separation process the breakage of particles is not observed. Hence, the DMT model is not suitable for modeling the particle size separation process.

2.4.3.4. The Johnson-Kendall-Roberts model

The Johnson-Kendall-Roberts, JKR, model is an improvement over the Hertzian contact model, and represents only dry loading and unloading conditions (Johnson et al., 1971). The JKR model takes into account the surface energy at the contact. This theory correlates the contact area of two contacting particles to the elastic material properties and the interfacial interaction strength. The cohesive force can be formed during the unloading cycle of contact as a force resisting separation. The JKR contact between two particles leads to the radius 'a' of the contact zone to be described by:

$$a^3 = \frac{R^*}{E^*}\left[f_n + 3\pi R^* \Upsilon_{surf} + \sqrt{(6\pi R^* \Upsilon_{surf} f_n + \left(3\pi R^* \Upsilon_{surf}\right)^2)} \right. \qquad (2\text{-}19)$$

where, Υ_{surf} is the surface energy in J/m^2 . The separation of the two particles is obtained from a maximum tensile force given by:

$$f_{JKR} = -\frac{3}{2}\pi R^* \Upsilon_{surf} \qquad (2\text{-}20)$$

The total normal force of contact with cohesion can be written as:

$$f_n = \frac{4a^2 E*}{3R*} - \sqrt{(8\pi E^* a^3 \Upsilon_{surf})} \qquad (2\text{-}21)$$

This represents a fully elastic model with cohesion between particles in the contact zone (Johnson et al., 1971; Johnson, 1987; Radjai and Dubois, 2011). Figure 2-6 provides an example of the JKR model and illustrates the tensile force between the particles in cohesive contact.

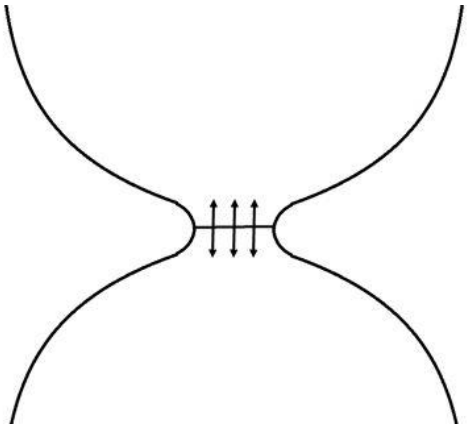

Figure 2-6: The Johnson-Kendall-Roberts model.

(Source: Radjai and Dubois, 2011).

The JKR approximation is accurate for large cohesive energies and larger particles with low Young's modulus. The model does not provide resistance in the tangential shearing direction. This limits the effect cohesion on material flow, because material is allowed to slide past each other with little resistance. Since, the present dissertation work is aimed at modeling the van der Waals forces between the finer particles; this model could not be adapted as it suits for modeling the cohesive energies between the larger particles with low Young's modulus.

2.4.3.5. Hertz-Mindlin with JKR cohesion model

Hertz-Mindlin with JKR cohesion model is cohesive contact model, which accounts for the influence of Van der Waals forces within the contact zone and allows to model strongly cohesive systems, such as dry powders or wet materials (DEM solutions, 2013). The model uses

the same calculations as the Hertz-Mindlin (no slip) contact model for tangential elastic, normal dissipation, and tangential dissipation forces.

JKR normal force depends on the normal overlap δ and the interaction parameter surface energy γ, in the following form as (DEM solutions, 2013):

$$f_{JKR} = -4\sqrt{\pi\gamma E^*}\, a^{\frac{3}{2}} + \frac{4E^*}{3R^*}\, a^3 \tag{2-22}$$

$$\delta = \frac{a^2}{R^*} - \sqrt{4\pi\gamma a / E^*} \tag{2-23}$$

where, the equivalent Young's Modulus E^*, the equivalent radius are defined as (DEM solutions, 2013):

$$\frac{1}{E^*} = \frac{(1-v_i^2)}{E_i} + \frac{(1-v_j^2)}{E_j} \tag{2-24}$$

$$\frac{1}{R^*} = \frac{1}{R_i} + \frac{1}{R_j} \tag{2-25}$$

where, the equivalentE_i, v_j, and R_i are being the Young's Modulus, Poisson ratio, and radius of each sphere in contact.

The maximum gap between the particles with non-zero force is given by (DEM solutions, 2013):

$$\delta = \frac{a_c^2}{R^*} - \sqrt{4\pi\gamma a_c / E^*} \tag{2-26}$$

$$a_c = \left[\frac{9\pi\gamma R^{*2}}{2E^*}\left(\frac{3}{4} - \frac{1}{\sqrt{2}}\right)\right]^{\frac{1}{3}} \tag{2-27}$$

The advantage of the EDEM Hertz-Mindlin JKR cohesion model is that it provides attractive cohesive force even if the particles are not in physical contact. This model could be

used to mathematically explain the cohesive forces between wheat flour particles and also in predicting the sieve efficiency and sieve blinding phenomena.

The above studies indicate that understanding the inter-particle cohesion and the eventual flowability of wheat flour is a more complex problem which requires a fundamental approach. An in-depth understanding of the cohesive behavior of wheat flour during sieving process is needed in order to develop an appropriate solution to flow problems during particle size separation process. Therefore, the primary focus of this dissertation effort is to pursue a fundamental investigation on the cohesive behavior of wheat flour.

2.5. References

Abu-Hardan, M., & Hill, S. E. (2010). Handling properties of cereal materials in the presence of moisture and oil. *Powder Technology*, 198, 16–24.

Aguilera, J. M., del Valle, J. M., & Karel, M. (1995). Caking phenomena in amorphous food powders. *Trends in Food Science and Technology*, 6, 149–155.

Aoki, R., & Suzuki, M. (1971). Effect of particle shape on the flow and packing properties of non-cohesive granular materials. *Powder Technology*, 1–3.

Ata, A., Rabinovich, Y. I., & Singh, R. K. (2002). Role of surface roughness in capillary adhesion. *Journal of Adhesion Science and Technology*, 16, 337–346.

Baerns, M. (1966). Effect of interparticle adhesive forces on fluidization of fine powders. *Industrial & Engineering Chemistry Fundamentals*, 5, 508–516.

Baruch, D. W. (1974). Wheat flour particle size distribution related to compressibility and bridging tests. *New Zealand Journal of Science*, 17, 21.

Bell, T. A. (2001). Solids flowability measurement and interpretation in industry, in: Levy, A., Kalman, H. (Eds.), *Handbook of Conveying and Handling of Particulate Solids*. pp. 3–13.

Bhandari, B., Bansal, N., Zhang, M., & Schuck, P. (2013). Handbook of food powders processes and properties. Woodhead Publishing Ltd., Cambridge, U.K.

Bian, Q., Sittipod, S., Garg, A., & Ambrose, R. P. K. (2015). Bulk flow properties of hard and soft wheat flours. *Journal of Cereal Science*, 63, 88–94.

Billings, S. W., Bronlund, J. E., & Paterson, A. H. J. (2006). Effects of capillary condensation on the caking of bulk sucrose. *Journal of Food Engineering*, 77, 887–895.

Boac, J. M., Kingsly, A. R. P., Casada, M. E., Maghirang, R. G., & Maier, D. E. (2014). Applications of discrete element method in modeling of grain postharvest operations. *Food Engineering Reviews*, 6, 128–149.

Bradley, R. S. (1932). The cohesive force between solid surfaces and the surface energy of solids. *Dublin Philosophical Magazine and Journal of Science*, 13, 853–862.

Campbell, G. M., Fang, C., & Muhamad, I. I. (2007). On predicting roller milling performance VI - Effect of kernel hardness and shape on the particle size distribution from first break milling of wheat. *Food and Bioproducts Processing*, 85, 7–23.

Capace, M., Ho, R., Strong, J., & Gao, P. (2015). Prediction of powder flow performance using a multi-component granular Bond number. *Powder Technology*, 286, 561–571.

Carr, R. L. (1965). Evaluating flow properties of solids. *Chemical Engineering*, 72, 163–167.

Castellanos, A. (2005). The relationship between attractive interparticle forces and bulk behaviour in dry and uncharged fine powders, *Advances in Physics*, 54, 263–376.

Chong, Y. S., Ratkowsky, D. A., & Epstein, N. (1979). Effect of particle shape on hindered settling in creeping flow. *Powder Technology*, 23, 55–66.

Chung, Y., & Ooi, J. (2008). A study of influence of gravity on bulk behavior of particulate solid. *Particuology*, 6, 467–474.

Cleary, P. W. (2001). Recent advances in DEM modelling of tumbling mills. *Minerals Engineering*, 14, 1295–1319.

Cleary, P. W. (2010). DEM prediction of industrial and geophysical particle flows. *Particuology*, 8, 106–118.

Cundall, P. A., & Strack, D. L. (1979). A discrete numerical model for granular assemblies. *Geotechnique*, 1, 47–65.

DEM Solutions. (2013). EDEM 2.5 User Guide. DEM Solutions, Ltd., Edinburgh, UK.

Deng, X.L., & Davé, R. N. (2013). Dynamic simulation of particle packing influenced by size, aspect ratio and surface energy. *Granular Matter*, 15, 401–415.

Eben, H. (2008). *Development of a composite index for pharmaceutical powders*, Unpublished Ph. D dissertation, North-west University, Potchefstroom, South Africa.

Fitzpatrick, J. J., Iqbal, T., Delaney, C., Twomey, T., & Keogh, M. K. (2004). Effect of powder properties and storage conditions on the flowability of milk powders with different fat contents. *Journal of Food Engineering*, 64, 435–444.

Freeman, R. (2007). Measuring the flow properties of consolidated, conditioned and aerated powders. A comparative study using a powder rheometer and a rotational shear cell. *Powder Technology*, 174, 25–33.

Gonzalez-Montellano, C., Fuentes, J. M., Ayuga-Tellez, E., & Ayuga, F. (2012). Determination of the mechanical properties of maize grains and olives required for use in DEM simulations. *Journal of Food Engineering*, 111, 553–562.

Griffith, E. J. (1991). Cake formation in particulate systems. VCH Publishers, Weinheim, Federal Republic of Germany.

Hamaker, H. C. (1937). The london-van der waals attraction between spherical particles. *Physica*, 4, 1058–1072.

Hareland, G. A. (1994). Evaluation of flour particle size distribution by laser diffraction, sieve analysis and near-infrared reflectance spectroscopy. *Journal of Cereal Science*, 20, 183–190.

Härtl, J., & Ooi, J. Y. (2008). Experiments and simulations of direct shear tests: porosity, contact friction and bulk friction. *Granular Matter*, 10, 263–271.

Hausner, H. H. (1967). Friction conditions in a mass of metal powder. *International Journal of Powder Metallurgy*, 3, 7–13.

Huang, Z., Scicolone, J., Gurumuthy, L., & Davé, R. (2014). Flow and bulk density enhancements of pharmaceutical powders using a conical screen mill: a continuous dry coating device, *Chemical Engineering Science*, 125, 209–224.

Iqbal, T., & Fitzpatrick, J. J. (2006). Effect of storage conditions on the wall friction characteristics of three food powders. *Journal of Food Engineering*, 72, 273–280.

Israelachvili, J. (1992). Intermolecular and Surface Forces, Academic Press, London.

Itasca. (2003). PFC 3D user manual. Itasca consulting group Inc, Minneapolis.

Jallo, L., Chen, Y., Bowen, J., Etzler, F., & Dave, R. (2011). Prediction of inter-particle adhesion force from surface energy and surface roughness, *Journal of Adhesion Science and Technology*, 25, 367–384.

Jenike, A. W. (1964). Storage and Flow of Solids, Bulletin No. 123. Utah Engineering Station, Salt Lake City, Utah.

Johanson, K. (2009). Effect of particle shape on unconfined yield strength. *Powder Technology*, 194, 246–251.

Johnson, K. L. (1987). Contact mechanics. Cambridge university press, Edinburgh, London.

Johnson, K. L., Kendall, K., & Roberts, A. D. (1971). Surface energy and the contact of elastic solids. Mathematical and physical sciences, 324, 301–313.

Kaerger, J. S., Edge, S., & Price, R. (2004). Influence of particle size and shape on flowability and compactibility of binary mixtures of paracetamol and microcrystalline cellulose. *European Journal of Pharmaceutical Sciences*, 22, 173–9.

Kamath, S., Puri, V. M., & Manbeck, H. B. (1994). Flow property measurement using the Jenike cell for wheat flour at various moisture contents and consolidation times. *Powder Technology*, 81, 293–297.

Kuakpetoon, D., Flores, R. A., & Milliken, G. A. (2001). Dry mixing of wheat flours: Effect of particle properties and blending ratio. *LWT - Food Science and Technology*, 34, 183–193.

Landillon, V., Cassan, D., Morel, M. H., & Cuq, B. (2008). Flowability, cohesive, and granulation properties of wheat powders. *Journal of Food Engineering*, 86, 178–193.

Levy, A. (2001). Handbook of conveying and handling of particulate solids, Elsevier Science.

Li, J., Langston, P. A., Webb, C., & Dyakowski, T. (2004). Flow of sphero-disc particles in rectangular hoppers—a DEM and experimental comparison in 3D. *Chemical Engineering Science*, 59, 5917–5929.

Li, Y., Xu, Y., & Thornton, C. (2005). A comparison of discrete element simulations and experiments for ‘sandpiles’ composed of spherical particles. *Powder Technology*, 160(3), 219–228.

Liu, F. P., Rials, T. G., & Simonsen, J. (1998). Relationship of wood surface energy to surface composition. *Langmuir*, 14, 536–541.

Liu, L. X., & Litster, J. D. (1991). The effect of particle shape on the spouting properties of non-spherical particles. *Powder Technology*, 66, 59-67.

London, F. (1937). The general theory of molecular forces. *Transactions of Faraday Society*, 33, 8–26.

Maugis, D. (1992). Adhesion of spheres: the JKR-DMT transition using a Dugdale model. *Journal of Colloid and Interface Science*, 150, 243–269.

Moreyra, R., & Peleg, M. (1981). Effect of equilibrium water activity on the bulk properties of selected food powders. *Journal of Food Science*, 46, 1918–1922.

Muller, V. M., Yushchenko, V. S., & Derjaguin, B.V. (1980). On the influence of molecular forces on the deformation of an elastic sphere and its sticking to a rigid plane. *Journal of Colloid and Interface Science*, 77(1):91–101.

Nase, S. T. (2000). *Characterization of wet granular flow*: *application to mixing and segregation.* Unpublished M.S Thesis. University of Pittsburgh, PA, U.S.A.

Neel, D. V. (1982). *Parameters affecting the flowability of hard wheat and soft wheat flours and their relationship to sifting.* Unpublished PhD Thesis. Kansas State University, KS, U.S.A.

Neel, D. V., & Hoseney, R. C. (1984a). Sieving characteristics of soft and hard wheat flours. *Cereal Chemistry*, 61, 259–261.

Neel, D. V., & Hoseney, R. C. (1984b). Factors affecting flowability of hard and soft wheat flours. *Cereal Chemistry*, 61, 262–266.

Newitt, D. M., & Conway-Jones, J. M. (1958). A contribution to the theory and practice of granulation. *Transactions of Institution of Chemical Engineers*, 36, 422–442.

O'Sullivan, C., & Bray, J. D. (2004). Selecting a suitable time step for discrete element simulations that use the central difference time integration scheme. *Engineering Computations*, 21, 278–303.

O'Sullivan, C. (2011). Particle-Based Discrete Element Modeling: Geomechanics Perspective. *International Journal of Geomechanics*, 11, 449–464.

Peleg, M. (1977). Flowability of food powders and methods for its evaluation – a review. *Journal of Food Process Engineering*, 1, 303–328.

Peschl, I. A. S. Z, & Colijn, H. (1977). New rotational shear testing technique. *Journal of Powder and Bulk Solids Technology*, 3, 55–60.

Pietsch, W. (1991). Size enlargement by agglomeration, fundamentals of agglomeration, John Wiley & Sons.

Pietsch, W. B. (1969). Adhesion and agglomeration of solids during storage and handling. *Transactions of ASME*, 5, 435–448.

Pilpel, N. (1969). The cohesiveness of powders. *Endeavour*, 28, 73.

Posner, E. S., & Hibbs, A. N. (2005). Wheat flour milling, second edition. St. Paul, Minn.: AACC International.

Quist, J. (2012). *Cone crusher modelling and simulation- Development of a virtual rock crushing environment based on the discrete element method with industrial scale experiments for validation.* Unpublished MS Thesis, Chalmers University of Technology, Goteborg, Sweden.

Radjai, F., & Dubois, F. (2011). Discrete-element modeling of granular materials. Wiley.

Remy, B., Khinast, J. G., & Glasser, B. J. (2009). Discrete element simulation of free-flowing grains in a four-bladed mixer. *AIChE Journal*, 55(8), 2035–2048.

Rhodes, M. (1998). Introduction to particle technology. John Wiley and Sons, New York, U.S.A.

Ricklefs, R. (2002). New NOVA sieve applications and equipment. *Association of Operative Millers Technical Bulletin*, August, 7825.

Roberts, T. A., & Beddow, J. K. (1968). Some effects of particle shape and size upon blinding during sieving. *Powder Technology*, 2, 121–124.

Rumpf, H. (1961). The strength of granules and agglomerate, in: Knepper, W. (Ed.), Agglomeration. Wiley Interscience, New York. U.S.A.

Schroeder, J. (2000). The evolution of sifting media and its effect on sifter performance and sieve frame design. *Association of Operative Millers Technical Bulletin*, May, 7451.

Schubert, H. (1987). Food particle technology – Part I: properties of particles and particulate food systems. *Journal of Food Engineering*, 6, 1–32.

Schulze, D. (1994). A New Ring Shear Tester for Flowability and Time Consolidation Measurements, in: 1st International Particle Technology Forum. Denver, Colorado, USA, pp. 11–16.

Schulze, D. (2007). Powders and bulk solids: Behavior, characterization, storage and flow, *Journal of Statistical Mechanics: Theory and Experiment*. Springer Verlag.

Scoville, E., & Peleg, M. (1981). Evaluation of the effects of liquid bridges on the bulk properties of model powders. *Journal of Food Science*, 46, 174–177.

Seville, J. P. K., Tuzun, U., & Clift, R. (1997). Processing of Particulate Solids. Blackie Academic and Professional, London.

Stanley-wood, N. (2008). Bulk solids handling: equipment selection and operation, Bulk Solids Handling.

Teunou, E., & Fitzpatrick, J. J. (1999). Effect of relative humidity and temperature on food powder flowability. *Journal of Food Engineering*, 42, 109–116.

Teunou, E., Fitzpatrick, J. J., & Synnott, E. C. (1999). Characterization of food powder flowability. *Journal of Food Engineering*, 39, 31–37.

Thakur, S. C. (2014). *Mesoscopic discrete element modelling of cohesive powders for bulk handling applications.* Unpublished PhD Thesis, The University of Edinburgh, Scotland.

Wang, L., & Flores, R. A. (2000). Effects of flour particle size on the textural properties of flour tortillas. *Cereal Chemistry*, 31, 263–272.

Wensrich, C. M., & Katterfeld, A. (2012). Rolling friction as a technique for modelling particle shape in DEM. *Powder Technology*, 217, 409–417.

Wu, C. -Y., & Cocks, A. C. F. (2006). Numerical and experimental investigations of the flow of powder into a confined space. *Mechanics of Materials*, 38, 304–324.

Yu, A., Feng, C., Zou, R., & Yang, R. (2003). On the relationship between porosity and interparticle forces, *Powder Technology*, 130, 70–76.

Zhou, C., & Ooi, J. Y. (2009). Numerical investigation of progressive development of granular pile with spherical and non-spherical particles. *Mechanics of Materials*, 41, 707–714.

Zou, R. P., & Yu, A. B. (1996). Evaluation of the packing characteristics of mono-sized non-spherical particles. *Powder Technology*, 88, 71–79.

Chapter 3 - Wheat Flour Particle Surface and Shape Characteristics

Abstract

The separation efficiency of wheat flour particles based on size, with minimum bran contamination, is important for a flour mill. Separation of flour during fractionation depends on the surface characteristics and shape of flour particles. Wheat flour particle characteristics such as surface lipid content, roughness, and morphology with respect to particle size were studied to better understand the differences between hard and soft wheat flours. Fractal analysis using image analysis was used to ascertain surface roughness. That was in turn verified by atomic force microscopy measurements. Soft wheat flours (soft red winter and soft white) had a higher degree of surface roughness than the hard wheat flours (hard red spring, hard red winter, and hard white). The fractal dimension values ranged from 2.67 to 2.78 and from 2.28 to 2.55 for soft and hard wheat flours, respectively. The surface lipid content increased with particle size in hard wheat but decreased in soft wheat flours. The surface lipid levels ranged from 1.02 to 1.18 and from 2.55 to 2.58% (% of total area) for 45 μm particles in hard wheat flours (hard red spring, hard red winter, and hard white) and soft wheat flours (soft red winter and soft white), respectively. For the 90 μm particles the lipid levels ranged from 1.54 to 1.62 and from 1.70 to 1.83% (% of total area) for flour particles in hard wheat flours (hard red spring, hard red winter, and hard white) and soft wheat flours (soft red winter and soft white), respectively. Surface lipid content and roughness values showed that soft wheat flours will be more cohesive than hard wheat flours. The morphology values revealed the irregularity in flour particles, irrespective of wheat class and particle size, owing to nonuniform fragmentation of protein and starch matrix of the wheat endosperm.

The results have been published, with the citation shown below:

Journal paper:

Siliveru, K., J. W. Kwek, G. Lau, and R. P. K. Ambrose. 2016. Image analysis approach to understand the differences in flour particle surface and shape characteristics. Cereal Chemistry, 93, 234-241.

3.1. Introduction

Wheat (*Triticum* spp.) is one of the most commonly produced and consumed cereal grains in the world. The majority of the wheat produced is converted into flour and used in the manufacture of bread, cakes, cookies, pasta, and couscous, whereas a small fraction is directed toward animal feed. For wheat, the end product of the milling is classified as flour in which "not less than 98 percent of the flour passes through a cloth having openings not larger than those of woven wire cloth designated 212 μm (No. 70)" (U.S. Code of Federal Regulations 2013). Wheat flours are classically obtained through a series of milling and sifting operations whereby the bran and germ are separated from the endosperm and by which the maximum amount of flour is extracted (Campbell et al. 2007).

It has been shown both experimentally and computationally that particle shape has a significant effect on powder behavior (Roberts and Beddow 1968; Liu and Litster 1991; Wu and Cocks 2006). In general, higher aspherical shape results in poorer powder flowability because of intermittencies in flow rate (Fraige et al. 2008). The fluidization velocities and bed voidage can be affected by particle shape (Flemmer et al. 1993; Xu and Zhu 2006). Mechanical interlocking with irregular shaped particles could result in larger bed voidages and higher minimum fluidization velocities (Kodam et al. 2009). These nonspherical particles develop greater rolling resistance that elevates the angle of repose compared with the relative rolling ease of spheres (Jensen et al. 1999). Consequently, the estimation of shape factors for wheat flour particles can be a valuable contribution to understanding the dynamics of wheat powders during handling and processing.

Different wheat classes, in particular hard and soft wheat, can have differences in sieving efficiency. A substantial loss in throughput is often encountered in soft wheat flours. Using the

sieving index, Neel and Hoseney (1984b) concluded that the loss was largely controlled by the flour cohesiveness. Based on the bulking number and bridging threshold tests, they identified further that moisture content, particle size distribution, and particle surface roughness were responsible for flour cohesion (Neel and Hoseney 1984a). In addition, Neel and Hoseney (1984b) reported that the presence of fat is a significant contributor to cohesiveness and that defatting removed some of the natural cohesiveness of the wheat flour systems. To account for the flow difficulties that come from surface lipid content, knowing the area of lipid over the wheat flour particle is necessary.

Surface roughness, which is a significant contributor to cohesiveness, controls the interparticle interaction by van der Waals forces and by mechanical linkages (Landillon et al. 2008). In recent years, the availability of modern measuring technology and the advent of atomic force microscopy (AFM) have enabled us to characterize the surface roughness of powder particles. The fractal dimension (FD) is commonly used to characterize the surface roughness of food and biological materials (Quevedo et al. 2002) at the macroscopic level. Higher values of FD mean more complex or rougher shapes, whereas lower values of FD are associated with simpler or smoother particles (Arzate-Vázquez et al. 2011). AFM allows three-dimensional (3D) imaging and measurement of particle roughness at the microscopic level. AFM has a sharp probe attached to a cantilever. During scanning, the forces between the tip of the probe and surface create deflections of the cantilever. A laser beam is focused onto the back of the cantilever, and by monitoring its movements a 3D image of the surface is built up (Allen et al. 1997). Because the probe is of nanometer dimensions and it is feasible to scan all the areas on a single particle, AFM is a powerful tool to discriminate between surface roughness levels at the microscopic level.

The objectives of this study were to 1) quantify the surface lipid content of flour particles, 2) define the shape factors of flour particles, 3) quantify the FD of flour particles with image analysis, and 4) calculate the surface roughness of flour particles with AFM.

3.2. Materials and Methods

3.2.1. Sample preparation

Samples of five different classes of wheat, hard red spring (HRS), hard red winter (HRW), hard white winter (HWW), soft red winter (SRW), and soft white winter (SWW) were procured from Montana Flour and Grains, Fort Benton, MT, U.S.A at a moisture content of 10 ± 0.5% wet basis (w.b.). The initial and final moisture contents of the wheat kernels were determined by drying 10 g whole grain samples, in triplicate at 130 °C for 19 h according to ASABE standard S 352.2 (ASABE, 2012). Wheat was cleaned with a dockage tester (CD-XT 3, Carter-Day, Minneapolis, MN, U.S.A.) before milling. Based on the methods of Posner (2000) and Seib et al. (2000), the HRS, HRW, HWW, and soft wheat samples (SRW and SWW) were tempered by adding water to adjust moisture contents to 16.5, 15.5, 15, and 14.5% (w.b.) and stored for 36, 24, 16, and 10 h, respectively. Different tempering times were used in the study because hard wheats absorb moisture more slowly than do soft wheats. The wheat samples were milled using the lab scale Bühler mill (MLU-202, Bühler Industries, Uzwil, Switzerland). For milling hard wheats and soft wheats, roll gap adjustments, dial settings, and sieve cloth adjustments followed were same as mentioned in the AACC international methods 26-21.02 and 26-31.01, respectively. Thus obtained flour samples were stored at 5 ± 1 °C, for the entire period of study.

The milled flour samples were then separated based on particle size (90, 75, and 45 μm diameter, respectively) using a Rotap sieve analyzer (model RX-29, Mentor, OH) with 170, 200, and 325 U.S. standard sieve sizes. Particles retained at each sieve were then collected and used for the surface physical and lipid content analysis.

3.2.2. Surface lipid content by staining

Lipid on flour particles was measured using dye solution binding (Sudan IV, Sigma Aldrich, St. Louis, MO) dissolved in 99% ethylene glycol (Sigma Aldrich, St. Louis, MO) at a concentration of 0.35 g/100 ml. The Chiffelle and Putt (1951) method was used for dye solution preparation. Staining of flour particles was accomplished by placing two to three drops of dye solution on a 75 x 25 mm glass slide, and a 50 x 22 mm cover glass was used to spread and cover the flour particles. Great care was taken during the sample preparation process to assure even distribution of flour particles without air bubbles. For each sample, at least 50 slides with samples were prepared to obtain a minimum of 30 particles for each sample. The slides were then analyzed under a light microscope (BX51, Olympus, Center Valley, PA), equipped with digital camera (DP 70, Olympus America Inc., Melville, NY) and the stained images were acquired at ×100. Stage automation software was used to collect the images from the sample area on the microscope slide. All viewing parameters were kept constant for all slides. Color images were captured, stored and used to differentiate between lipids (reddish-orange color) from rest of the flour particle surfaces. The color images were processed using the color feature extraction code written using MATLAB program (R2013a, MathWorks, Natick, MA). Individual particles were segmented by thresholding (Choudhary et al. 2008) followed by filtering the images using two-dimensional finite impulse response (FIR) filter. The pixels outside the individual particles were removed so that the features from the particles alone were extracted (Rani et al. 2013).

After color segmentation, the color images were then converted into binary image based on number of pixels per micrometer (1 μm = 98 pixels). The outputs, total area of the flour particle and the lipid area on a single flour particle, from all the processed images were saved as Microsoft excel files. The average total area of the particle, the lipid area on the particle, and percentage (%) of lipid area on the particle were used for the statistical analysis.

3.2.3. Morphology of flour particles

Scanning electron microscope (SEM) images were used to quantify the morphology of the wheat flour particles. From the SEM images, surface roughness of particles can be described using the fractal dimension (FD) parameter. In addition, several shape factors can be determined from a two dimensional (2-D) projection of the three dimensional particle on a plane surface because the particle is in its most mechanically stable plane and the 2-D projection of a particle represents its largest projection area of the particle (Saad et al. 2011). The SEM images were obtained using a high resolution scanning electron microscope (JSM-6700F, JEOL, Japan) operating at 2kV. The samples were first mounted on aluminum metal stubs via an electrically conductive carbon tape and then sputter coated with gold for 2 minutes (Sputter Coater 208HR, Cressington Scientific Instruments ltd., Watford, UK). Single particle images were obtained at ×500 magnification. At least 25 images of flour from each particle size and wheat class were obtained for shape factor and fractal analysis.

3.2.4. Surface topography measurements

Two surface topography measurements were made in the present study. One, FD analysis, serves as a characterizing tool to differentiate particles with high degree of roughness (higher FD values) from smoother particles (lower FD values) at the macroscopic level and

considering the entire particle. The other measurement technique, AFM was focused on the microscopic level, characterizing the areas on a single particle with different degree of roughness. This also serves as a validating tool for the FD study.

3.2.4.1. Fractal analysis

From the 2-D SEM images, the texture feature of the image (fractal dimension) was calculated using the Mapfractalcount plug-in (version 1.0) available in the ImageJ software. ImageJ is a Java-based, multithreaded, freely available, open source, platform independent, and public domain image processing analysis program developed at the National Institute of Health (NIH), USA (Rasband 2007). One way of determining the FD is by analyzing the surface intensity (SI), obtained by plotting the (*x*, *y*) pixel coordinates versus gray level of each pixel (z axis) and using either the fractal Brownian motion method, frequency domain method, and/or box counting method there on (Quevedo et al. 2002). In the box counting method, the cubic boxes of constant size (the length of the side of the box [r] is 4) are mounted into columns and intercepted with the SI, counting the number of boxes intercepted (N) for each iteration. The FD is determined from the slope of the least-squares linear regression of the logarithmic plot of number of boxes intercepted (N) versus 1/r. In the present study, the Shifting Differential Box Counting method (FD_{SDBC}) which corresponds to the 2-D grey level crumb images as proposed by Wen-Shiung et al (2003) was used as shown in Eq. 3-1, where "N" is the number of boxes and "r" is the length of the side of box.

$$FD_{SDBC} = \frac{\log(N)}{\log\left(\frac{1}{r}\right)} \qquad (3\text{-}1)$$

The FD is regarded as an index of irregularity and complexity, so a particle with higher FD will be more complex or rougher, while lower values of FD can be associated with simpler or smoother particles (Arzate-Vázquez et al. 2011).

3.2.4.2. Surface roughness quantification

The surface topography and roughness of wheat flour particles were measured using an atomic force microscope (NX-10 AFM, Park Systems Corp., Korea). For surface measurement using AFM, 90 and 45 µm flour particles from HRW and SRW was used. Altogether 100 images were analyzed for HRW and for SRW flour particles. All the AFM imaging on single particles were carried out at ambient laboratory conditions (21 ^{o}C, 55 – 60 % Relative Humidity) using non-contact mode operation. A fresh rectangular beam pre-mounted silicon cantilever (SSS-NCHR, NanoSensors^{TM}, NanoWorld AG, Switzerland), oscillating at a nominal resonant frequency of 330 kHz, was used for the wheat flour particles. The images were captured at a scan rate of 0.5 Hz for scan size of 5 x 5 µm^2 and were then analyzed using the accompanying software (XEI, version 1.8.2.Build1, Park Systems Corp., Korea).

On the basis that any surface has some distribution of height, Kiely and Bonnel (1997) proposed equations that involves parameters such as root-mean-square (RMS) roughness (R_q) and roughness average for evaluating the surface roughness. In the present study, RMS roughness (R_q) is quantified for a single particle and defined as standard deviation of the elevation (Z values) within the given area, is calculated using

$$R_q = \frac{1}{N}\sqrt{\sum_{i=1}^{N}(Z_i - Z_{ave})^2} \qquad (3\text{-}2)$$

where, Z_{ave} is the average of the Z values within the given area, Z_i is the Z value for a given point, and N is the number of points within the given area.

3.2.5. Shape factor analysis

Many of the powder physical and flow properties depend on particle morphology (Tanguy et al. 1999). In this study, the particle shape of wheat flour from different classes, at different particle size, was assessed with respect to four shape factors: form factor, roundness, aspect ratio, and compactness (Russ 1995).

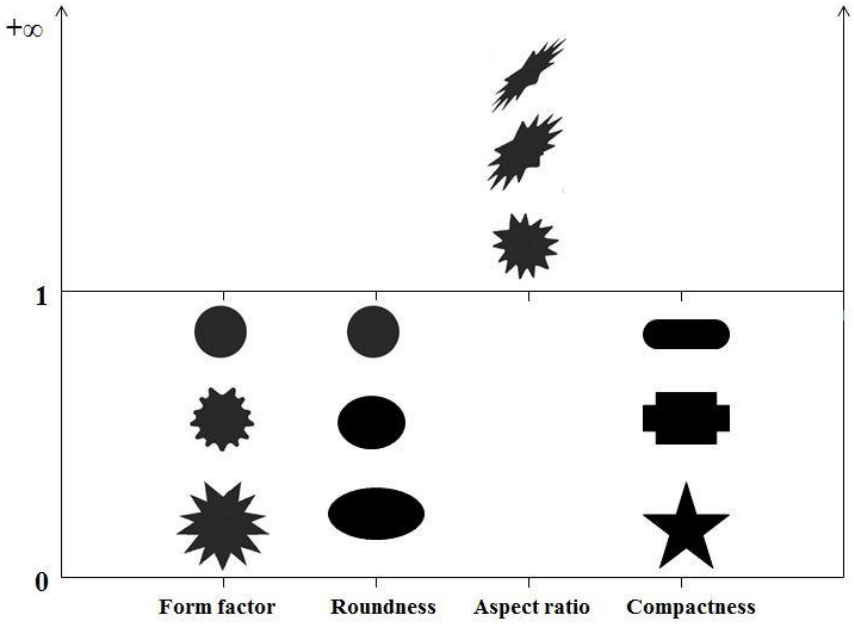

Figure 3-1: Shape factor values for regular shaped objects.

As described in Figure 3-1, values were normalized either between 0 and 1 (for form factor, roundness, and compactness) or between 1 and positive infinity (aspect ratio). The shape descriptors of wheat flour particles were calculated from the 2-dimensional SEM images using the Shape descriptors plug in (V 1.48) in the ImageJ software as follows:

i. Image pretreatment: It includes conversion of grey scale image to binary image, particle's border killing (removes the edges of the other particles that are in contact with the selected wheat flour particle/region of interest), filling of holes that may have formed due to dead

pixels, and morphological cleaning for removing the background noise from the subtracted area of interest.

ii. Generation of threshold value based on the histogram analysis results to verify if the environmental conditions were equivalent for different particles, image acquisition. Based on the histogram values generated, a threshold value was quantified to separate the particle (region of interest) from the background.

iii. Calibration step for the translation of pixel unit of the particle into metric units (1 μm = 207 pixels). This was done based on the scale obtained from the SEM image and the number of pixels were quantified for every image to make sure that 1 μm = 207 pixels.

iv. The measured particle dimensions and the processed images were saved as Microsoft excel format files and the calculated average shape factors are presented in this study.

The calculated shape factors are described below:

Form factor was measured using Eq. 3-3, from the area and the perimeter of the flour particles, and it provides a measure that describes the shape of a particle (Russ 1995). The particles that have the same area, but differing in perimeter will cause the wider range of values for form factor. The form factor of a circle is 1.

$$Form\ factor = \frac{4\ \pi Area}{Perimeter^2} \qquad (3\text{-}3)$$

Roundness describes the particle's resemblance to a circle; it was measured using Eq. 3-4 (Russ 1995). For a circle the roundness value equals 1. Roundness value decreases (< 1) when the projected shape of the particle deviates from a circle, either due to high surface roughness or elongation.

$$Roundness = \frac{4\ Area}{\pi max.diameter^2} \qquad (3\text{-}4)$$

Aspect ratio is defined as the ratio of maximum diameter over minimum diameter of the particle (Eq. 3-5) (Russ 1995). Thus the aspect ratio from this definition will be greater than or equal to 1.0.

$$Aspect\ ratio = \frac{Maximum\ dimeter}{Minimum\ diameter} \quad (3\text{-}5)$$

Compactness (Eq. 3-6) value equals 1 for a rectangular or square shaped object (Russ 1995). The compactness increases (< 1) when the particle departs from the simple form of a square or rectangle.

$$Compactness = \frac{\sqrt{\left(\frac{4}{\pi}\right)Area}}{Maximum\ diameter} \quad (3\text{-}6)$$

3.2.6. Statistical analysis

The effect of wheat class, and particle size on different surface physical and chemical characteristics of wheat flour particles were evaluated by statistical analysis. A general linear model (GLM) procedure was tested for each property to determine whether significant differences existed using a Type I (α) error rate of 0.05; if so, then a least significant difference (LSD) test at a 95% confidence interval was conducted using SAS (SAS version 9.3, SAS Institute, Inc., Cary, NC, U.S.A.).

3.3. Results and Discussions

3.3.1. Surface lipid quantification

The surface lipid of flour at all particle sizes were significantly different ($p \leq 0.05$) within each wheat class and the same trend was observed for flour particles across the wheat classes. The soft wheats (SRW and SWW) had higher lipid areas than did the hard wheat classes (HRW, HRS, and HWW) (Table 3-1). This result may be due to the significant effect of hardness on the

quantitative distribution of polar lipids on the surface of starch (Finnie et al. 2010). Greenblatt et al (1995) indicated that the polar lipids are found mainly on the surface of starch particles in soft wheat classes, but they were not present on the surface of hard wheat varieties.

However, the higher surface lipid on soft wheats is not only due to presence of polar lipids, but also from the presence of free lipids. Morrison and Laignelet (1983) showed that, the hard wheats have less free lipids compared to that of soft wheats. The other factor could be due to the presence of starch lipids, as in soft wheats the levels of damaged starch are low compared to hard wheats, the lipids might have been retained over the surface of starch portion of the particles (Pomeranz, 1988), and might have exposed during staining. In flour from hard wheat classes (HRW, HRS, and HWW), lipid increased in the range of about 0.20% with increase in particle size range selected in this study (Table 3-1). In contrast, the surface lipid content decreased with increase in particle size for the flour from soft wheat classes (SRW and SWW). This difference could be owing to association of higher levels of lipids with smaller starch granules (Raeker et al. 1998); hence the 45 µm particles, which could have smaller starch granules, might have retained lipids over them.

Table 3-1: Surface lipid content of wheat flour particles.

Wheat class	Mean particle size (µm)	Total Area (µm^2)[b]	Lipid Area (µm^2)	%Lipid Area
HRW	45	1611.39 (42.51)	17.92 (0.59)	1.11 (0.07)cC
	75	4578.15 (92.88)	64.65 (1.83)	1.41 (0.03)bD
	90	6368.85 (102.40)	98.80 (1.83)	1.55 (0.12)aD
HRS	45	1605.45 (16.64)	16.41 (0.46)	1.02 (0.03)cD
	75	4613.28 (50.60)	63.97 (2.55)	1.39 (0.05)bD
	90	6348.02 (42.50)	97.97 (2.02)	1.54 (0.03)aD
HWW	45	1609.94 (39.31)	19.01 (0.59)	1.18 (0.03)cB
	75	4538.06 (167.73)	66.50 (1.36)	1.47 (0.06)bC
	90	6327.22 (193.32)	102.64 (2.05)	1.62 (0.04)aC
SRW	45	1707.53 (90.43)	44.00 (2.64)	2.58 (0.11)aA
	75	4683.27 (104.55)	83.58 (4.11)	1.79 (0.09)bB
	90	6356.07 (47.95)	107.94 (4.81)	1.70 (0.07)cB
SWW	45	1618.77 (45.56)	41.30 (1.41)	2.55 (0.04)aA
	75	4539.61 (120.48)	89.41 (3.25)	1.97 (0.04)bA
	90	6399.54 (124.89)	117.26 (2.80)	1.83 (0.03)cA

[a] Values followed by the same lowercase letters indicates no significant difference among the particle sizes for a particular wheat class (p = 0.05, LSD). Values followed by the same upper case letter indicates no significant difference between wheat classes at a given particle size (p = 0.05, LSD). Values in parenthesis are standard deviations.
[b] Total area represents surface area of wheat flour particles obtained by imaging.

3.3.2. Fractal dimension

The images used for FD measurements from HRS and SRW wheat classes (45 µm and 90 µm) are presented in Figure 3-2. At ×500 magnification, significant irregularities on wheat flour particle were visualized. The surface texture was analyzed by the surface intensity (SI). This was obtained by plotting the (x, y) pixel coordinates versus the gray level of each pixel (z-axis) and

their respective gray level intensity maps or SI of the surface of wheat flour particles that is presented in Fig. 3-3. The surface image of 45 µm particles (HRS and SRW) appeared rougher than that of the 90 µm particles (HRS and SRW) (Fig. 3-2). Similar to visual observation, the SI map of 45 µm particles is more rugged and shows a greater range of pixel intensities (gray level) than that of 90 µm particles. The calculated FD_{SDBC} is significantly higher for 45 µm particles (2.52, 2.76) than for 90 µm particles (2.44, 2.69) for HRS and SRW respectively. The finer particles (45 µm) had higher FD values compared to larger particles (75, and 90 µm) irrespective of wheat class. This higher FD could be owing to increase in the degree of grinding in the production of finer particles, which might have led to more rugged surfaces on finer particles.

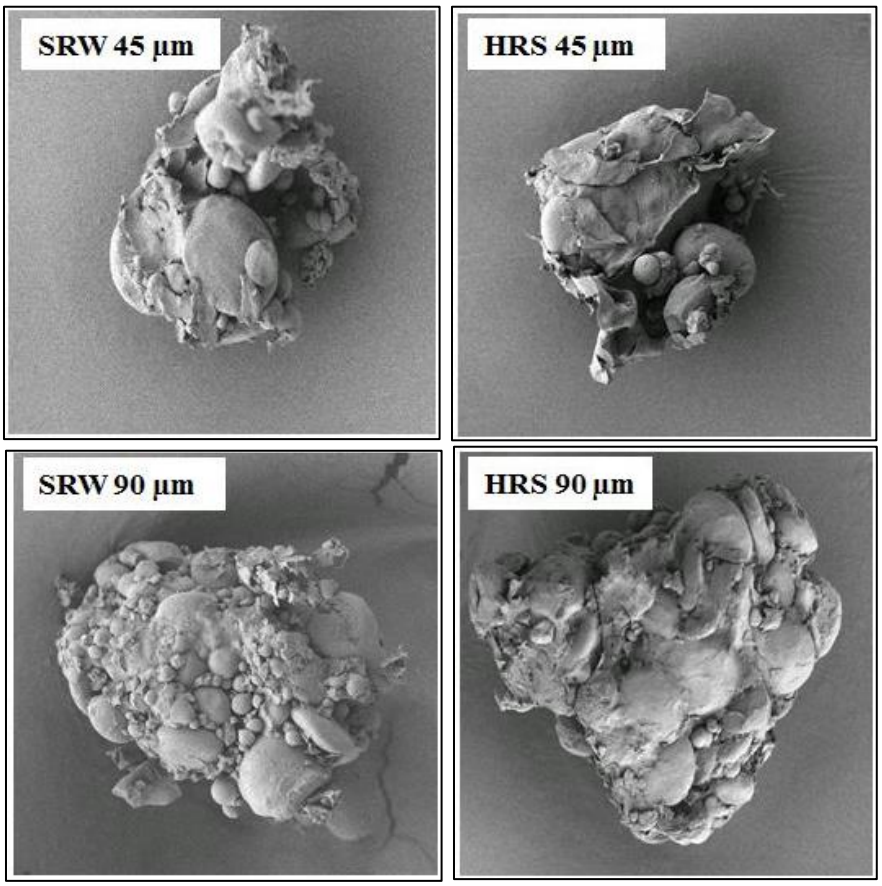

Figure 3-2: SEM images of hard and soft wheat flour particles.

Table 3-2 presents the average of FD values of wheat flour particles calculated from 25 images from each particle size and wheat class. Particle size had a significant effect on the FD values ($p = 0.05$) within each wheat class and also on FD of flour particles from different wheat classes (Table 3-2). The hard wheat flour particles appear to have rough and smooth faces, which could be owing to the presence of exposed starch granules (spherical in shape) and protein matrix, whereas soft wheat flour particles had a rough surface texture (Fig. 3-3 and 3-4).

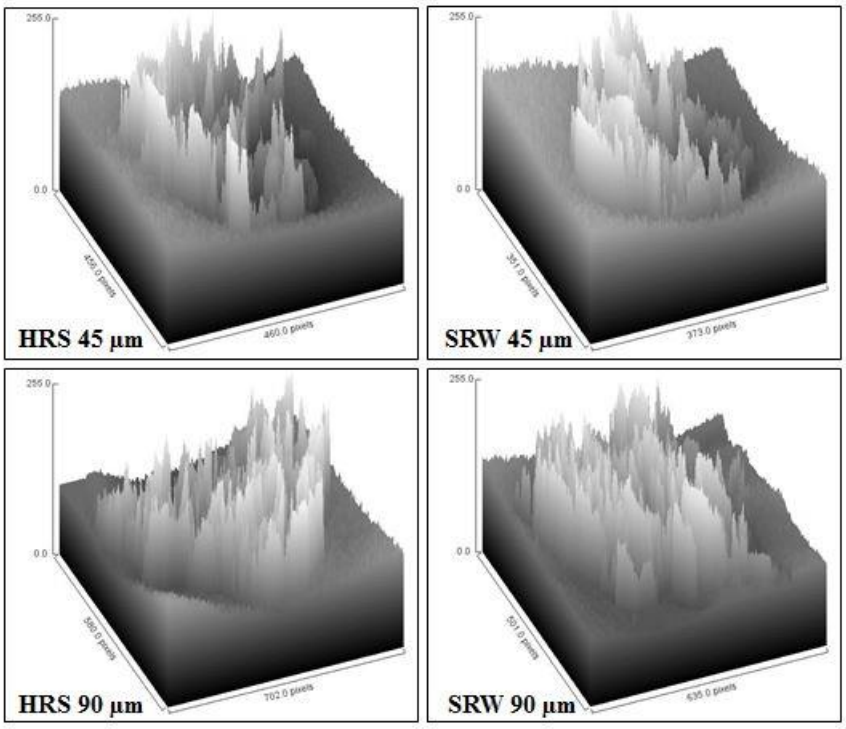

Figure 3-3: Surface intensity plots of wheat flour.

This is due to the manner in which soft wheats break down on impact or upon crushing (Simmonds 1974). Because of weaker adhesion forces, between starch and protein or between cell walls and cell contents, soft wheats are readily crushed and starch is released through cell wall rupture (Neel and Hoseney 1984b). With the release of starch granules from protein matrix, the inner cells of protein matrix create the unusual rough texture of soft wheat flour (Neel and

Hoseney 1984a). However, the cell contents and walls are coherent in hard wheats (Simmonds 1974), causing breakage at the weakest point, either through starch granules and the protein layer or along the cell wall (Neel and Hoseney 1984a).

Table 3-2: Fractal dimension from surface images of wheat flour particles.

Wheat class	Mean particle size (μm)	Fractal dimension (dimensionless)
HRW	90	2.37 (0.05)cD
	75	2.50 (0.03)bB
	45	2.55 (0.03)aC
HRS	90	2.44 (0.04)bC
	75	2.50 (0.03)aB
	45	2.52 (0.04)aD
HWW	90	2.28 (0.04)cE
	75	2.41 (0.03)bC
	45	2.50 (0.03)aD
SRW	90	2.69 (0.02)bB
	75	2.71 (0.02)bA
	45	2.76 (0.04)aB
SWW	90	2.67 (0.04)cA
	75	2.72 (0.03)bA
	45	2.78 (0.03)aA

[a] Values followed by the same lowercase letters indicates no significant difference among the particle sizes for a particular wheat class (p = 0.05, LSD). Values followed by the same upper case letter indicates no significant difference between wheat classes at a given particle size (p = 0.05, LSD). Values in parenthesis are standard deviations.

3.3.3. Validation of fractal analysis with AFM surface roughness

For validation of the fractal dimension values obtained through image analysis (Table 3-2), RMS surface roughness (R_q) was calculated for selected wheat classes at 45 and 90 μm size.

The 3-D AFM topographical roughness of HRW and SRW particles at 90 and 45 µm sieve size are shown in Fig. 3-4. Because a larger contrast in the 3-D topographical image would imply a rougher surface (Bennett 1992), it is apparent from Fig. 3.4 that the SRW 90 µm flour particle has a rougher surface. The statistical average of the R_q values for SRW-90 µm particles was rougher (456 nm) compared with HRW-90 µm (370 nm) particles. However, there was no significant difference in the surface roughness between HRW and SRW at 45 µm. In addition, the surface roughness values increased with decrease in particle size. This roughness increase might be due to increase in degree of grinding in the production of finer particles, which could have resulted in an increase in surface roughness with a reduction particle size.

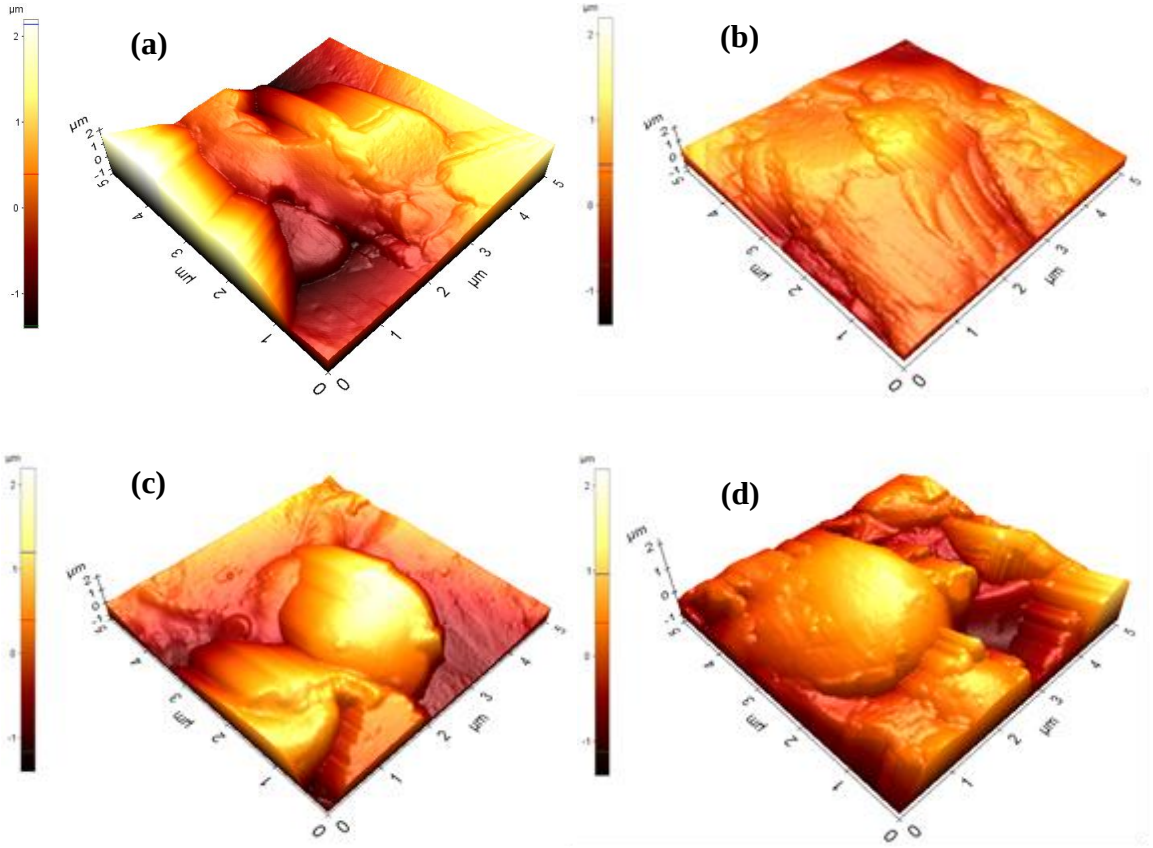

Figure 3-4: AFM 3D surface topography of (a) HRW-90 µm and (b) SRW-90 µm, (c) HRW-45 µm, and (d) SRW-45 µm particles.

It is further evident from Fig. 3-6 that, SRW (90 µm) had a higher percentage of areas (~ 41%) with surface roughness greater than 501 nm than did HRW (90 µm) (~ 21%). This higher roughness implied that a higher surface heterogeneity exists for SRW flour particles at 90 µm. The number of areas having higher surface roughness values increased with a decrease in particle size. A 50% increase in the number of areas having surface roughness values of 501– 600 nm was found for particles from SRW (Fig. 3-5). Surface roughness results obtained using the AFM were thus in good agreement with the fractal dimensions illustrated in Table 3-2, with regard to roughness differences between SRW and HRW at a defined sieve size and also in the trend of the surfaces becoming rougher with decrease in particle size. However, at 45 µm sieve size, the AFM did not reveal significant difference between SRW and HRW whereas the fractal dimension results showed significant difference between them. This difference could be because the calculation of the FD is from the contour of a 2D projection of the particle. Thus, the stable position of a particle at rest could influence the calculated FD values. Because the AFM results corroborate the calculated FD values, an image analysis approach would an inexpensive way of characterizing the surface roughness of flour particles. Surface roughness influences the friability, adhesion, flow, permeability, blend homogeneity, and packing of flour particles. Based on the final use and purpose, surface roughness characterization would help to optimize the processing conditions. For example, SRW wheat flour would require a higher mixing time to achieve blend uniformity compared with HRW flour.

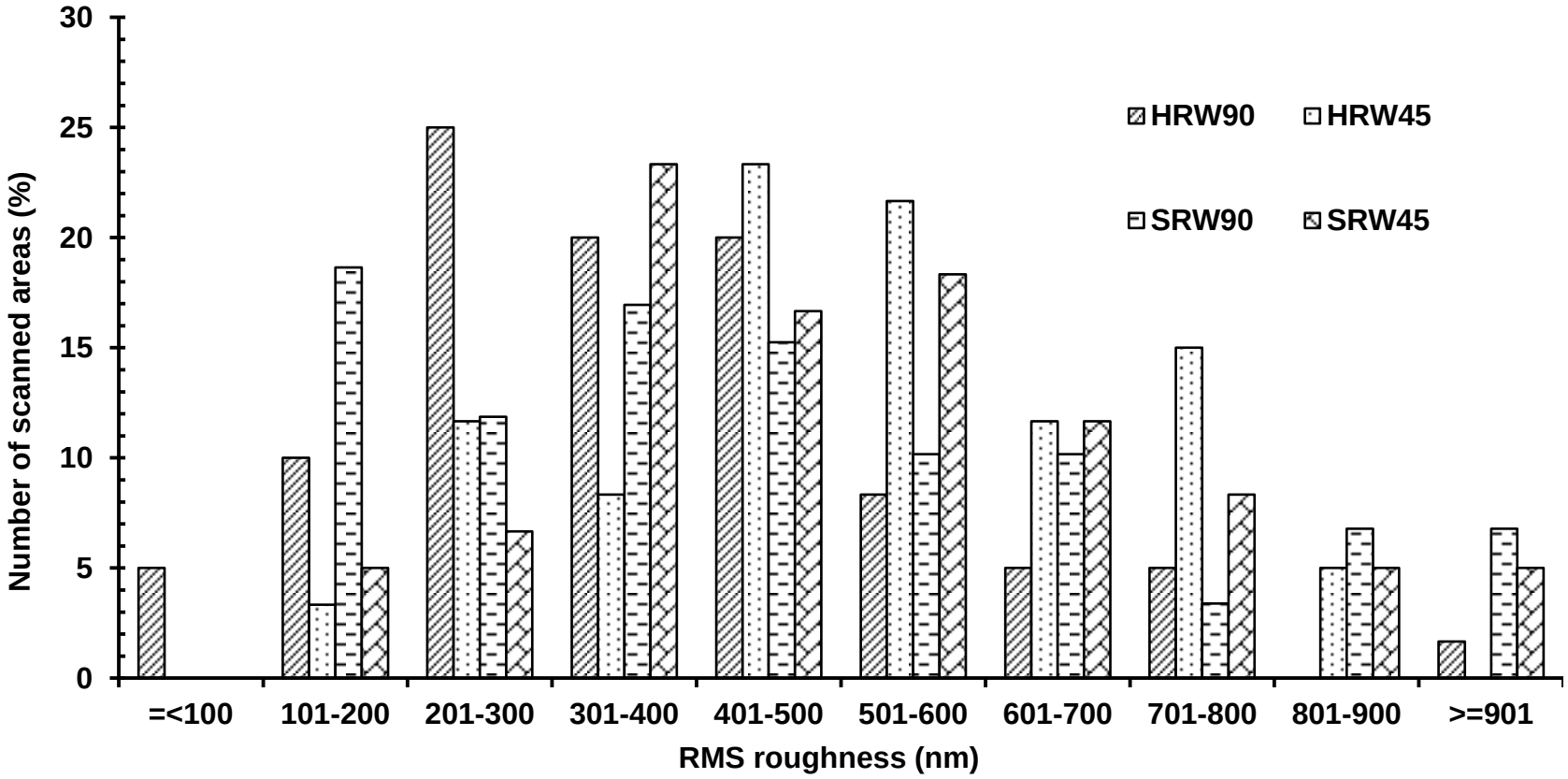

Figure 3-5: RMS roughness for HRW and SRW particles at 90 and 45 µm sizes.

3.3.4. Particle shape descriptors

Preliminary experiments (results not reported) quantified, the number of particles needed for accurate determination of shape descriptor at each particle size. Based on those results, 25 single particle images were selected to measure shape descriptors. Because higher magnification (×500) was used in this study, great care was taken in selecting the individual particles based on size, to avoid sampling variability. The four selected shape factors (form factor, roundness, aspect ratio, and compactness) were measured and calculated from 2D projection of the particles.

The differences in the shape descriptors were not statistically significant (Table 3-3). Saad et al (2011) carried out a similar study on shape factors (elongation, circularity, compactness, and convexity) for flour particles (diameter <125 μm, 125-160 μm, and > 160 μm) and for semolina fractions (diameter < 315 μm and >315 μm) and reported a similar observation. They concluded that the wider distribution of shape factor values was owing to the variability in shape of the particles in the bulk powder and also might be owing to the analytical procedure of shape measurement that employs 2D projections. In this study, we selected particles within narrow size range (45–90 μm), and selection of particles was done with greater care and at higher magnification (×500). For compactness, the results obtained in this study (0.80–0.85 with standard deviation values ranging from 0.07 to 0.09) were comparable to the results for compactness (0.70 with standard deviation value of 0.13) obtained by Saad et al. (2011).

Table 3-3: Shape descriptor values for wheat flour particles.

Wheat class	Mean particle size (µm)	Form factor	Roundness	Compactness	Aspect Ratio
HRW	45	0.70 (0.07)	0.71 (0.09)	0.84 (0.07)	1.45 (0.19)
	75	0.71 (0.08)	0.67 (0.13)	0.82 (0.08)	1.57 (0.49)
	90	0.70 (0.07)	0.69 (0.12)	0.83 (0.07)	1.50 (0.27)
HRS	45	0.66 (0.08)	0.66 (0.13)	0.81 (0.09)	1.57 (0.36)
	75	0.68 (0.07)	0.73 (0.12)	0.85 (0.07)	1.42 (0.25)
	90	0.65 (0.07)	0.66 (0.13)	0.81 (0.08)	1.57 (0.33)
HWW	45	0.72 (0.07)	0.71 (0.13)	0.84 (0.08)	1.45 (0.31)
	75	0.71 (0.08)	0.68 (0.12)	0.82 (0.07)	1.52 (0.30)
	90	0.69 (0.06)	0.65 (0.12)	0.80 (0.08)	1.60 (0.32)
SRW	45	0.64 (0.08)	0.72 (0.11)	0.84 (0.07)	1.43 (0.25)
	75	0.63 (0.10)	0.69 (0.14)	0.83 (0.08)	1.50 (0.34)
	90	0.65 (0.08)	0.66 (0.12)	0.81 (0.07)	1.56 (0.31)
SWW	45	0.66 (0.07)	0.72 (0.11)	0.85 (0.07)	1.42 (0.22)
	75	0.68 (0.07)	0.74 (0.11)	0.86 (0.06)	1.38 (0.21)
	90	0.64 (0.07)	0.73 (0.12)	0.85 (0.07)	1.41 (0.36)

The form factor values (0.63–0.72) indicated that the wheat flour particles, from all wheat classes, did not have a regular shape. The roundness values (0.65–0.74) confirmed the irregularity of the particles (Table 3-3). A higher degree of surface roughness and fragmentation of endosperm into aspherical components resulted in lower form factor and roundness values. Starch particles are more spherical than the protein fragments. However, protein fragments

attached to starch particles might have reduced the roundness values. The aspect ratio of the wheat flour particles ranged from 1.38–1.60 (Table 3-3), which indicated that the difference between maximum and minimum diameter of the particle was not high. The average aspect ratio values and their standard deviations indicated that most of the particles were irregular and aspherical.

Saad et al. (2011) concluded that the lower level of distortion in the shape of smaller flour particles was owing to the presence of exposed starch granules (which are mostly convex shaped) when compared with larger particles. In many published studies, researchers made the assumption that granular particles are spherical (Andrzejczak and Wodzinski 1994; Li et al. 2003) and calculated sifter efficiencies based on this assumption. But in general, the flour particles are not spherical, which influences the production process conditions. Particle irregularity increases the angle of repose, coefficient of friction, and angle of internal friction, which will affect the flow of flour through any processing and handling systems. For example, in a flour sifter irregularity of particles could reduce the sifting rate, load on sifters, and passage of particles through the screens. In addition, irregularity of particles increases the tendency to break into fragments owing to abrasion. A size-based segregation, owing to irregular shaped particles, could affect the overall quality of flour.

3.4. Conclusions

This study quantified the surface morphology and chemical (lipid) content of wheat flour particles from different wheat classes. The surface characteristics, particle morphology, and surface roughness data provide the basis for understanding particle cohesion and the movement of flour particles during the sifting and purification processes. The surface lipid content increased with particle size in hard wheat flours, but decreased in soft wheat flours. The surface lipid

content ranged from 1.02 to 1.18 and from 2.55 to 2.58% (% of total area) for the 45 μm flour particles in hard and soft wheat flours, respectively. Surface lipid content increases the cohesion between flour particles and could limit the loading rate in sifters. The data indicate that soft wheat flours will be cohesive and could increase the stickiness and agglomeration, limiting the flowability characteristics. For the 90 μm particles, the surface lipid levels ranged from 1.54 to 1.62 and 1.70 to 1.83% (% of total area) in hard and soft wheat flours, respectively. The morphology of particles including FD and shape factors (form factor, roundness, aspect ratio, and compactness) was calculated by using image analysis from the 2D projection of particles. The FD values ranged from 2.67 to 2.78 and 2.28 to 2.55 for soft and hard wheat flours, respectively. The surface roughness of HRW and SRW flour particles was also measured using AFM. The results confirmed the higher surface roughness characteristics of soft wheat flour particles compared with flour particles from hard wheat. Percolation of smaller particles through bigger particles is an important phenomenon during size-based separation processes. Surface roughness could hinder percolation owing to interlocking of soft wheat flour particles. The protein fragments attached to the spherical starch particles resulted in aspherical flour particles. This irregularity increased the interparticle friction and influenced the passage of flour through sieves. The differences in surface characteristics could lead to segregation or agglomeration of flour particles that could affect the product quality and uniformity.

3.5. References

AACC International. Approved Methods of Analysis, 11th Ed. Method 26-21.02. Experimental Milling-Bühler Method for Hard Wheat. Approved October 12, 1988. Method 26-31.01. Experimental Milling-Bühler Method for Soft Wheat Straight-Grade Flour. Approved October 12, 1988. Available online only. AACC: St. Paul, MN.

Allen, S., Davies, M. C., Roberts, C. J., Tendler, S. J., and Williams, P. M. 1997. Atomic force microscopy in analytical biotechnology. Trends Biotechnol. 15:101–105.

Andrzejczak, P., and Wodzinski, P. 1994. Model of screening in the layer. Powder Handling and Processing 6:263–272.

Arzate-Vázquez, I., Chanona-Pérez, J. J., Perea-Flores, M. J., CalderónDomínguez, G., Moreno-Armendáriz, M. A., Calvo, H., GodoyCalderón, S., Quevedo, R., and Gutiérrez-López, G. 2011. Image processing applied to classification of avocado variety Hass (*Persea americana Mill*.) during the ripening process. Food Bioprocess Tech. 4:1307–1313.

ASABE. 2012. S 352.2: Moisture measurement-unground grain and seeds. In: ASAE Standards. St. Joseph, MI.

Bennett, M. J. 1992. Recent developments in surface roughness characterization. Meas. Sci. Technol. 3:1119–1127.

Campbell, G. M., Fang, C., and Muhamad, I. I. 2007. On predicting roller milling performance: Part VI. Effect of kernel hardness and shape on the particle size distribution from first break milling of wheat. Food Bioprod Process. 85:7–23.

CFR. 2013. 21 CFR 137.105: Requirements for specific standardized cereal flours and related products. Code of Federal Regulations, Washington, D.C.

Chiffelle, T. L., and Putt, F. 1951. Propylene and ethylene glycol as solvents for Sudan IV and Sudan black B. Stain Technol. 26:51–56.

Choudhary, R., Paliwal, J., and Jayas, D. S. 2008. Classification of cereal grains using wavelet, morphological, colour, and textural features of non-touching kernel images. Biosyst Eng. 99:330–337.

Finnie, S. M., Jeanuette, R., Morris, C. F., and Faubion, J. M. 2010. Variation in polar lipid composition among near isogenic wheat lines possessing different puroindoline haplotypes. J. Cereal Sci. 51:66–72.

Flemmer, R. L. C., Pickett, J., and Clark, N. N. 1993. An experimental study on the effect of particle shape on fluidization behavior. Powder Technol. 77:123–133.

Fraige, F. Y., Langston, P. A., and Chen, G. Z. 2008. Distinct element modelling of cubic particle packing and flow. Powder Technol. 186:224–240.

Greenblatt, G. A., Bettge, A. D., and Morris, C. F. 1995. The relationship among endosperm texture, friabilin occurrence, and bound polar lipids on wheat starch. Cereal Chem. 72:172–176.

Jensen, R. P., Bosscher, P. J., Plesha, M. E., and Edil, T. B. 1999. DEM simulation of granular media–structure interface: effects of surface roughness and particle shape. Int. J. Numer. Anal Met. 23:531–547.

Kiely, J. D., and Bonnell, D. A., 1997. Quantification of topographic structure by scanning probe microscopy. J. Vac. Sci. Technol. 15:1483–1493.

Kodam, M., Bharadwaj. R., Curtis, J., Hancock, B., and Wassgren, C. 2009. Force model considerations for glued-sphere discrete element method simulations. Chemical Eng. Sci. 64:3466–3475.

Landillon, V., Cassan, D., Morel, M. H., and Cuq, B. 2008. Flowability, cohesive, and granulation properties of wheat powders. J. Food Eng. 86:178–193.

Li, J., Webb, C., Pandiella, S. S., and Campbell, G. M. 2003. Discrete particle motion on sieves-a numerical study using the DEM simulation. Powder Technol. 133:190–202.

Liu, L. X., and Litster, J. D. 1991. The effect of particle shape on the spouting properties of non-spherical particles. Powder Technol. 66:59–67.

Morrison, W. R., and Laignelet, B. 1983. An Improved Colorimetric Procedure for Determining Apparent and Total Amylose in Cereal and Other Starches. J. Cereal Sci. 1:9–20.

Neel, D. V., and Hoseney, R. C. 1984a. Sieving characteristics of soft and hard wheat flours. Cereal Chem. 61:259–261.

Neel, D. V., and Hoseney, R. C. 1984b. Factors affecting flowability of hard and soft wheat flours. Cereal Chem. 61:262–266.

Pomeranz, Y. 1988. Composition and functionality of wheat flour components. Pages 219–370 in: Wheat Chemistry and Technology. Y. Pomeranz, ed. Am. Assoc. Cereal Chem., St. Paul, MN.

Posner, E. S. 2000. Wheat processing. Pages 9–30 in: Handbook of Cereal Science and Technology. K. Kulp and J. G. Ponter, eds. CRC press: New York, NY.

Quevedo, R., Carlos, L. G., Aguilera, J. M., and Cadoche, L. 2002. Description of food surfaces and microstructural changes using fractal image texture analysis. J. Food Eng. 53:361–371.

Raeker, M. O., Gaines, C. S., Finney P. L., and Donelson, T. 1998. Granule size distribution and chemical composition of starches from 12 soft wheat cultivars. Cereal Chem 75:721–728.

Rani, P. R., Chelladurai, V., Jayas, D. S., White, N. D. G., and Kavitha-Abirami, C. V. 2013. Storage studies on pinto beans under different moisture contents and temperature regimes. J. Stored Prod. Res. 52:78–85.

Rasband, W. S. 2007. ImageJ Bethesda, Maryland. U.S. National Institute of Health. http://rsb.info.nih.gov/ij/.

Roberts, T. R., and Beddow, J. K. 1968. Some effects of particle shape and size upon blinding during sieving. Powder Technol. 2:121–124.

Russ, J.C. 1995. The image processing handbook, second ed. CRC Press, London.

Saad, M., Sadoudi, A., Rondet, E., and Cuq, B. 2011. Morphological characterization of wheat powders, how to characterize the shape of particles. J. Food Eng. 102:293–301.

Seib, P. A., Liang, X., Guan, F., Liang, Y. T., and Yang, H. C. 2000. Comparison of Asian noodles from some hard white and hard red wheat flours. Cereal Chem. 77:816–822.

Simmonds, D. H. 1974. Chemical basis of hardness and vitreosity in the wheat kernel. Bakers Dig. 48:16.

Tanguy, P. A., Thibault, F., Dubois, C., and Ait-Kadi, A. 1999. Mixing hydrodynamics in a double planetary mixer. Chem. Eng. Res. Des. 77:318–324.

Wen-Shiung, C., Shang-Yuan, Y., and Chih-Ming, H. 2003. Two algorithms to estimate fractal dimension of gray-level images. Opt. Eng. 42:2452–2464.

Wu, C. Y., and Cocks, A. C. F. 2006. Numerical and experimental investigations of the flow of powder into a confined space. Mech. Mater 38:304–324.

Xu, C., and Zhu, J. 2006. Parametric study of fine particle fluidization under mechanical vibration. Powder Technol. 161:135–144.

Chapter 4 - Shear Flow Properties of Wheat Flour

Abstract

Size based fractionation of flour particles is an important process in wheat flour milling. Inter particle cohesion could affect the dynamic separation process and result in loss in throughput. This study quantifies the effect of particle characteristics that includes physical and chemical on the shear flow properties of wheat flour. The specific aim of this study is to investigate the effect of particle size on the shear flow properties of wheat flour. The values of cohesion and flow function obtained for the three moisture contents (10%, 12%, and 14%), three particle sizes (75-106, 45-75, and <45 μm), three sifter loads (0.5, 1.0, and 1.0 kPa) were significantly different ($P < 0.05$). The triggering moisture content and particle size where the flowability shifts from 'easy flowing' to 'very cohesive' were found to be 14% (wet basis) and < 45 μm, respectively. The high correlation observed between the chemical composition (damaged starch, protein, and fat) on the physical (bulk, tapped, and true densities) and flow properties (cohesion, flow function, and angle of internal friction (AIF)) demonstrates that chemical composition significantly contributes towards the differences in cohesion and flowability wheat flours.

4.1. Background

The wheat flour manufacturing process involves multiple size reduction and size based fractionation steps. Compositional quality of wheat flour depends on the wheat type (soft or hard), color (red or white), growing season (spring or winter), and milling process specifications (tempering moisture, degree of milling, roll disposition and roll differential). Wheat flour is a raw material for wide variety of food applications. The need for quality final product has driven

the researchers to carry out studies on the effects of differences in particle size and composition on the end product quality (Wang and Flores, 2000). But, most of the studies focused on the technological aspects towards food applications and there is a lack of fundamental understanding on the engineering properties of wheat flour.

Many published studies have stressed the need for understanding the flowability of wheat flours during storage and processing, due to its heterogeneity and anisotropic nature (Teunou et al., 1999). Due to the inherent characteristics, wheat flour, in general, has been described as a ‘‘complex” powder (Landillon et al., 2008). Several inherent characteristics of wheat flour have been correlated to flow properties, such as cohesiveness (Baruch, 1974; Neel and Hoseney, 1984a, 1984b). Kamath et al. (1994) reported that the increase in moisture content did not significantly influence the cohesive property of wheat flour. They also demonstrated that the storage times (12 and 24 h) did not have a significant effect on the flow properties of wheat flour at 11.8% (dry basis) moisture content. But, the wheat flour is inherently cohesive as reported by Teunou et al. (1999). This study, by comparing the Jenike’s flow index value of wheat flour with milk, tea, and whey powders reported that wheat flour is ‘cohesive powder with some difficult flow’. Similar studies, conducted under varying stress conditions, reported that an increase in moisture content resulted in increased cohesiveness, wall friction, and the effective angle of wall friction (Teunou et al., 1999; Teunou and Fitzpatrick, 1999; Iqbal and Fitzpatrick, 1999).

Particle size is an important factor that increases the interparticulate cohesive forces. The median particle size of hard and soft wheat flours is 75 and 45 μm, respectively (Neel and Hoseney, 1984a). The presence of smaller particles (45 μm) in greater number increases the cohesiveness in soft wheat flours (Neel and Hoseney, 1984b). In the same study, even though the particle sizes of wheat flours from all classes made similar with the standardized milling process

the measured flow properties were found to be different. Bian et al. (2015) reported that the soft wheat flour is cohesive than the hard wheat flour. Higher cohesiveness in soft wheat flours could be due to the presence of surface fat, higher surface roughness, and low density (Neel and Hoseney, 1984b; Kuakpetoon et al., 2001; Siliveru et al., 2016). The effect of chemical composition on the cohesive properties of wheat flour is not a well understood phenomenon. The difference in wheat flour composition originates from their differences in class, roller milling specifications and the fractionation process (Wang and Flores, 2000).

During sieving, the stresses acting on wheat flour leads to sieve blinding and agglomeration of flour in sifter screens, causing changes in bulk density. In addition, with the continuous movement of sifter stack (vibrational and centrifugal action), the fluctuation in density of flour changes the inter-particulate interactions. For example the size based separation output reduces during sieving soft wheat flour compared to that of hard wheat flour. According to Hareland (1994) soft wheat flours do not pass freely through the sieve openings, whereas hard wheat flours pass without adhering to the sieve mesh.

The specific aim of this study is to compare the cohesive properties of wheat flours as influenced by chemical composition with other factors remaining constant. Thus, the objective of the present work is to investigate the physical and shear properties of wheat flours from the five different wheat classes at varying moisture content, particle size and load conditions.

4.2. Materials and Methods

4.2.1. Sample preparation

The median particle size distribution of hard wheat and soft wheat flours are 75 and 45 µm, respectively (Neel and Hoseney, 1984a). To measure the variation in cohesion values with respect to differences in particle sizes, wheat flours were obtained at three particle sizes (75-106,

45-75, and <45 μm diameter, respectively) using an Alpine jet sieve analyzer (model e 200 LS, Hosokawa Alpine Ag & Co, Augsburg, Germany) with 140, 200, and 325 U.S. standard sieve sizes. To address the variation in moisture content, the flour at each particle size were then conditioned to 10, 12, and 14% m.c (w.b.). Higher moisture contents of 12 and 14 (% w.b.) were achieved by placing the samples in a relative humidity chamber maintained at 50-55% relative humidity (r.h) and 25 °C for 4-5 hr. The lower moisture content of 10 (% w.b.) was achieved by drying the samples at room temperature. The moisture content of the flours was determined using the AOAC standard 925.10 (AOAC International, 2006) on drying 2-3 g of the sample in a hot air oven at 130 °C for 60 min. The final moisture contents were within ± 0.25% (w.b.) of the target moisture content.

4.2.2. Chemical composition analyses

Proximate analysis and damaged starch content determination was performed on the flour samples from an external laboratory. The analysis methods used included AACC 46-30.01 for crude protein, AACC 30-25.01 for crude fat, AACC 32-10.01 for crude fiber, AACC 08-01.01 for ash content, AACC 76-30.02 for damaged starch content (AACC International, 1999), and AOAC 996.11 for total starch content (AOAC International, 2006).

4.2.3. Density measurements

The bulk density of the samples was measured using a Winchester cup arrangement (Seedburo Equipment Co., Des Plaines, IL, USA). The samples were made to fall from a hopper into a one pint cup (4.732×10^{-4} m^3) from a height of 10 cm, to maintain a natural flow into the cup. The cup was allowed to fill completely until excess sample began to overflow. The excess

sample was scrapped off by making a zigzag motion with a scrapper. The bulk density was then calculated from the weight of the flour and volume of the flour in the cup of known volume.

The tapped density, or compacted bulk density was measured using an auto tap density analyzer (Quantachrome Instruments, FL, U.S.A.). A cylinder of known volume was filled with flour sample, and the cylinder was then tapped 750 times (260 taps min^{-1}). The tapped density was calculated from the volume of flour after tapping and weight of the sample.

The true density of the flour samples was measured using a gas pycnometer (AccuPync II 1340, Micromeritics, Norcross, GA, U.S.A). Helium was used to fill the chamber containing the sample to determine the volume occupied by the particles. The true density was calculated from the weight and volume occupied by the solid particles.

4.2.4. Shear flow tests

The FT4 powder rheometer (Freeman Technologies, Gloucestershire, UK) was used to evaluate the shear flow properties. To address the variations in sifter load, shear flow properties were measured at different applied pressures (0.5, 1.0, and 1.5 kPa) which were calculated based on the flour retained on 1 m^2 sifter screen area. The cohesion (*C*), major principal stress (σ_1), unconfined yield strength (σ_c), and angle of internal friction (ø) were measured and these properties are extensively being used to design hoppers, silos, and becoming increasingly useful for general characterization of granular materials under different processing conditions (Bruni et al., 2007).

Detailed descriptions of the powder rheometer and shear cell tests can be found in Freeman (2007), Leturia et al. (2014), and Bian et al. (2015). The powder rheometer system consists of a vertical glass sample container (50 mm internal diameter and 85 mL volume). During the measurements, the powder sample was first conditioned by a rotating blade (48 mm

diameter and 10 mm height), which passes through the sample up and down, in clockwise and in anti-clockwise direction, to achieve a homogenous reproducible initial state, and then slowly pre-compacted under a determined normal load with a vented piston. After the conditioning, pre-consolidation steps, the sample was pre-sheared to achieve a 'critically consolidated state'. The shear stress (τ) necessary to cause failure and create flow was measured on lowering the normal stress (σ). The sequence of pre-shear/shear is programmed based on the applied pressures and the sequence is repeated for 5 times at decreasing normal loads and the curve thus obtained is called the 'yield loci'. Mohr circle analysis was then applied on the relationship between the normal and shear stress (yield loci) to calculate the shear properties (Leturia et al., 2014; Bian et al., 2015). Cohesive intercept stress and angle of internal friction were calculated using the Mohr-Coulomb equation (eqn. 1), by linear regression

$$\tau = c + \sigma \tan(ø) \qquad (4\text{-}1)$$

where τ = shear stress (kPa), c = cohesion (kPa), σ = normal stress (kPa), and $ø$ = angle of internal friction (°).

At each pre-shear load, the unconfined yield strength (UYS, σ_c) and major principal stress (MPS, σ_1) were calculated from the two Mohr's circles which were drawn tangent to the yield locus (Fitzpatrick et al., 2004). To characterize flowability, Jenike (1964) proposed the ratio of major principal stress (MPS) and the unconfined yield strength (UYS) called the flowability index (FF):

$$FF = \frac{\sigma_1}{\sigma_C} \qquad (4\text{-}2)$$

4.2.5. Data analysis

Density measurements and shear flow tests were performed in triplicate. The results were analyzed by ANOVA and compared by Fisher's test at a significance level of 0.05. The relationship between measured parameters was assessed by Pearson's test (*, ** significance levels at $P < 0.05$ and $P < 0.01$, respectively). A general linear model procedure was tested for shear properties to determine whether significant differences existed using a type I (α) error rate of 0.05; if so, then a least significance difference test at a 95% confidence interval was conducted with SAS software (SAS version 9.3, SAS Institute, Cary, NC, U.S.A.).

4.3. Results and Discussion

4.3.1. Chemical characteristics of flour fractions

The soft wheat flour fractions (SRW and SWW) have lower protein, fat, ash, and damaged starch contents than hard wheat flour fractions (HRW, HWW, and HRS) (Table 4-1). For hard wheat flour fractions, particle sizes were negatively correlated with protein (r = -0.94), ash (r = -0.94), damaged starch contents (r = -0.86), and positively correlated with fat (r = 0.99) and fiber contents (r = 0.84). For soft wheat flour fractions, particle sizes were correlated negatively with damaged starch (r = -0.90), and positively correlated with protein (r = 0.94), ash (r = 0.94), fat (r = 0.99), and fiber contents (r = 0.96). These results were in agreement with Wang and Flores (2000), and Kuakpetoon et al. (2001), who reported that a similar relationship between particle size with ash and protein content of wheat flour. In soft wheat flours, the <45 μm particle fractions had lower protein content than other fractions, which indicated that the small spherical B-type starch granules (<10 μm) and large lenticular A-type granules (25 – 40 μm) were readily released from the protein matrix during grinding due to weaker adhesion forces between starch and protein (Neel and Hoseney, 1984b). Whereas, an opposite trend was

observed for hard wheats due to coherent nature of cell walls and cell contents causing breakage at the weakest point either through starch granules or along the cell walls, creating smaller fractions (<45 µm) of starch granules that were embedded in protein matrix (Simmonds, 1974; Neel and Hoseney, 1984b). For both hard and soft wheat flour fractions a negative correlation was observed between the particle size and damaged starch content, similar to the findings by Wang and Flores (2000) and Kuakpetoon et al. (2001). Flour fractions from hard wheats presented significantly higher damaged starch content than fractions from soft wheat (Table 4-1). Hard and soft wheat differ in the ease and manner in which they break during crushing (Simmonds, 1974). Due to weaker adhesion forces between starch and protein matrices, the starch granules are readily released in soft wheat, whereas stronger adhesion forces results in higher starch damage in hard wheats (Neel and Hoseney, 1984b). In soft wheat flours, the <45 µm fractions had higher fat content than other fractions (Table 4-1) due to presence of free lipids (Morrison and Laignelet, 1983) and also due to the association of higher levels of lipids with smaller starch granules (Raeker et al., 1998). The presence of higher fat in soft wheats could be one of the reasons for lower sieve throughput, as it has been proven to hinder the flow characteristics (Neel and Hoseney, 1984b; Fitzpatrick et al., 2004). The presence of higher levels of fat on the surface provides the necessary sites on individual flour particle surfaces for the formation of liquid bridges between the particles (Neel and Hoseney, 1984b).

Table 4-1: Chemical characteristics of the flour fractions.

	Particle size (µm)	Protein content (%)	Fat content (%)	Ash content (%)	Damaged starch (%)	Total starch (%)	Fiber content (%)
HRW	<45	12.64	0.87	0.71	12.33	64.20	0.45
	45-75	10.16	1.15	0.56	6.23	68.40	0.96
	75-106	9.50	1.38	0.52	4.92	69.20	1.03
HWW	<45	11.99	0.69	0.58	21.61	65.60	0.48
	45-75	10.88	0.88	0.47	12.38	67.65	0.83
	75-106	9.95	1.13	0.40	8.40	67.65	1.27
HRS	<45	13.03	0.82	0.54	16.70	67.90	0.98
	45-75	11.82	0.91	0.49	8.90	69.00	1.36
	75-106	11.22	1.15	0.42	6.24	69.30	1.82
SRW	<45	8.21	1.61	0.37	8.28	78.70	0.62
	45-75	8.85	1.39	0.41	4.71	78.95	1.02
	75-106	10.15	1.28	0.48	3.30	79.75	1.09
SWW	<45	4.45	1.10	0.27	4.94	68.90	1.03
	45-75	6.51	0.74	0.30	2.50	71.10	1.21
	75-106	7.01	0.44	0.34	1.85	72.50	1.57

[*] Content of protein, fat, ash, damaged starch, total starch, and fiber content on 12% moisture content (% wet basis); Mean values of duplicates with variance less than 3%.

4.3.2. Density of wheat flours

The bulk density for wheat flour samples decreased in the range of about 10 kg m^{-3} with increase in moisture from 10 to 14% (w.b.) for the samples from all the particle sizes and all the five wheat classes (Fig. 4-1). A linear negative relationship of bulk density to moisture content (with r = -0.98) has been found. Patwa et al. (2014) observed a similar trend of decrease in bulk density for wheat flour samples (particle size ranging from 2 to 400 µm) when moisture content increased from 12 to 14% (w.b.). However, in the same study, they reported an increase in bulk density, with further increase in moisture content from 14 to 16% (w.b.). For different millet

flours, Subramanian and Viswanathan (2007) found that the bulk density increased with increase in moisture content. This indicates that, the bulk density of a powder is not dependent on the moisture content alone, but also dependent on the size and shape of the particles (Brown and Richards, 1970). At lower moisture contents, size, shape and chemical composition could play a bigger role on the wheat particle properties.

The bulk density measurements shown in Fig. 4-1 indicate that the particle size has significant influence ($P < 0.05$) on the bulk density of the wheat flour samples. The finer flour particles (<45 µm) had lower bulk density compared to that of other two particles sizes (45-75, 75-106 µm) for the flours from all the wheat classes and at different moisture contents (Fig. 4-1). This is due to the fact that, the finer particles pack more loosely than larger granules (Brown and Richards, 1970), due to differences in surface roughness and shape factors. Siliveru et al. (2016) noted that the finer particles are comparatively rough and have a wide range of shapes when compared to larger particles. The other possible reason for lower bulk density of fine particles (<45 µm) is that they are mostly protein fractions and the protein has lower density than starch granules (Kuakpetoon et al., 2001)

In this study, it was confirmed that the bulk density of hard wheat flours is significantly different from soft wheat flours ($P < 0.05$) as stated by Bian et al. (2015). The hard wheat flours occupied most of the available volume whereas soft wheat flours formed an open structure with greater proportion of void spaces (Bian et al., 2015). However, within the hard wheat classes (i.e. between HRW, HRS, and HWW) and soft wheat classes (i.e. between SRW and SWW) no significant difference was observed in the bulk densities (Fig. 4-1), due to similarities in hardness and breakage pattern during milling.

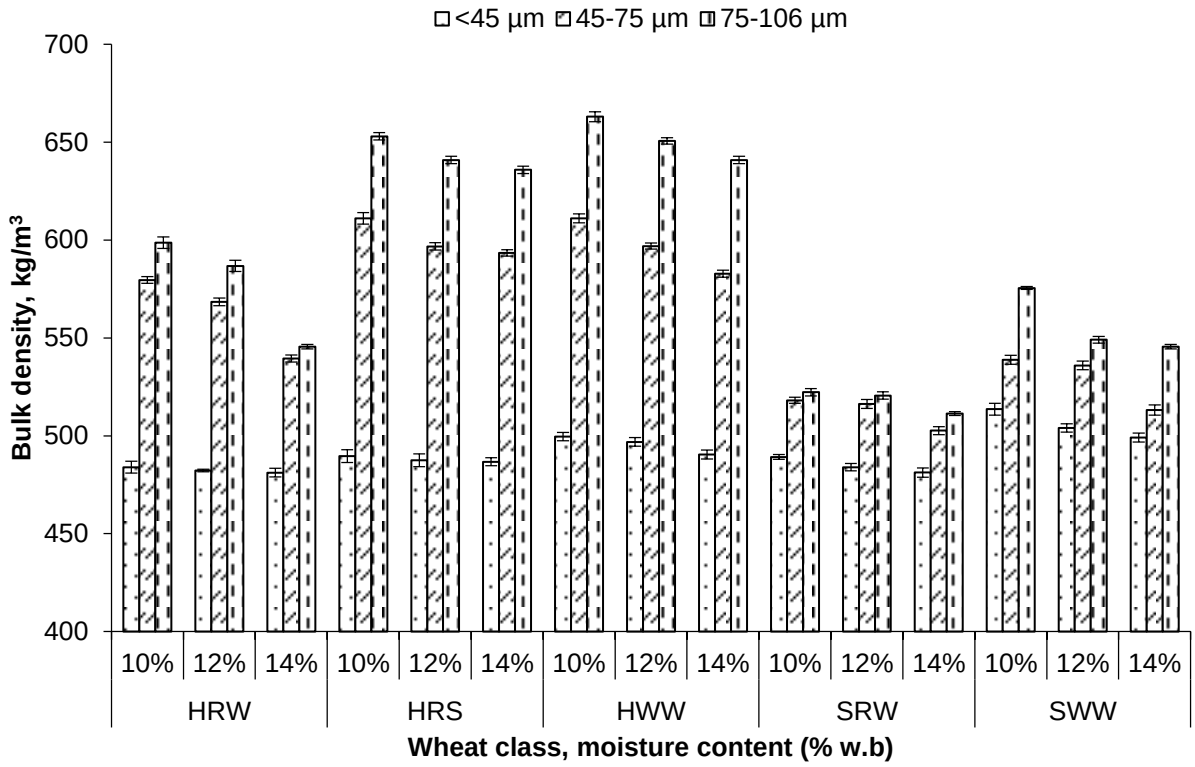

Figure 4-1: Bulk density of wheat flour samples at three moisture levels and three particle sizes.

Note: Error bars represent the standard deviations.

A positive correlation (r = 0.96) has been found between the tapped density and moisture content. For all the particle sizes, the tapped density significantly increased with increase in moisture content (Fig. 4-2) and this could be due to the fact that, interparticulate void spaces are being occupied by the particles and the collapse of mechanical interlocking during tapping could have reduced the volume of the samples. A similar trend was observed in the study carried out by Abu-Harden and Hill (2010) on wheat flour and starches. However, Patwa et al. (2014) observed an opposite trend for the wheat flour samples (particle size ranging from 2 to 400 µm), i.e. decrease in tapped density values with increase in moisture content from 12 to 16%. This deviation might be due to a wider particle size distribution of flour used in their study. In a wider

distribution, smaller particles easily fill the intergranular void space between larger particles resulting in a better compaction of the solids.

The values shown in Fig. 4-2 indicate that the particle size has significant influence on the tapped densities of the wheat flour samples, with a high positive correlation ($r = 0.99$). This is due to the fact that the finer particles pack more loosely than larger granules due to irregular shape (Brown and Richards, 1970), which increases the volume and the intergranular void space (Abu-Harden and Hill, 2010).

This study also confirms that the tapped density of hard wheat flours is significantly different from soft wheat flours ($P < 0.05$), as stated by Bian et al. (2015). Siliveru et al. (2016) reported that the roughness quotient of soft wheat flour is higher than the hard wheat flours. The roughness and the comparative non-uniform shape could be preventing the soft wheat flour particles from rearranging and packing.

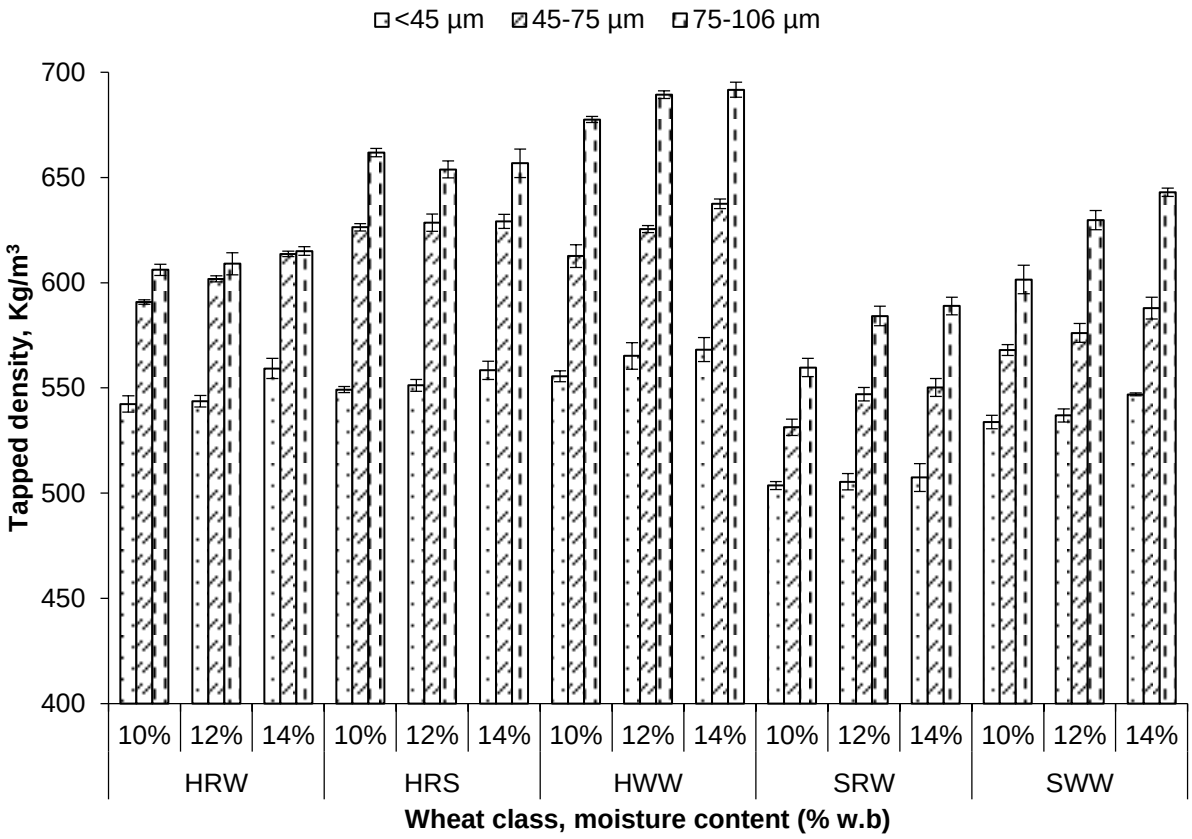

Figure 4-2: Tapped density of wheat flour samples at three moisture levels and three particle sizes.

Note: Error bars represent the standard deviations.

A high negative correlation (r = -0.99) has been found between the true density and moisture content of wheat flours (Fig. 4-3). This might have been due to the swelling of starch granules at higher moisture content and led to a higher increase in volume compared to that of increase in mass. Particle size has a significant influence ($P < 0.05$) with a positive correlation for hard wheat flour (r = 0.99) and a negative correlation for the soft wheat flour (r = -0.97). This can be related to their respective protein contents (Table 4-1), a high negative correlation (r = -0.87) has been found between the true density and protein content. Wang and Flores (2000) observed that, the finer fractions of flour (<38 µm) had more low molecular weight fraction

(LMW) proteins compared to the larger particle sizes of flour. The presence of LMW proteins in greater amounts in hard wheat smaller particles (<45 µm) might have led to the lower true density values, since the proteins has lower density than starch granules (Kuakpetoon et al., 2001). This study also confirms that the true density of soft wheat flours is significantly different from hard wheat flours ($P < 0.05$) due to the differences in composition.

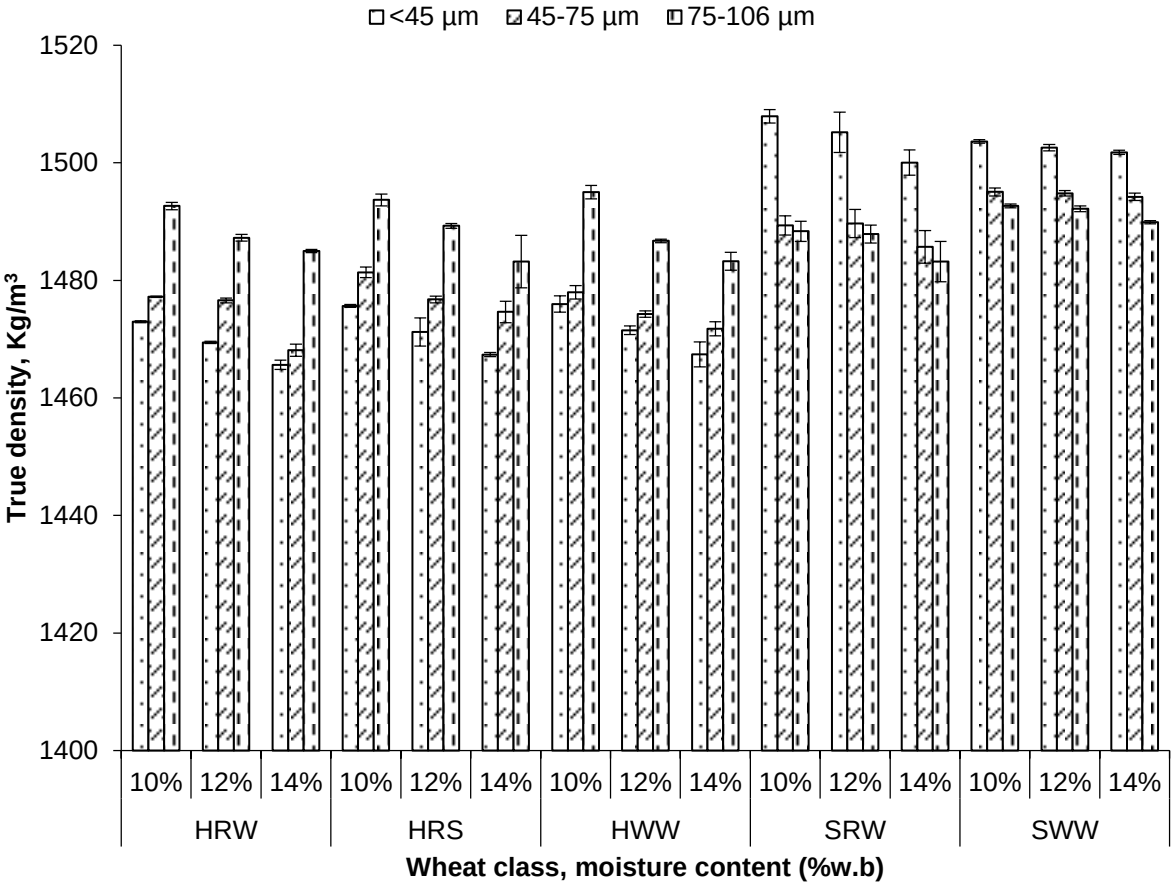

Figure 4-3: True density of wheat flour samples at three moisture levels and three particle sizes.

Note: Error bars represent the standard deviations.

4.3.3. Shear flow properties

The shear flow properties (cohesion, flow function, and AIF) at three moisture levels, three particle sizes, and three sifter loads have been investigated for the wheat powders from five different wheat classes (three hard wheats, two soft wheats). As there is no significant difference ($P < 0.05$, results not reported) among the shear flow properties within the hard wheats (i.e. between HRW, HRS, and HWW) and within the soft wheats (i.e. SRW and SWW). One wheat class from each variety (HRW and SRW) that differs extremely in hardness, milling procedure, and chemical composition was chosen to investigate the effect of variety (hardness and chemical composition) on shear flow properties (Table 4-2).

4.3.3.1. Effect of moisture on shear flow properties

The cohesion values for wheat flour samples increased in the range of about 0.05 – 0.20 kPa with increase in moisture from 10 to 14 (% w.b.) for the samples depending on their particle size and applied pressure. A positive correlation (r = 0.98) between moisture content and cohesion and negative correlation (r = -0.98) between moisture content and FF was observed (Table 4.3). The lower value of FF indicates the increase in cohesive nature (hard to flow) nature of the powders (Jenike, 1964). The FF values for wheat flour samples decreased in the range of about 0.20 – 0.45 with increase in moisture from 10 to 14 (% w.b.), indicating the drop in their nature of flow from ‘easy flowing’ to ‘very cohesive’. From the FF values, it can be seen that the moisture content of the flour will likely to play a bigger role in the flow of wheat flour during dynamic flow through a sifter stack and other processing equipment. The results (c, FF) obtained in this study were in close agreement with the results reported by Teunou and Fitzpatrick (1999) and Iqbal and Fitzpatrick (2006). The moisture content does not have significant effect on AIF (Table 4-2). The results from this study indicate that, moisture increases the adhesion

characteristics of wheat flour, thereby increasing the powder cohesivity. Major differences in cohesion values could be seen between the two wheat flours and at different particle sizes (Table 4-2), which could be due to differences in their surface properties. During the sample preparation (for 14% m.c), the powders were placed in a high relative humidity atmosphere (55 – 60% r.h), which might have caused increased thickness of the adsorbed liquid layer, thereby increasing the strength of liquid bridges formed between particles (Teunou and Fitzpatrick, 1999). The differences in cohesion values are not only due to differences in relative humidity, but also due to differences in chemical composition. The presence of starch granules and protein fractions had a significant effect on the adsorption of the water on the surface, which might have led to higher cohesion increment, specifically in soft wheats (Table 4-2). Abu-Hardan and Hill (2010) reported that there is significant difference in cohesive index of wheat flours and wheat starches, due to differences in the hydration capacity. Ambrose et al. (2016) stated that the ability to absorb and adsorb water within a powder bulk depends on structural arrangement of the chemical components on each particle.

This study was conducted within the range of production moisture content of flour that is common in wheat flour industry. A key understanding is the transformation of wheat flour at a specific moisture level (>12%) from ‘easy flowing’ to ‘very cohesive’. Therefore, to avoid agglomeration of flour over the sifter screen it would be critical to maintain the moisture content of the wheat flour below 12 (% w.b.). In the milling facilities, the increase in moisture of the flour could happen either due to high tempering moisture or relative humidity of the ambient air.

4.3.3.2. Effect of particle size on shear flow properties

The cohesion values for wheat flour samples decreased in the range of about 0.02 – 0.34 kPa with increase in particle size from < 45 μm to 75-106 μm for the samples depending on their

wheat class and applied pressure (Table 4.2). The cohesion of flour particles decreased with increasing in particle size (r = -0.92) from <45 μm to 75-106 μm (Table 4-3). The FF values for wheat flour samples increased in the range of about 0.07 – 2.05 with increase in particle size from < 45 μm to 75-106 μm, indicating the change in the nature of flow from 'very cohesive' to 'easy flowing' powders (Table 4-2). From the cohesion values, it is obvious that the particle size of the flour significantly impacts the flow behavior of wheat flour on the sifter causing agglomeration and blockage (blinding) of screen surfaces. On considering the particle size as a dependent variable, it is evident that the particle size is a significant contributor for cohesivity (average r = -0.94). A high negative correlation (r = -0.94) has been observed between particle size and AIF. For the wheat powders, reduction in particle size tends to increase cohesion behavior because the particle surface area per unit mass increases, creating a greater number of contact points for interparticulate bonding and additional interparticulate interactions. The other factor for higher cohesion values for < 45 μm particles (0.80 – 0.94 kPa at 1.5 kPa applied pressure) is due to increase in surface roughness. Siliveru et al. (2016) observed that 45 μm particles have higher surface roughness values due to the differences in breakage pattern of hard and soft wheats. The particle surface roughness could increase the interparticle interaction by increased Van der Waals forces and by mechanical linkages (Landillon et al., 2008).

The three particle sizes (75-106, 45-75, and <45 μm) used in this study, on the basis of median size distribution of wheat particles during milling helps us to understand the exact particle size distribution that could initiate flow challenges, as well as formation of agglomerates (very cohesive) on the sifter screens. Based on the cohesion values (Table 4-2), this study further hypothesizes that, the wheat flour particles of < 45 μm could be a significant contributor for sieve blinding.

4.3.3.3. Effect of sifter load on shear flow properties

The cohesion values for wheat flour samples increased in the range of about 0.20 – 0.56 kPa with increase in applied pressure from 0.5 kPa to 1.5 kPa for the samples depending on the wheat class and particle sizes (Table 4-2). A high positive correlation (r = 0.99) was observed between sifter load and cohesion while a negative correlation (r = -0.95) was observed between sifter load and FF, respectively (Table 4-3). The FF values for wheat flour samples increased in the range of about 6.50 – 0.35 with increase in applied pressure from 0.5 to 1.5 kPa, indicating the change from 'easy flowing' to 'very cohesive' powders. In the range of applied pressures, the increment in cohesion values (0.5 – 0.7 kPa) for <45 μm particles is higher than that for 75-106 μm (0.02 – 0.15 kPa) particles (Table 4-2). This indicates that the presence of higher amounts of <45 μm particles on the sieve surface would lead to agglomeration of particles and could cause flowability issues when compared to bigger sized particles. From the cohesion values it is obvious that sifter load will have a significant influence on the sieve blinding issues often faced by wheat flour processing facilities. From the cohesion values determined in this study (Table 4-2), a significant transformation of particle flow behavior could be observed on increasing the sifter load from 1.0 to 1.5 kPa. So, the maintenance of mass of flour on screen surface from time to time would be critical, which could be achieved by monitoring the roll parameters during milling.

Table 4-2: Shear flow properties of HRW and SRW wheat powders.

Sample characteristics			HRW			SRW		
Moisture content, (% w.b)	Particle size, μm	Applied pressure, kPa	Cohesion, kPa	FF	AIF, °	Cohesion, kPa	FF	AIF, °
10	<45	0.5	0.20 (0.01)b	1.50 (0.03)a	40.5 (3.05)a	0.24 (0.01)a	1.32 (0.02)a	36.5 (6.42)a
		1.0	0.41 (0.01)b	1.26 (0.04)a	32.53 (1.29)a	0.48 (0.01)a	1.21 (0.02)a	30.97 (0.15)a
		1.5	0.74 (0.01)b	1.15 (0.04)a	24.3 (1.90)a	0.78 (0.01)a	1.12 (0.02)a	23.37 (0.91)a
	45-75	0.5	0.08 (0.01)a	3.50 (0.05)a	32.9 (4.02)a	0.09 (0.01)a	3.27 (0.04)b	35.1 (1.79)a
		1.0	0.15 (0.01)a	2.98 (0.03)a	27.4 (4.02)a	0.17 (0.01)a	2.92 (0.07)b	32.1 (2.44)a
		1.5	0.31 (0.01)b	2.47 (0.08)a	27.8 (1.46)a	0.38 (0.01)a	2.41 (0.06)a	28.03 (0.84)a
	75-106	0.5	0.07 (0.01)a	9.52 (0.16)a	32.87 (0.87)a	0.04 (0.01)a	7.01 (0.09)b	31.33 (2.89)a
		1.0	0.11 (0.01)a	5.96 (0.16)a	27.87 (0.91)a	0.08 (0.01)a	5.72 (0.09)a	31.97 (0.15)a
		1.5	0.22 (0.01)a	3.52 (0.09)b	27.43 (0.67)a	0.14 (0.01)b	5.24 (0.06)a	30.4 (0.3)a
12	<45	0.5	0.24 (0.01)b	1.31 (0.05)a	37.47 (0.65)a	0.28 (0.01)a	1.24 (0.05)a	33.6 (4.34)a
		1.0	0.45 (0.01)a	1.11 (0.04)a	35.80 (2.21)a	0.49 (0.01)a	1.18 (0.01)a	34.5 (0.61)a
		1.5	0.90 (0.01)a	1.02 (0.02)a	21.52 (1.59)a	0.80 (0.01)b	1.08 (0.04)a	22.5 (2.25)a
	45-75	0.5	0.09 (0.02)a	2.68 (0.07)b	35.57 (0.23)a	0.09 (0.01)a	2.96 (0.05)a	37.50 (1.13)a
		1.0	0.24 (0.01)a	2.40 (0.03)b	27.83 (1.16)a	0.19 (0.01)b	2.56 (0.06)a	33.30 (0.67)a
		1.5	0.40 (0.01)a	2.24 (0.09)a	26.77 (0.71)a	0.40 (0.01)a	2.22 (0.07)a	28.21 (1.10)a

	75-106	0.5	0.07 (0.01)a	4.31 (0.03)a	29.07 (2.40)a	0.06 (0.01)a	4.00 (0.14)b	32.53 (3.17)a
		1.0	0.14 (0.01)a	3.50 (0.07)b	27.77 (2.11)a	0.14 (0.01)a	3.75 (0.09)a	30.03 (2.07)a
		1.5	0.27 (0.01)a	3.35 (0.06)a	27.03 (0.12)a	0.21 (0.01)b	3.48 (0.05)a	29.63 (0.47)a
14	<45	0.5	0.28 (0.01)a	1.03 (0.02)a	39.27 (2.66)a	0.30 (0.01)a	1.10 (0.08)a	41.07 (4.54)a
		1.0	0.49 (0.01)a	1.04 (0.01)a	39.37 (2.44)a	0.51 (0.01)a	1.05 (0.03)a	38.37 (2.07)a
		1.5	0.95 (0.01)a	1.03 (0.01)a	27.50 (1.64)a	0.84 (0.01)b	1.02 (0.03)a	25.17 (3.95)a
	45-75	0.5	0.13 (0.01)a	2.03 (0.11)b	32.93 (1.96)a	0.11 (0.01)a	2.66 (0.04)a	35.07 (0.90)a
		1.0	0.32 (0.02)a	1.69 (0.12)b	31.53 (0.80)a	0.23 (0.01)b	2.41 (0.05)a	33.50 (0.95)a
		1.5	0.54 (0.01)a	1.48 (0.03)b	26.00 (1.47)a	0.44 (0.01)b	1.89 (0.07)a	27.30 (0.40)b
	75-106	0.5	0.07 (0.01)a	4.18 (0.06)a	29.07 (2.40)a	0.08 (0.00)a	3.60 (0.02)b	34.31 (1.06)a
		1.0	0.15 (0.02)a	3.27 (0.03)a	27.77 (2.11)a	0.17 (0.01)a	3.23 (0.09)a	29.62 (1.73)a
		1.5	0.29 (0.01)a	3.06 (0.06)a	27.03 (0.12)a	0.30 (0.01)a	2.73 (0.10)b	26.87 (0.51)a

*Values in the parenthesis are standard deviations.

** The values followed by the same letters are not significantly different for HRW and SRW at particular moisture level, particle size and sifter load.

Table 4-3: Correlations between different physical and chemical properties on shear flow properties of wheat powders.

	Cohesion	FF	AIF
MC	0.98**	-0.98**	ns
PS	-0.92**	0.96**	-0.94
SL	0.99**	-0.95**	-0.83
DS	0.92**	-0.82**	ns
Protein	0.91* (Hard)	-0.84* (Hard)	ns
	-0.73* (Soft)	0.91* (Soft)	
Crude fat	-0.64** (Hard)	0.74** (Hard)	ns
	0.92* (Soft)	-0.86* (Soft)	

Moisture content (MC), particle size (PS), sifter load (SL), damaged starch (DS), flow function (FF), angle of internal friction (AIF).

**, * Indicate significance at $P < 0.01$ and $P < 0.05$, respectively; ns, not significant.

4.3.3.4. Effect of chemical composition on shear flow properties

The cohesion and flow function values of flour for the hard wheats (HRW) and soft wheats (SRW) at all moisture levels, particle sizes, and sifter loads were significantly different ($P < 0.05$) as shown in Table 4-2. The cohesion values for soft wheats (at 10 and 14% m.c) were significantly higher than that of hard wheats. It is observed in this study that at 12% (w.b.) moisture content, irrespective of particle size and applied pressure, the cohesion and FF values of hard and soft wheat flour were similar (Table 4-2). So, the dynamic flow properties of soft and hard wheat flours would be similar provided the particle size and sifter loads are kept constant.

The cohesion of flour particles increased with the damaged starch content (r = 0.92) (Table 4-3). This could be due high water absorption capacity of damaged starch (Landillon et al., 2008). It was expected that protein and fat will also have a similar trend on the cohesion

values due to the contribution of these components in strengthening the interparticle interactions through chemical bonding. Protein and fat molecules tend to form non-covalent hydrogen bonds (proteins), chemicals links (protein and fats), or liquid fat bridges (fats) (Landillon et al., 2008). However, the cohesion of flour particles increased with increasing in protein content ($r = 0.91$) for hard wheats, whereas an opposite trend was observed for soft wheats ($r = -0.73$) (Table 4-3). A similar trend was reported between cohesion and fat content of flours ($r = 0.92, -0.64$, for hard and soft wheats, respectively). No clear functional link can be proposed on this phenomenon, as total proximate compositions (fat and protein) were used in the correlation analysis. Additional extensive analysis of the surface composition of wheat flours is needed to explain the cohesion and chemical composition of wheat flour.

4.4. Conclusions

This study quantified the effect of moisture content, particle size, sifter load, and chemical composition on the shear flow properties of wheat flour. Results demonstrate a large diversity in physical and cohesive properties for the selected wheat flours. Besides the wheat class as a variable, the three levels each of moisture, particle size, and of sifter loads were tested. The high correlation reported in between the physical independent variables (moisture content, particle size, sifter load), chemical composition (damaged starch, protein, and fat) on the flow properties (cohesion, flow function, and AIF) demonstrated that each parameter had a significant contribution on the cohesion and flowability of wheat flour. The moisture content and particle size where the flowability shifts from ‘easy flowing’ to ‘very cohesive’ were found to be 12% (wet basis) and 45 μm, respectively. The chemical components (protein and fat) had mixed effects on the cohesive properties of hard and soft wheat flours and needs further investigation to understand the effects of composition on the cohesive properties. This understanding of the

physical and shear flow properties of flour particles could eventually be instrumental to improve the efficiency of size based fractionation of flour from various wheat classes.

4.5. References

AACC International. (1999). Approved Method of Analysis. (Methods 08-01.01; 30-25.01; 32-10.01; 46-30.01; 76-30.02, 11th ed.,). St. Paul, Minnesota.

AACC International. (1988). Approved Methods of Analysis. (Method 26-21.02. Experimental Milling-Buhler Method for Hard Wheat. Method 26-31.01.Experimental Milling-Buhler Method for Soft Wheat Straight-Grade Flour, 11th ed.,). St. Paul, Minnesota.

Abu-Hardan, M., & Hill, S. E. (2010). Handling properties of cereal materials in the presence of moisture and oil. *Powder Technology*, 198, 16–24.

Ambrose, R. P. K., Jan, S., & Siliveru. K. (2016). A review on flow characterization methods for cereal grain based powders. *Journal of the Science of Food and Agriculture*, 96, 359–364.

AOAC International. (2006). Official Methods of Analysis. (17th ed.,). Gaithersburg Maryland.

Barbosa-Cánovas, G. V., & Juliano, P. (2005). Compression and compaction characteristics of selected food powders. *Advances in Food and Nutrition Research*, 49, 233–307.

Baruch, D. W. (1974). Wheat flour particle size distribution related to compressibility and bridging tests. *New Zealand Journal of Science*, 17, 21.

Bian, Q., Sittipod, S., Garg, A., & Ambrose, R. P. K. (2015). Bulk flow properties of hard and soft wheat flours. *Journal of Cereal Science*, 63, 88–94.

Brown, R. L., & Richards, J. C. (1970). Principles of Powder Mechanics, Pergamon Press, Oxford.

Bruni, G., Lettieri, P., Newton, D., & Barletta, D. (2007). An investigation of the effect of the interparticle forces on the fluidization behaviour of fine powders linked with rheological studies. *Chemical Engineering Science*, 62, 387–396.

Fitzpatrick, J., Barringer, S. A., Iqbal, T. (2004). Flow property measurements of food powders and sensitivity of Jenike's hopper design methodology to the measured values. *Journal of Food Engineering*, 61, 399–405.

Freeman, R. (2007). Measuring the flow properties of consolidated, conditioned and aerated powders. A comparative study using a powder rheometer and a rotational shear cell. *Powder Technology*, 174, 25–33.

Hareland, G. A. (1994). Evaluation of flour particle size distribution by laser diffraction, sieve analysis and near-infrared reflectance spectroscopy. *Journal of Cereal Science*, 20, 183–190.

Iqbal, T., & Fitzpatrick, J. J. (2006). Effect of storage conditions on the wall friction characteristics of three food powders. *Journal of Food Engineering*, 72, 273–280.

Jenike, A. W. (1964). Storage and Flow of Solids, Bulletin No. 123. Utah Engineering Station, Salt Lake City, Utah.

Kamath, S., Puri, V. M., & Manbeck, H. B. (1994). Flow property measurement using the Jenike cell for wheat flour at various moisture contents and consolidation times. *Powder Technology*, 81, 293–297.

Kuakpetoon, D., Flores, R. A., & Milliken, G. A. (2001). Dry mixing of wheat flours: Effect of particle properties and blending ratio. *LWT - Food Science and Technology*, 34, 183–193.

Landillon, V., Cassan, D., Morel, M. H., & Cuq, B. (2008). Flowability, cohesive, and granulation properties of wheat powders. *Journal of Food Engineering*, 86, 178–193.

Leturia, M., Benali, M., Lagarde, S., Ronga, I., & Saleh, K. (2014). Characterization of flow properties of cohesive powders: a comparative study of traditional and new testing methods. *Powder Technology*, 253, 406–423.

Morrison, W. R., & Laignelet, B. (1983). An improved colorimetric procedure for determining apparent and total amylose in cereal and other starches. *Journal of Cereal Science*, 1, 9–20.

Neel, D. V., & Hoseney, R. C. (1984a). Sieving characteristics of soft and hard wheat flours. *Cereal Chemistry*, 61, 259–261.

Neel, D. V., & Hoseney, R. C. (1984b). Factors affecting flowability of hard and soft wheat flours. *Cereal Chemistry*, 61, 262–266.

Patwa, A., Malcolm, B., Wilson, J., & Ambrose, R. P. (2014). Wheat mill stream properties for discrete element method modeling. *Transactions of the ASABE*, 57, 891–899.

Raeker, M. O., Gaines, C. S., Finney, P. L., & Donelson, T. (1998). Granule size distribution and chemical composition of starches from 12 soft wheat cultivars. *Cereal Chemistry*, 75, 721–728.

Siliveru, K., Kwek, J.W., Lau. G., & Ambrose, R.P.K. (2016). An image analysis approach to understand the differences in flour particle surface and shape characteristics. *Cereal Chemistry*, 93, 234-241.

Simmonds, D. H. (1974). Chemical basis of hardness and vitreosity in the wheat kernel. *Baker's Digest*, 48, 16–29.

Subramanian, S., & Viswanathan, R. (2007). Bulk density and friction coefficients of selected minor millet grains and flours. *Journal of Food Engineering*, 81, 118–126.

Teunou, E., & Fitzpatrick, J. J. (1999). Effect of relative humidity and temperature on food powder flowability. *Journal of Food Engineering*, 42, 109–116.

Teunou, E., Fitzpatrick, J. J., & Synnott, E. C. (1999). Characterization of food powder flowability. *Journal of Food Engineering*, 39, 31–37.

Wang, L., & Flores, R. A. (2000). Effects of flour particle size on the textural properties of flour tortillas. *Cereal Chemistry*, 31, 263–272.

Chapter 5 - Prediction of Bulk Flow Behavior of Wheat Flour Using Granular Bond Number

Abstract

In order to improve the fundamental understanding of wheat flour flow behavior, which is essential for the success of sieving and other particulate size based separation processes, this study investigates the relationship between particle properties and the flow function coefficient, a metric used to assess the flow performance. The granular Bond number quantified from the inter-particle cohesion force using the multi-asperity model, which is modification of Rumpf equation, correlates well with the flow function coefficient. The lower values of standard error of prediction (0.007 to 0.01) for flow function coefficient of size segregated wheat flours, flour blends indicates that the developed model agreed well with the experimental measurements. It was established that, the variations in the surface chemical composition of flours could have a significant impact on the flow behavior of wheat flours. The modeling effort put forth in this study, can be used to guide the millers to obtain the required throughput on increasing the sieve efficiency by preventing the particle agglomeration and also to assess the flow behavior of wheat flour blends.

5.1. Introduction

The end product of the wheat milling process is classified as flour in which "not less than 98 percent of the flour passes through a cloth having openings not larger than those of woven wire cloth designated 212 μm (No. 70)" (U.S. Code of Federal Regulations CFR, 2013). To manage the bulk flow of these finer flour particles, milling industries rely on the empirical knowledge and technical knowhow of the operators. Due to differences in particle cohesion, a

significant loss in throughput is observed when sieving soft wheat flour in comparison to that of hard wheat flour (Neel and Hoseney, 1984a). Several characteristics of wheat flour have been considered to discuss these differences in flowability, such as cohesiveness, particle size, and the particle physical and chemical composition (Neel and Hoseney, 1984a, 1984b; Siliveru et al., 2016). With the "inherently complex" nature of the granular materials, the particulate processes remain exceedingly difficult to model, design, and control (Andreotti et al., 2013). This complex and diverse bulk-scale behavior originates from contact and non-contact interactions among particles and their surroundings, thus the particle-scale interactions are difficult to resolve (Capece et al., 2015).

Due to the heterogeneity and anisotropic nature of the wheat flour, many published studies stressed the need for understanding the flowability issues of the wheat flours during storage and processing operations (Teunou et al., 1999; Landillon et al., 2008). Given that uniform flowability of flour is essential for better process control, there has been devoted efforts on this topic with most studies focusing on the effect of moisture content (Kamath et al., 1994; Teunou et al., 1999; Iqbal and Fitzpatrick, 2006; Landillon et al., 2008), particle size distribution (Neel and Hoseney, 1984a, 1984b; Landillon et al., 2008), and wheat class (Landillon et al., 2008; Bian et al., 2015). But, these studies omit the underlying mechanisms responsible for poor flow behavior of cohesive finer flour particles such as the cohesive forces that exist between the finer particles. Most importantly, the effect of surface chemical composition on the flow behavior of wheat flour is not a well understood phenomenon. The differences in chemical composition may lead to molecular bonding forces due to the formation of non-covalent hydrogen bonds, chemical links, or liquid fat bridges (Landillon et al., 2008).

In general, to assess or predict the flowability, flow function coefficient (ff_c) is the commonly used parameter that is determined by shear analysis. Mathematically modeling ff_c is limited to coarse powders (particles of 100 µm size or more). For coarse powders, bulk density is the criterion used for model development and is used extensively in assessing the gravity induced flows (Shultz, 2008). The same approach cannot be adapted for fine powders, since the inter-particle cohesive forces are highly dependent on the fundamental particle characteristics. For fine powders, the concept of Bond number introduced by Capece et al. (2015) allowed the prediction of flowability from the particle parameters such as particle size, surface roughness (asperities), surface energy, and density. For fine, dry, and uncharged particles, van der Waals force is dominated compared to the other forces like liquid bridging and mechanical interlocking (Castellanos, 2005). Because the van der Waals force can be orders of magnitude greater than particle weight; the ratio of which is predominantly referred to as granular Bond number (Capece et al., 2015). As the granular Bond number can be approximated from the measurable particle properties (Capece et al., 2015), an attempt was made in this study to propose a model for predicting the flow behavior of wheat flours based on granular Bond number concept using the particle physical and chemical characteristics.

5.2. Materials and Methods

5.2.1. Materials

Flour particles from two wheat classes (hard red winter, [HRW] and soft red winter [SRW]), which differ in hardness, milling procedure, and chemical composition were used in this study. The flour sample preparation is discussed in detail in Chapter 3 (3.2.1). The median particle size of hard and soft wheat flours was 75 and 45 µm, respectively. To measure the variation in flow behavior due to the difference in size and size distribution, wheat flours were

segregated at three particle size ranges (75-106, 45-75, and <45 μm) using an Alpine jet sieve analyzer (model e 200 LS, Hosokawa Alpine Ag & Co, Augsburg, Germany) with 140, 200, and 325 U.S. standard sieve sizes. The separated wheat flour particles were then conditioned to a moisture content of 12 ± 0.25 % (w.b.), which is the average production moisture content of flour in wheat milling industry. The target moisture content (12%, w.b.) was achieved by placing the samples in relative humidity chamber maintained at 50-55% relative humidity (r.h) at 25 °C for 4-5 hr. The initial and final moisture content of the flours was determined by drying 2-3 g of the samples, in triplicate, at 130 °C for 60 min (AOAC standard 925.10, AOAC International, 2006).

5.2.2. Particle size and chemical characterization of wheat flours

The particle size analysis of the wheat flours, after segregation, was carried out on the Morphologi G3-ID morphologically directed Raman system (Malvern Instruments, Worcestershire, UK). For equal distribution of the particles over the slide holders, a dry air dispersion technique was used by applying a pressure of 0.5 bar. For the entire period of image analysis, a standard settling time of 300 s was chosen, in order to give ample of time for the dispersed particles to settle down over the glass slide. The flours were then visualized through an Episcopic bright field illumination. The images of the samples were then obtained using the optical system equipped with camera (Nikon CFI 60) operated with an objective lens set at ×50. At least 125 images of flour from each particle size and wheat class were obtained for Sauter mean and asperity diameters measurements.

In this study, it was also hypothesized that the variation in flow behavior of wheat flours was not only due to the particle size distribution (75-106, 45-75, and <45 μm), but also due to their surface chemical composition. To investigate the differences in surface chemical

composition of wheat flours, the flour samples of two distinct particle sizes (<45 μm and 75-106 μm) from HRW and SRW were used in the study. The methodology used by Jin et al. (2016) was used in this study. The samples were analyzed using a Renishaw inVia Raman Spectrometer (Renishaw Inc., IL, U.S.A.) under a ×20 microscope objective. To minimize the noise that could occur due to aberrant surfaces of wheat flours during spectroscopic measurements, the flours samples, pure starch, and gluten samples were made into compacts using a manual tablet press (Model 3912, Carver Inc., U.S.A.). About 200 mg of sample was weighed into the stainless steel die of 10 mm diameter. A compression force of ~ 2000 psi was exerted for 2 min to make the compacts. From each compact, about 4 Raman maps of 300 × 300 μm size were collected over the spectral range of 100-1825 cm^{-1} with excitation at a wavelength of 785 nm. Raman measurement spectral values for pure components (starch and gluten) obtained on following the similar procedure. The spectral values for lipid obtained from Piot et al. (2001) were used for comparative analysis. A total of 196 spectra (from 49 pellets) from each particle size were used in the analysis.

The collected Raman spectra of individual flour particles were analyzed using Band-Target Entropy Minimization (BTEM) algorithms, using the MATLAB program (R2013a, MathWorks, Natick, MA, U.S.A.). In order to obtain the pure component spectral estimates of the constituents and the percentage signal contribution of the components, the BTEM algorithm was used. The percentage signal contributions of components (starch, protein, and lipid) obtained in this study are Raman intensity values and does not reflect the exact percentage of each component over the surface of flour particle.

5.2.3. Preparation of flour blend

Flour blends were prepared using a lab scale rotary mixer. Mixing was performed in a cylindrical glass jar with a height of 20 cm and an inner diameter of 12 cm loaded with 100 g of flour. The flour was mixed for 20 min with the jar rotating at 60 rpm. From the three particle sizes used (75-106, 45-75, and <45 μm) in this study, four separate blends were prepared: 33.3/33.3/33.3; 16.6/41.7/41.7; 41.7/16.6/41.7; and 41.7/41.7/16.6.

5.2.4. True density

The true density of the individual flour samples was measured using a helium gas pycnometer (AccuPync II 1340, Micromeritics, Norcross, Ga.). The true density was calculated from the weight and volume occupied by the solid particles. Ten measurements were taken for each sample and the mean was reported.

5.2.5. Surface energy

The dispersive surface energy of the individual flour particle samples was measured using inverse gas chromatography (IGC-SEA, Surface Measurement Systems, London, U.K.) equipped with a flame ionization detector. To prevent the sample movement during the experiment, each sample was packed into a separate pre-silanized columns (300 × 4 mm ID) with silanized glass wool sealed at each end. The mass required for each sample was adjusted to a total surface area of 0.25 m^2 based on the preliminary experiments (results not reported). An infinite dilution method was followed using the heptane, octane, nonane, and decane (HPLC grade, Sigma-Aldrich, Poole, U.K.) as probe molecules as mentioned by Schultz et al. (1987). Helium was used as the carrier gas with a flow rate of 10 standard cubic centimeters per minute (sccm) and methane was used for dead volume determination. The surface energies were

measured in triplicate, at a relative humidity (r.h) of 30% and temperature of 30 °C. The Frenkel relation (Eq. 5-1) was used for the Hamaker constant calculation based on the dispersive surface energy (γ_d) (J/m^2) and the cut-off distance (D_0, m) (Frenkel, 1955). In the present study, the cut-off was assumed to be 0.165 nm, as mentioned by Israelachvili (1992).

$$A = 24\pi D_0^2 \gamma_d \qquad (5\text{-}1)$$

5.2.6. Theoretical prediction of wheat flour flowability

For particles in close contact, their interparticulate interaction depends on molecular forces due to differences in chemical composition, capillary, electrostatic, and van der Waals (vdW) forces. During the model development it was assumed that the sieving process happens in a controlled atmosphere (at constant r.h conditions). Therefore, the capillary forces between the particles were neglected. The electrostatic forces were known to be of tertiary importance and about 10 times weaker than vdW forces under typical dry atmospheric conditions (25-50% r.h) (Podczeck, 1998). Thus, during the model development, the discussion of forces was restricted to molecular interactions and vdW forces. The dipole-induced attraction between the constituent molecules (molecular interactions) from two interacting particles originates the vdW forces. The magnitude of these forces depends on particle characteristics such as; particle size, geometry, surface roughness, surface energy, and surface chemistry. Fine particle size flour, i.e. ~ 100 µm and smaller, can cause severe agglomeration resulting in non-ideal flour flowability (cohesive behavior) (Castellanos, 2005).

Therefore, due to the dominance of vdW forces for fine flours, in this study, the expression for cohesive force was developed by modifying the Rumpf cohesion model (Eq. 5-2) proposed by Chen et al. (2008). This modified model also considers the non-contact interaction

between two particles separated by distance H_0 and the contact forces between particles and asperities (Capace et al., 2015).

$$F_{cohesion} = \frac{A}{12z_0^2}\left(\frac{d_p}{2(^{H_0}/_{z_0})^2} + \frac{3d_{asp}d_p}{d_{asp}+ d_p}\right) \quad (5\text{-}2)$$

where A is Hamaker constant (J), Z_0 is the equilibrium separation distance assumed to be 0.4 nm (Chirone et al., 2016), d_p is the particle diameter (m), H_0 is the separation distance (Capace et al., 2015), and d_{asp} is asperity diameter (m). The first term within the parenthesis on the right hand side of Eq. (2) accounts for the non-contact force between two particles separated by distance H_0, whereas the second term accounts for the contact forces between the particles.

To determine the particle's overall cohesiveness, a multitude of other body and surface forces must be considered along with the force of cohesion. In sieving and other dynamic processes, the force of gravity (W_g), a competing force to vdW force is most relevant and applicable in all the unit operations. To account for W_g, a dimensionless parameter known as the granular bond number (Bo_g) (which is described as the ratio of cohesive force to the non-cohesive forces (W_g)), is used to quantify the interparticle cohesion (Eq. 5-3) (Castellanos, 2005).

$$Bo_g = \frac{F_{cohesion}}{W_g} \quad (5\text{-}3)$$

Based on the preliminary experiments, a good correlation between the Bo_g and flow function coefficient (ff_c) was observed (Figure A-2). The Bond number concept used in this study, has been shown to correlate well with other bulk-scale flour properties such as bulk density (Yu et al., 2003; Capece et al., 2014), angle of repose (Jallo et al., 2011), and flow function coefficient (Huang et al., 2014; Capece et al., 2015). Due to the good correlation between these two

parameters, a formal relationship can be established using the empirical expression as shown in Eq. (5-4).

$$ff_c = \alpha\left(Bo_g\right)^{-\beta} \quad (5\text{-}4)$$

The power law relationship (Eq. 5-4), has also been observed for angle of repose (Jallo et al., 2011), powder bed porosity (Yu et al., 2003; Capece et al., 2014), and flow function coefficient (Huang et al., 2014; Capece et al., 2015). The parameters α and β used in the model (Eq. 4) are material independent, since Bo_g takes into account all the relevant material properties.

5.2.7. Granular Bond number model development for flour blends

To explain the flow behavior of flours blends, the Eq. (5-4) was further extended to blended flour (ternary mixture prepared by mixing different particle size flours) containing three different particle sizes (75-106, 45-75, and <45 μm). The relationship between the flow function coefficient and Bond number of the flour mixture was established using the equation below:

$$ff_{c,Mix} = \alpha(Bo_{g,Mix})^{-\beta} \quad (5\text{-}5)$$

Since, the Bond number of individual sized flours was determined by the interaction between the two particles of similar material (i.e. material having same physical, surface, and chemical properties), the Bond number of a multicomponent mixture must account for all the possible interactions of all the particles in contact. Thus, the Bond number of a mixed system is defined as the weighted harmonic mean of the granular Bond number between three components (i, j, and k) (Eq. 5-6).

$$Bo_{g,Mix} = \left(\sum_{i=1}^{N}\sum_{j=1}^{N}\sum_{k=1}^{N}\frac{w_{ijk}}{Bo_{g,ijk}}\right)^{-1} \quad (5\text{-}6)$$

w_{ijk} represents the weighting function and can be determined using the fractional surface area (f_{SA}) of the particles in close contact and calculated using Eq. (5-7).

$$w_{ijk} = f_{SA,i} f_{SA,j} f_{SA,k} \quad (5\text{-}7)$$

The fractional surface area was calculated based on the ratio of Sauter mean diameter surface area to the particle diameter surface area as in denoted in Eq. (5-8). The Sauter mean diameter was obtained from the particle size distribution.

$$f_{SA} = \frac{(d_{32})^2}{(d_p)^2} \quad (5\text{-}8)$$

The Sauter mean diameter is expressed as the relation of the particle volume to the particle surface area shown in Eq. (5-9).

$$d_{32} = 6\frac{V_p}{S_p} \quad (5\text{-}9)$$

The granular Bond number between three components was assessed using Eq. (5-10).

$$Bo_{g,ijk} = \frac{F_{c,ijk}}{W_{ijk}} \quad (5\text{-}10)$$

The force of cohesion was calculated based on Eq. (5-2) using geometric mean of Hamaker constant and harmonic means of particle diameter, asperity diameter and particle weight (Eq.5-11 to Eq. 5-14) (Katainen et al., 2006).

$$A = \sqrt{A_i A_j A_k} \quad (5\text{-}11)$$

$$d_p = \frac{3 d_{p,i} d_{p,j} d_{p,k}}{d_{p,i} + d_{p,j} + d_{p,k}} \quad (5\text{-}12)$$

$$d_{asp} = \frac{3 d_{asp,i} d_{asp,j}\, d_{asp,k}}{d_{asp,i} + d_{asp,j} + d_{asp,k}} \quad (5\text{-}13)$$

$$W_{ijk} = \frac{3 W_i W_j W_k}{W_i + W_j + W_k} \quad (5\text{-}14)$$

5.2.8. Experimental characterization of flow performance

The flow performance of flours was evaluated using the FT4 Powder Rheometer (Freeman Technologies, Gloucestershire, UK). The detailed description of the powder rheometer

and shear flow cell tests can be found elsewhere (Bian et al., 2015). The sample holder system consists of a vertical glass container of 50 mm internal diameter and 85 ml volume. The flour contained within the cell was sheared using a head cell (2 cm height) consisting of 18 equally spaced vanes of 2.5 mm height. To address the variations in sifter load, a pre-consolidation stress (i.e. normal consolidation stress at pre-shear) of 1 kPa was chosen based on the average sifter load (flour retained on 1 m^2 sifter screen area). The samples were sheared to failure under normal stresses of 200, 400, 600, 800, and 1000 Pa to obtain the yield locus. From the yield locus and Mohr circle analysis, the unconfined yield strength (UYS, σ_c) and major principal stress (MPS, σ_1) at each pre-shear load can be determined. The ff_c is characterized based on the Eq. (5-15) proposed by Jenike (1964). The σ_1 must be higher than σ_c to cause a powder bed to yield or flow, accordingly a larger ff_c value, refers to a better flowing powder (Jenike, 1964). All samples were stored at 35±1% r.h in a controlled humidity chamber prior to testing. All the measurements were conducted in triplicate.

$$ff_c = \frac{\sigma_1}{\sigma_C} \qquad (5\text{-}15)$$

5.2.9. Data analysis

The results were analyzed by ANOVA and compared by Fisher's test at a significance level of 0.05 using SAS software (SAS version 9.3, SAS Institute, Cary, NC, U.S.A.). The measure of accuracy of the predictions (i.e., mean standard deviation between the predicted and actual values) was estimated by calculating the standard error of prediction (SEP).

$$SEP = \sqrt{\frac{\sum(Y-Y')^2}{N}} \qquad (5\text{-}16)$$

where Y = experimental ff_c value, Y' = predicted ff_c value, and N = number of observations.

5.3. Results and Discussion

5.3.1. Significance of surface chemical composition on the model development

The surface composition obtained as % Raman intensity are the approximates of the actual surface composition (Table 5-1). The soft wheat flour fractions (< 45 and 75-106 μm) had lower surface protein and higher starch and lipid content than the hard wheat flour fractions (< 45 and 75-106 μm) and the values were significantly different ($p < 0.05$) (Table 5-1). This trend was due to the significant differences in the proximate compositions of hard and soft wheats. The higher surface protein in hard wheats is not only due to the differences in proximate composition, but also due to differences in breakage pattern of endosperm during milling (Siliveru et al., 2016). It is further evident from Table 5-1 that the <45 μm particle fractions of soft wheats had lower surface protein content than other fractions, which indicated that the small spherical B-type starch granules (<10 μm) and large lenticular A-type granules (25 – 40 μm) were readily released from the protein matrix during grinding due to weaker adhesion forces between starch and protein (Neel and Hoseney, 1984b). Whereas in hard wheats, the smaller fractions (<45 μm) have higher surface protein content due to the coherent nature of cell walls and cell contents in hard wheats creating smaller starch granules (<45 μm) embedded in protein matrix (Simmonds, 1974; Neel and Hoseney, 1984b).

The surface lipid content of flour samples from different wheat classes and particle sizes were significantly different ($p < 0.05$). The <45 μm particle fractions of soft wheats had higher surface lipid content than other fractions, owing to the distribution of polar lipids on the surface of starch due to significant difference in hardness (Finnie et al., 2010). A similar trend was reported in the study conducted by Siliveru et al. (2016), who stated that the difference is not

only due to distribution of polar lipids but also due to the presence of free lipids (Morrison and Laignelet, 1983).

It is evident from the above results that the surface chemical compositions of hard and soft wheat flours at various particle sizes were significantly different ($p < 0.05$). So, the difference in flow behavior of wheat flours could not only be due to the difference in particle physical characteristics, but also from the differences in surface chemical composition. To further understand the influence of surface chemical composition, the dispersive surface energies (γ_d) were calculated for the respective flour samples. The surface energy of the samples increased with increase in particle size (Table 5-1). No clear functional link was identified on this phenomenon, as the estimated surface energies were some combination of surface energies of starch, protein, and lipid. Because the purpose of this study was to calculate the surface energy to include in the model, no additional extensive analysis of the surface energies of individual pure components (starch, gluten, and lipid) were conducted to explain the increasing or decreasing trend of surface energies.

Table 5-1: Relative surface chemical composition (% Raman intensity) and surface energy of wheat flour samples.

Wheat class	Particle size (μm)	Starch (%)	Protein (%)	Lipid (%)	Dispersive surface energy, γ_d (mJ/m^2)
HRW	<45	72.85 (2.65)c	25.45 (2.23)a	0.80 (0.01)d	30.8
	75-106	78.73 (2.11)b	19.87 (1.57)b	1.38 (0.07)c	32.8
SRW	<45	85.60 (2.25)a	8.30 (0.71)d	2.11 (0.12)a	30.4
	75-106	86.96 (2.35)a	11.93 (1.98)c	1.60 (0.04)b	35.1

Values in parentheses are standard errors. *The same letter in the same column for a given sample indicates no significant difference ($p < 0.05$)

5.3.2. Flow performance of flours with uniform particle size

To establish a correlation between inter-particle cohesiveness and flour flow performance, the Bo_g's and the ff_c's were determined individually for HRW and SRW flours with particle sizes of 75-106, 45-75, and <45 μm, respectively. A negative correlation (r = -0.92) was observed between Bond number and flow function coefficient, which indicates that the Bo_g used in this study has the potential to predict the flowability of wheat flour. A simple linear regression was used to determine the flow function values from the calculated Bond number. Based on the linear regression model, the model parameters (α and β) were estimated for the flours from different wheat classes. The α and β values for HRW flours were found to be 53.68 and 0.43, whereas for SRW flours the values were 63.38 and 0.45, respectively.

The flow function coefficient decreases (poor flow) as the Bond number increases (high inter-particle cohesion) (Table 5-2). The trend is similar for both hard and soft wheat classes. Data presented in Table 2 clearly demonstrates that, all the particle size ranges (75-106, 45-75, and <45 μm) from the both hard and soft wheat classes tend to have flow problems (low experimental ff_c values) based on the classification proposed by Jenike (1964). The particles of 75-106 μm have 'easy flowing behavior' (model ff_c = 6.01 and 5.81 for HRW and SRW, respectively), i.e. these flours are free-flowing low-cohesive particles as they have lower unconfined yield strengths and can yield at lower stresses. Whereas, the particles of 45-75 and <45 μm sizes falls under the category of 'cohesive' and 'very cohesive' category, due to their low flow function coefficient values. It is because of the fact that, the low-cohesive particles can re-orient and move past neighboring particles with greater ease, when compared to that of high cohesive particles (Capece et al., 2015). Reduction in particle size increases the particle surface area per unit mass, thereby creating a greater number of contact points for interparticulate

bonding and additional interparticulate interactions which in turn results in higher cohesion. The other factor for higher cohesion values for < 45 μm particles is due to increase in surface roughness and surface lipid composition (Siliveru et al., 2016). The particle surface roughness could increase the interparticle interaction by increased Van der Waals forces and by mechanical linkages (Landillon et al., 2008). Siliveru et al. (2016) reported that the <45 μm size particles of soft wheats have higher surface lipids due to the association of lipid content with smaller starch granules and also due to presence of free lipids (Morrison and Laignelet, 1983). The presence of higher surface lipid in soft wheats could be another reason for lower ff_c values, as lipids provide necessary sites for the formation of liquid bridges between the individual flour particle surfaces (Neel and Hoseney, 1984b).

The developed model predicts the ff_c values of HRW and SRW flours within narrow particle size range (i.e. 75-106, 45-75, and <45 μm sizes) with high accuracy based on the standard error of prediction (SEP). The average SEP for hard and soft wheat flour were found to be 0.07 and 0.06, respectively. It proves that, reasonable flow pattern approximation of flours within narrow size range can be obtained by using the developed model based on granular Bond number. Similar conclusions were reported on fine flours by Yu et al. (2003) in predicting the flour bed porosity and Capece et al. (2014) in predicting the flow function coefficients.

Table 5-2: Particle properties, granular Bond number, and flow function coefficients of flour samples with narrow particle size range.

Material	Sauter mean diameter, d_{32} (μm)	Asperity diameter, d_{asp} (nm)	True density, ρ (kg/m^3)	Dispersive surface energy, γ_d (mJ/m^2)	Hamaker constant, A (J)	Granular Bond number, Bo_g	Flow function coefficient, ff_c		SEP
							Predicted	Experimental*	
HRW									
<45	35.6	517.9	1469.4	30.8	6.32×10^{-20}	7.23×10^{3}	1.21	1.18 (0.02)	0.04
45-75	62.4	443.9	1478.0	31.8	6.50×10^{-20}	7.41×10^{2}	2.94	3.02 (0.03)	0.08
75-106	85.8	370.0	1487.2	32.8	6.74×10^{-20}	1.80×10^{2}	6.01	5.95 (0.10)	0.10
SRW									
< 45	35.3	516.0	1505.2	30.4	6.24×10^{-20}	7.18×10^{3}	1.17	1.12 (0.03)	0.06
45-75	62.6	486.0	1497.0	32.7	6.72×10^{-20}	7.95×10^{2}	2.86	2.83 (0.11)	0.04
75-106	87.0	456.0	1487.9	35.1	7.20×10^{-20}	2.18×10^{2}	5.81	5.74 (0.07)	0.10

* Flow function coefficient determined using 1 kPa pre-consolidation stress. Values in parentheses are standard errors within replicates.

5.3.3. Predicting the flow performance of flour blends

For predicting the flow behavior of flour blends, the model parameters (i.e. α and β values) determined for uniform particle size of HRW and SRW flours were used and the flow function coefficients were measured for different flour blends (Table 5-3). For HRW samples, with an increase in <45 μm mass fraction in the blend, the flow behavior changed from 'easy flow' (predicted ff_c = 3.96) to 'cohesive' (predicted ff_c = 2.76). Though there is 'no shift' in terms of the flow behavior for soft wheats with an increase <45 μm mass fraction in the mixture, the ff_c values significantly dropped from 3.76 to 2.59. Thus, the bulk flour behavior is substantially affected by <45 μm fraction in the blend. This could be due to the higher surface area of <45 μm (d_{32} = 35 μm) particles. It is a well-known fact that increase in particle surface area per unit mass creates a greater number of contact points which increases the interparticulate bonding there by resulting in higher cohesion. The model predicts the flow function coefficient of all the flour blends with an average standard error of prediction of 0.11 (Table 5-3). The reason for this deviation is that, in this study it was assumed that the cohesion force between the particles was only due to vdW force. So the deviation in the model prediction was only due to the inability to determine the exact cohesion force between particles.

5.3.4. Application of the developed flow prediction model

The experimental values for the flow function coefficient of various compositions of HRW and SRW are shown in Fig. 5-1 and 5-2, respectively, along with the model prediction for any blend composition shown as colored ternary plot. As the ternary diagrams show, the flow behavior of HRW and SRW wheat flours, with different compositions, can be predicted from the particle characteristics. It can be seen from Fig. 5-1 and 5-2 that, with increase in the mass fraction of 75-106 μm particles in the flour mixture the flow behavior of blend tends to move

towards ‘easy flow nature’. It is because of the fact that the low-cohesive particles (75-106 µm size) can re-orient and move past neighboring particles with greater ease, when compared to that of high cohesive particles (<45 µm size) (Capece et al., 2015). Based on the predicted flow behavior, necessary corrective actions such as increase or decrease in sifting time, introduction of different sieve cleaners, or change of sieve cloth can be done to prevent agglomeration of particles which decreases the throughput. If the number of components in mixture increases or if there is significant change in the flour particle parameters due to change in milling conditions, the developed model can significantly reduce experimental work, save material and time in assessing the flow behavior.

The ability to predict the flow behavior based on particle properties can be very useful in the flour sieving process. The multi-component granular Bond number prediction model presented in this study could be extended to any blend of hard and soft wheat flours and provides guidance not only during their sieving but also in other processing operations. The predictive capacity of the model may also be used to identify the right sifter load setting, proportion of blend (i.e. particle size combination), and moisture content of flour to prevent the flour from blinding the screen surfaces.

Table 5-3: Granular Bond numbers and flow function coefficients for ternary mixtures of HRW and SRW flours.

Component	Mass fraction	Fractional surface area	$Bo_{g,\ Mix}$	Flow function coefficient, ff_c		SEP
				Predicted	Experimental	
HRW <45/45-75/75-106	0.333/0.333/0.333	0.219/0.241/0.283	6.20×10^2	3.32	3.34 (0.07)	0.06
	0.166/0.417/0.417	0.109/0.302/0.354	4.37×10^2	3.96	3.85 (0.19)	0.19
	0.417/0.166/0.417	0.274/0.120/0.354	5.73×10^2	3.47	3.39 (0.05)	0.09
	0.417/0.417/0.166	0.274/0.302/0.141	1.02×10^3	2.76	2.62 (0.10)	0.16
SRW <45/45-75/75-106	0.333/0.333/0.333	0.233/0.251/0.288	6.92×10^2	3.24	3.26 (0.04)	0.04
	0.166/0.417/0.417	0.116/0.315/0.360	4.96×10^2	3.76	3.69 (0.12)	0.12
	0.417/0.166/0.417	0.292/0.125/0.360	6.44×10^2	3.32	3.32 (0.04)	0.03
	0.417/0.417/0.166	0.292/0.315/0.144	1.11×10^3	2.59	2.48 (0.16)	0.17

* Flow function coefficient determined using 1 kPa pre-consolidation stress. Values in parentheses are standard errors.

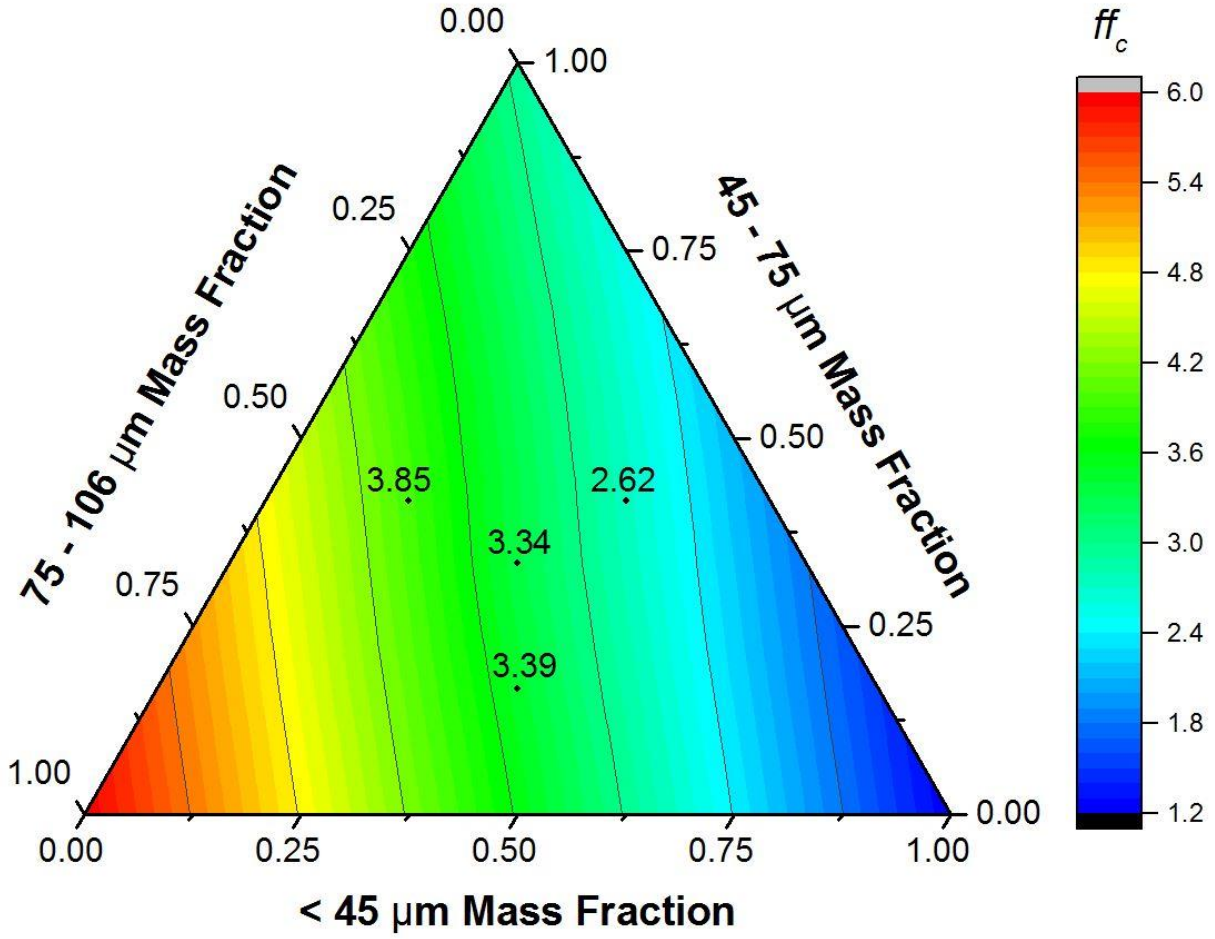

Figure 5-1: Flow function coefficients determined experimentally for ternary mixtures of HRW flour samples (<45, 45-75, and 75-106 µm particle sizes) represented as solid markers. The color gradients represent the flow functions predicted from the developed model.

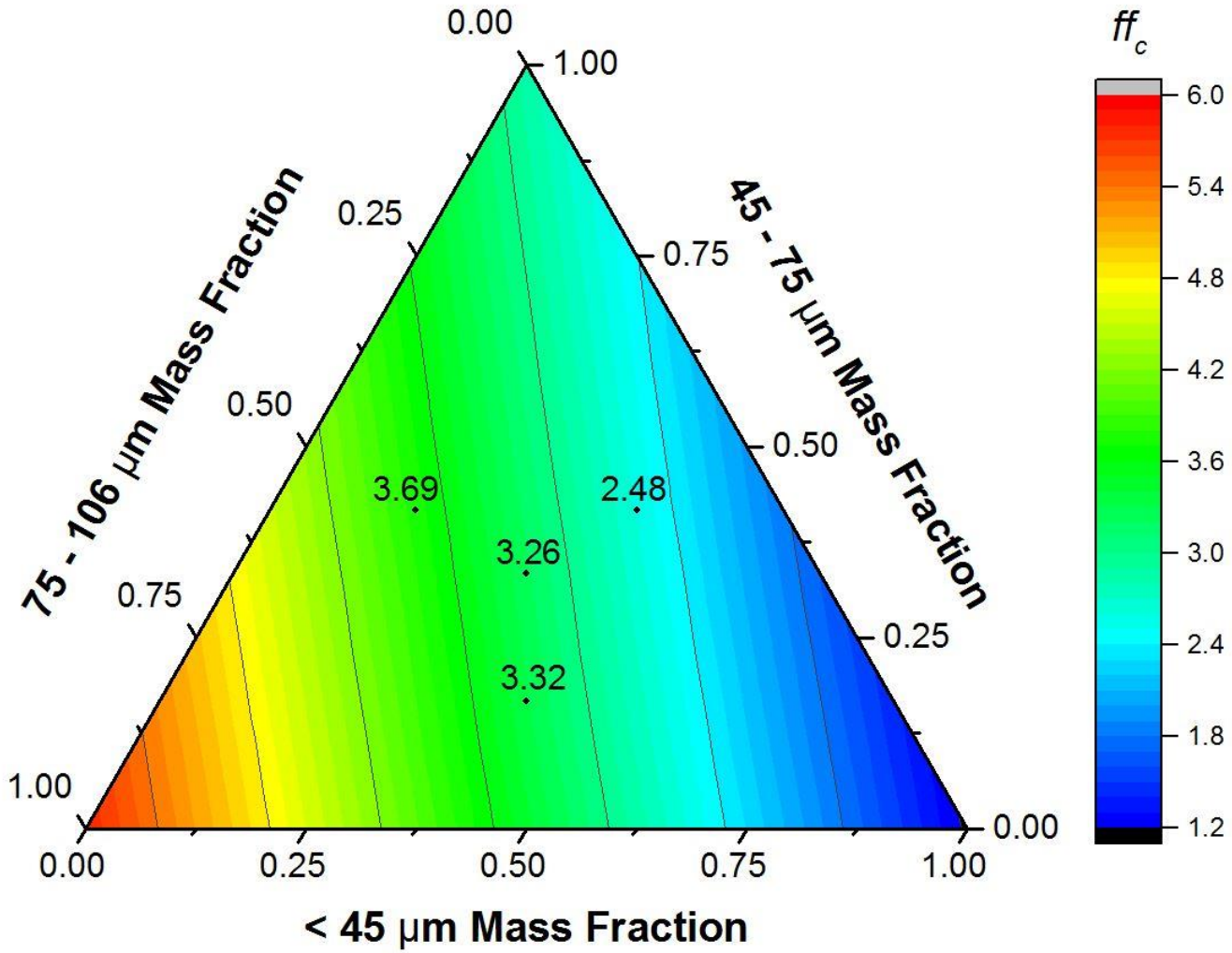

Figure 5-2: Flow function coefficients determined experimentally for ternary mixtures of SRW flour samples (<45, 45-75, and 75-106 µm particle sizes) represented as solid markers. The color gradients represent the flow functions predicted from the developed model.

5.4. Conclusions

Through experimental evaluation and mathematical analysis, this study explained the flow behavior of wheat flour and presented models to predict the flow behavior. Flour particle physical and surface chemical compositions were used to develop the predictions using the granular Bond number. The granular Bond number, defined as the ratio of the vdW force of cohesion to particle weight was successfully used to predict the flow function coefficient. It was also established that the variations in the surface chemical composition of flours could have a significant impact on the flow behavior. Though the variations in the surface chemical composition were not directly included in the model, the variations were addressed using the calculated dispersive surface energies (γ_d), which are a combination of the surface energies of the different components present on the surface.

The granular Bond number concept was also used to successfully predict the flow behavior of hard and soft wheat flour with a larger particle size distribution prepared by mixing flours of different particle size ranges. This modeling effort was found to be more appropriate for fine flours (~ 100 μm size), which are dominated by van der Waals force, and could be extended to other particulate materials by determining the appropriate model parameters.

5.5. References

AACC International. (1988). Approved Methods of Analysis. (Method 26-21.02. Experimental Milling-Buhler Method for Hard Wheat. Method 26-31.01.Experimental Milling-Buhler Method for Soft Wheat Straight-Grade Flour, 11th ed.,). St. Paul, Minnesota.

Andreotti, B., Yoel, F., & Pouliquen, O. (2013). Granular Media, Cambridge University Press, New York.

AOAC International. (2006). Official Methods of Analysis. (17th ed.,). Gaithersburg Maryland.

Bian, Q., Sittipod, S., Garg, A., & Ambrose, R. P. K. (2015). Bulk flow properties of hard and soft wheat flours. *Journal of Cereal Science*, 63, 88–94.

Campbell, G. M. (2007). Roller milling of wheat. *Powder Technology*, 12, 392–425.

Capace, M., Ho, R., Strong, J., & Gao, P. (2015). Prediction of powder flow performance using a multi-component granular Bond number. *Powder Technology*, 286, 561–571.

Capece, M., Huang, Z., To, D., Aloia, M., Muchira, C., Davé, R., & Yu, A. (2014). Prediction of porosity from particle scale interactions: surface modification of fine cohesive powders, *Powder Technology*, 254, 103–113.

Castellanos, A. (2005). The relationship between attractive interparticle forces and bulk behaviour in dry and uncharged fine powders, *Advances in Physics*, 54, 263–376.

CFR. (2013). 21 CFR 137.105: Requirements for specific standardized cereal flours and related products. Code of Federal Regulations, Washington, D.C.

Chen, Y., Yang, J., Dave, R., & Pfeffer, R. (2008). Fluidization of coated group C powders, *AIChE Journal*, 54, 104–121.

Chirone, R., Barletta, D., Lettieri, P., & Poletto, M. (2016). Bulk flow properties of sieved samples of a ceramic powder at ambient and high temperature. *Powder Technology*, 288, 379–387.

Finnie, S. M., Jeanuette, R., Morris, C. F., & Faubion, J. M. (2010). Variation in polar lipid composition among near isogenic wheat lines possessing different puroindoline haplotypes. Journal of Cereal Science, 51, 66–72.

Frenkel, J. (1955). Kinetic theory of liquids, Dover Publications, New York.

Huang, Z., Scicolone, J., Gurumuthy, L., & Davé, R. (2014). Flow and bulk density enhancements of pharmaceutical powders using a conical screen mill: a continuous dry coating device, *Chemical Engineering Science*, 125, 209–224.

Iqbal, T., & Fitzpatrick, J. J. (2006). Effect of storage conditions on the wall friction characteristics of three food powders. *Journal of Food Engineering*, 72, 273–280.

Israelachvili, J. (1992). Intermolecular and Surface Forces, Academic Press, London.

Jallo, L., Chen, Y., Bowen, J., Etzler, F., & Dave, R. (2011). Prediction of inter-particle adhesion force from surface energy and surface roughness, *Journal of Adhesion Science and Technology*, 25, 367–384.

Jenike, A. W. (1964). Storage and Flow of Solids, Bulletin No. 123. Utah Engineering Station, Salt Lake City, Utah.

Kamath, S., Puri, V. M., & Manbeck, H. B. (1994). Flow property measurement using the Jenike cell for wheat flour at various moisture contents and consolidation times. *Powder Technology*, 81, 293–297.

Katainen, J., Paajanen, M., Ahtola, E., Pore, V., & Lahtinen, J. (2006). Adhesion as an interplay between particle size and surface roughness, *Journal of Colloid and Interface Science*, 304, 524–529.

Kuakpetoon, D., Flores, R. A., & Milliken, G. A. (2001). Dry mixing of wheat flours: Effect of particle properties and blending ratio. *LWT - Food Science and Technology*, 34, 183–193.

Kwek, J. W., Siliveru, K., Cheng. S., Xu, Q., & Ambrose, R. P. K. (2016). Zein film functionalized atomic force microscopy and Raman Spectroscopic evaluations on surface differences between hard and soft wheat flour. *Journal of Cereal Science* (In review).

Landillon, V., Cassan, D., Morel, M. H., & Cuq, B. (2008). Flowability, cohesive, and granulation properties of wheat powders. *Journal of Food Engineering*, 86, 178–193.

Liu, F. P., Rials, T. G., & Simonsen, J. (1998). Relationship of wood surface energy to surface composition. *Langmuir*, 14, 536–541.

Morrison, W. R., & Laignelet, B. (1983). An improved colorimetric procedure for determining apparent and total amylose in cereal and other starches. *Journal of Cereal Science*, 1, 9–20.

Neel, D. V., & Hoseney, R. C. (1984a). Sieving characteristics of soft and hard wheat flours. *Cereal Chemistry*, 61, 259–261.

Neel, D. V., & Hoseney, R. C. (1984b). Factors affecting flowability of hard and soft wheat flours. *Cereal Chemistry*, 61, 262–266.

Piot, O., Autran, J. -C., & Manfait, M. (2001). Investigation by confocal Raman microspectroscopy of the molecular factors responsible for grain cohesion in the *Triticum aestivum* bread wheat. Role of the cell walls in the starchy endosperm. *Journal of Cereal Science*, 34, 191–205.

Podczeck, F. (1998). Particle–Particle Adhesion in Pharmaceutical Powder Handling, Imperial College Press, London.

Schultz, J., Lavielle, L., & Martin, C. (1987). The role of the interface in carbon fibre–epoxy composites, *Journal of Adhesion*, 23, 45–60.

Shultz, D. (2008). Powders and Bulk Solids, Springer, Berlin.

Siliveru, K., Kwek, J. W., Lau. G., & Ambrose, R. P. K. (2016). An image analysis approach to understand the differences in flour particle surface and shape characteristics. *Cereal Chemistry*, 93, 234-241.

Simmonds, D. H. (1974). Chemical basis of hardness and vitreosity in the wheat kernel. *Baker's Digest*, 48, 16–29.

Teunou, E., Fitzpatrick, J. J., & Synnott, E. C. (1999). Characterization of food powder flowability. *Journal of Food Engineering*, 39, 31–37.

Yu, A., Feng, C., Zou, R., & Yang, R. (2003). On the relationship between porosity and interparticle forces, *Powder Technology*, 130, 70–76.

Chapter 6 - Discrete Element Method (DEM) Modeling of Wheat Flour Sieving Process

Abstract

Sifting or size separation of flour particle is an important operation in wheat milling process. The flour particles often behave as imperfect solids with discontinuous flow and agglomeration during size separation. Many studies have indicated that the inter-particle cohesion is highly dependent on the particle parameters and significant deviations occur during the sieving process. To further improve the fundamental understanding of powder flow behavior which is essential to the success of sieving, this study presents the development of a discrete element method (DEM) model. The DEM model agreed with the experimental results in terms of the particle size distribution at different sieves. Based on the standard error of prediction (SEP) values in terms of percent weight retained over respective screens ranging from 0.13-9.67, it is demonstrated that the sieving process could be predicted through DEM simulations. The DEM model satisfactorily estimated the sieving performance in terms of weight percentage passing and sieve blinding phenomenon particularly when the effect of particle-particle interactions are significant.

6.1. Introduction

The discrete element method (DEM), developed by Cundall and Strack (1979), is being used as a tool for analyzing quasi-static problems related to granular material handling operations. DEM has increasingly been used in several research areas like engineering, material science, physics, geology, mineralogy, agriculture, and more (Thakur, 2014). Common application of DEM in the grain industry has involved modeling excavator bucket filling

(Coetzee et al., 2007), commingling of grains in bucket elevators (Boac et al., 2010), and in the bulk handling and storage of cereal grains (Gonzalez-Montellano et al., 2012). Another common application of DEM is to study the size reduction and breakage of granular material and agglomerates (Metzger and Glasser, 2013; Cleary, 2001) and modeling the particulate flow on vibrational screens (Dong et al., 2009; Chen and Tong, 2010).

Early research works on sieving were concerned with the establishment of factors influencing screening efficiency, including the prediction of sieving kinetics based on probability theories (Jansen and Glastonbury, 1968; Roberts and Beddow, 1968; Schroeder, 2000; Ricklefs, 2002). Due to the complex nature of particulate materials and the lack of advanced mathematical and experimental techniques applicable to particulate systems a physical understanding of this complex physical process has never been realized. As a result, most published information about sieving has been empirical (Standish, 1985). However, these probabilistic theories fail to account for the effects of inter-particle cohesion on the movement of particles over sieve and initiation of sieve blinding, the factors which have been identified as crucial to sieving performance. A full understanding of these physical phenomena is the key to optimize design and operation of a complex sieving process. Thus, the objective of this study was to develop and validate a DEM model to describe the wheat flour sieving process.

6.2. Materials and Methods

6.2.1. Model setup

The DEM simulations and model development were carried out using EDEM 2.6 software (DEM Solutions Ltd., Edinburgh, UK) installed in an 80-Core Xeon E7-8870 processor with 96 GB RAM in the Beocat computing cluster (Kansas State University, Manhattan, KS).

The DEM working principles are discussed in detail in Chapter 2 (2.4.2). The discussion here is restricted to the operation of the model and the simulation process.

6.2.2. Creating particles

The first step in developing a DEM model, for any process, is to create particles and assign these particles with the definite physical and mechanical properties. As an approximation, the flour particles were assumed to be spherical in shape. Table 6-1 lists the physical and mechanical properties used as input parameters to define the particles. The property value inputs for size (radius), density, and disruptive surface energy were measured using standard techniques. The Poissons ratio, shear modulus (Markauskas et al., 2010; Sarnavi et al., 2013; Weigler et al., 2012), coefficient of restitution, coefficient of static friction, and coefficient of rolling friction (Patwa et al. 2014) were obtained from the literature. The use of this set of selected properties enabled modeling the HRW at 10% and 14% m.c (% w.b.) and SRW at 10% m.c (% w.b.) flours, respectively.

6.2.3. Creating custom factory for particle generation

It is known that in sieving (i.e., a batch process of particle separation) of flours, all the material is introduced on the top screen at same time. To achieve this in the model a custom factory was created as described below:

i) Create a box of same area as that of the screen as mentioned in Table 6-2, at a distance of 5 cm above the top screen (i.e. 10.5 XX).

ii) Define the quantity of flour particles to be created in this geometry box; in this model the quantity of flour was chosen to be 0.01 g for all the simulations.

iii) Once the simulation begins, flour particles, equaling the defined quantity will be created in the box and fall freely onto the top screen.

6.2.4. Defining particle cohesion

After defining the flour particles and developing the custom factory, the cohesion between particles is defined. The JKR (Johnson-Kendall-Roberts) model is a commonly used contact model to implement cohesive forces between fine particles (Morrissey, 2013). The Hertz-Mindlin with JKR model was found to be appropriate and this model is available by default in EDEM (DEM Solutions, 2016). The current model accounts for the influence of van der Waals forces within the contact zone, and allows modeling of cohesive dry powders. For calculating the tangential elastic, normal and tangential dissipation forces, the model adapts the calculation procedure from Hertz-Mindlin (no slip) contact model. In JKR cohesion model, the normal force depends on the normal overlap (δ) and the interaction parameter i.e. surface energy (γ) and expressed as (DEM Solutions, 2013):

$$f_{JKR} = -4\sqrt{\pi\gamma E^*}\, a^{\frac{3}{2}} + \frac{4E^*}{3R^*}\, a^3 \qquad (6\text{-}1)$$

$$\delta = \frac{a^2}{R^*} - \sqrt{4\pi\gamma a / E^*} \qquad (6\text{-}2)$$

where, the equivalent Young's Modulus (E^*), and the equivalent radius (R^*) are defined as (DEM Solutions, 2013):

$$\frac{1}{E^*} = \frac{(1-\nu_i^2)}{E_i} + \frac{(1-\nu_j^2)}{E_j} \qquad (6\text{-}3)$$

$$\frac{1}{R^*} = \frac{1}{R_i} + \frac{1}{R_j} \qquad (6\text{-}4)$$

where, the equivalent E_i, v_j, a and R_i are the Young's Modulus, Poisson ratio, contact radius, and radius of each sphere in contact, respectively.

The maximum gap between the particles with non-zero force is given by (DEM Solutions, 2013):

$$\delta = \frac{a_c^2}{R^*} - \sqrt{4\pi\gamma a_c / E^*} \quad (6\text{-}5)$$

$$a_c = \left[\frac{9\pi\gamma R^{*2}}{2E^*}\left(\frac{3}{4} - \frac{1}{\sqrt{2}}\right)\right]^{\frac{1}{3}} \quad (6\text{-}6)$$

The advantage of the EDEM Hertz-Mindlin JKR cohesion model is that, it provides attractive cohesive force even if the particles are not in physical contact. The critical pull-off force, the force required to separate the two contacting particles is defined as:

$$P_{JKR} = -\frac{3}{2}\pi\gamma R^* \quad (6\text{-}7)$$

where, the equivalent γ is the surface energy and R^* is the equivalent radius as defined in equation (6-5).

6.2.5. Model input particle properties

The flour samples from hard red winter (HRW) and soft red winter (SRW) wheat were used in this study, because they differ in their hardness, chemical composition, particle size distribution, and breakage pattern. The flour sample preparation is discussed in detail in Chapter 3 (3.2.1). To address the variation in moisture content of flour that occurs during the wheat milling process, the HRW flour samples were conditioned to 10 and 14% m.c (w.b.). The higher moisture content (14% w.b.) was achieved by placing the flour samples in a relative humidity (rh) chamber maintained at 50-55% rh and 25 °C for 4-5 hr. The lower moisture content (10% w.b.) was achieved by drying the samples at room temperature. The flour moisture content was

determined using the AOAC standard 925.10 (AOAC International, 2006) by drying 2-3 g of the sample in a hot air oven at 130 °C for 60 min.. The physical and mechanical properties needed as input parameters for the model are given in Table 6-1.

The average particle diameter of HRW and SRW flour samples was measured using laser diffraction (Horiba LA-910, Horiba, Ltd., Kyoto, Japan) based on volume distribution. The samples were diluted (2 g in 20 mL) by mixing with de-ionized water then agitated by a set of agitating blades at 400 rpm for 5 min. To ensure proper dilution of the sample in the distilled water agitation was performed. To break down aggregated flour particles and to purge out the air bubbles, instrument uses ultrasonic vibrations (39 kHz) after agitation. The average particle diameter values are reported in Table 6-1.

The true density of the flour samples was measured using a helium gas pycnometer (AccuPync II 1340, Micromeritics, Norcross, Ga.). The true density was calculated from the weight and volume occupied by the solid particles. Ten measurements were taken for each sample and the mean was reported in Table 6-1.

6.2.6. Sieve geometry

The laboratory scale sieve stack geometry was created in PTC Creo Parametric design software (NxRev, Fremont, CA, USA) using a Great Western lab sifter (Great Western Manufacturing, Leavenworth, KS, USA) as the model (Figure 6-1) and imported into EDEM software (DEM Solutions, Edinburgh, UK) as a .stp extension file (Figure 6-1 (a) and (b)). Posner and Hibbs (2005) stated that the inefficient separation of flour particles in industrial scale rebolt sieves was because of the fact that most of the separation is done by first two or three sieves while remaining sieves remove very little. Similar to an industrial scale flour sifter, a

laboratory sieve stack consisting of 10.5 XX (125 µm), 12 XX (112 µm), 14 XX (95 µm), 20 XX (75 µm), and 25 XX (63 µm) sieves was used in this study.

The specifications of sieve stack used for the model development and simulation are given in Table 6-2.

Table 6-1: Property input values used for particles and sieve stack.

Moisture content, % w.b.	Average particle diameter, µm	Density, kg/m^3	Dispersive surface energy[a], mJ/m^2	Poissons ratio[b]	Shear modulus[b], MPa	Coefficient of restitution[c]	Coefficient of static friction[c]	Coefficient of rolling friction[c]
HRW								
10.00	72	1485.14 (2.21)	32.8	0.20	76.5	0.25	0.43	0.50
14.00	78	1473.46 (1.89)	32.8	0.20	76.5	0.27	0.43	0.55
SRW								
10.00	47	1491.35 (1.61)	30.4	0.20	76.5	0.28	0.44	0.39
Sieve cloth, poly amide								
	-	1140	-	0.41	760	-	-	-

*The respective mean values used in the simulation were obtained [a] from Table 5-1; [b] from Markauskas et al., 2010; Sarnavi et al., 2013; Weigler et al., 2012; [c] from Patwa et al. (2014).

Note: For all the properties only mean values were used for simulations.

Table 6-2: Specification of sieve parameters used for simulation and validation.

Sieve cloth	Poly amide
Weaving pattern	XX
Sieve stack	10.5 XX (125 µm), 12 XX (112 µm), 14 XX (95 µm), 20 XX (75 µm), and 25 XX (63 µm)
Sieve height, mm	25.4
Sieve area*, mm^2	11.22
Quantity of flour used for validation**, gm	100
Quantity of flour used for simulation**, gm	0.01
Motion of the sieve stack	Circulatory, with diameter of 10.5 cm
Frequency of the sieve stack, rpm	180

*Note: For simulation purpose the original sieve area was scaled down to 1/10000 times of the experimental size.

**Prof. Zworykin, 1911 stated that quantity of flour to be sifted is directly proportional to area of the sieve. For simulation the quantity of flour to be sifted was also scaled down by 1/10000 of the experimental quantity to match the simulated area.

6.2.7. Model validation

The Great Western lab scale sieve shaker and standard sieves shown in Figure 6-1 (a) (Great Western Manufacturing, Leavenworth, KS, USA) were used for the validation of sieving trials. The sieve stack consisted of five screens: PA 10.5 XX (125 µm), PA 12 XX (112 µm), PA 14 XX (95 µm), PA 20 XX (75 µm), PA 25 XX (63 µm) and a pan. Relative humidity plays a significant role on the flow behavior of wheat flour during the sieving process (Neel, 1982). To overcome this issue, all the experiments were conducted at room condition where the relative humidity was maintained at 48 ± 0.5%. A 100 g sample was used in all the sieving tests. The amount of flour retained over each screen was weighed at 5, 10, 15, and 20 s time intervals and

reported as percentage retained and were compared with the model results. All the lab scale sieving tests were performed in triplicate and the mean values were reported.

The measure of accuracy of the predictions (i.e., mean standard deviation between the predicted and actual values) was estimated by calculating the standard error (SEP).

$$\text{SEP} = \sqrt{\frac{\sum(Y-Y')^2}{N}} \qquad (6\text{-}8)$$

where, Y = experimental value, Y' = predicted value, and N = number of observations.

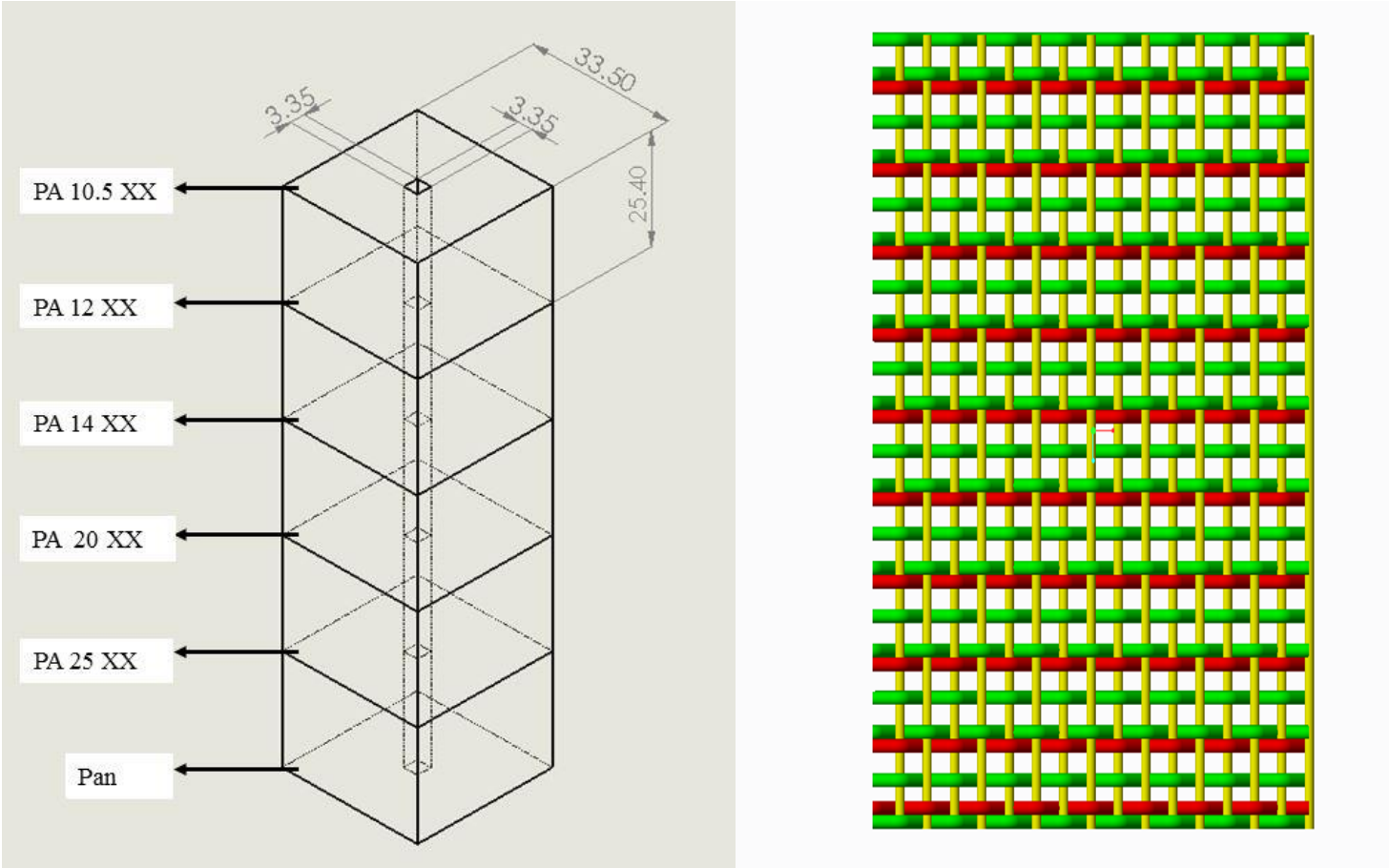

(a) (b)

Figure 6-1: (a) Sieve stack geometry used in the simulation and (b) Weaving pattern (XX style) of screen cloth.

*Note: Dimensions in the figure are in mm.

6.3. Results and Discussions

The model simulated 20 s of sieving which took an average of 916.4 h for completion. Upon completion of the simulations, the mass and particle size data for all the particles at the five screens and pan at each time step were exported into a Microsoft Excel spread sheet (Microsoft Corporation, WA, USA). The percentage of mass retained over each screen obtained from model prediction and lab scale validation trials for HRW samples at 10 % m.c, 14 % m.c, and SRW samples at 10 % m.c are presented in tables 6-3, 6-4, and 6-5, respectively. Though five screens were used in the study, the separation is done by first two or three sieves as shown in Tables 6-3, 6-4, and 6-5. So, the discussion was limited to PA 10.5 XX (125 µm), PA 12 XX (112 µm), and PA 14 XX (95 µm) sieves. For HRW flour sample at 10 % m.c, the model underpredicted the percentage of mass retained over 125 µm screen at all the time steps (Table 6-3). The reason for this deviation is that, during experimental validation, the flour is placed directly on the screen surface and the inter-particle cohesion already existed between the particles. Whereas, during model implementation the flour particles were created individually in the particle generation factory and the inter-particle cohesion was then initiated through the Hertz-Mindlin JKR cohesion model on the screen surface once all the created particles reached the screen. Figure 6-2 shows the particle generation and separation of undersized particles through 125 µm sieve at 0.1 s. Before the initiation of inter-particle cohesion some smaller flour particles passed through the 125 µm screen on to the bottom sieves. This led to over prediction of the percentage of mass retained over lower screen decks of 95, 75, 63 µm, and pan. The same trend was observed for all the simulations irrespective of moisture content and type of wheat class (Tables 6-3, 6-4, and 6-5). The standard errors of prediction (SEP) were within acceptable

limits with the maximum SEP of 9.27% at top screen (125 μm) for HRW flour at 10% moisture level.

Table 6-3: Experimental and predicted particle size distribution of HRW flour at 10 % moisture content.

Screen size, µm	Sieving time								SEP
	At 5 s		At 10 s		At 15 s		At 20 s		
	Predicted	*Experimental*	*Predicted*	*Experimental*	*Predicted*	*Experimental*	*Predicted*	*Experimental*	
125	78.38	84.70 (0.62)	74.21	78.45 (0.29)	70.19	76.37 (0.12)	70.19	75.88 (0.02)	9.27
112	7.49	10.59 (0.70)	11.26	13.08 (0.18)	15.21	12.77 (0.06)	15.19	10.93 ((0.24)	3.65
95	5.87	3.19 (0.06)	6.00	4.50 (0.45)	5.92	4.65 (0.01)	5.94	5.74 (0.13)	1.68
75	3.16	0.93 (0.02)	3.27	2.04 (0.13)	3.29	2.91 (0.04)	3.26	3.02 (0.08)	1.29
63	3.92	0.45 (0.07)	4.03	1.55 (0.36)	4.14	1.95 (0.08)	4.16	3.04 (0.16)	2.48
Pan	1.16	0.15 (0.07)	1.23	0.40 (0.12)	1.26	1.36 (0.18)	1.26	1.40 (0.11)	0.67

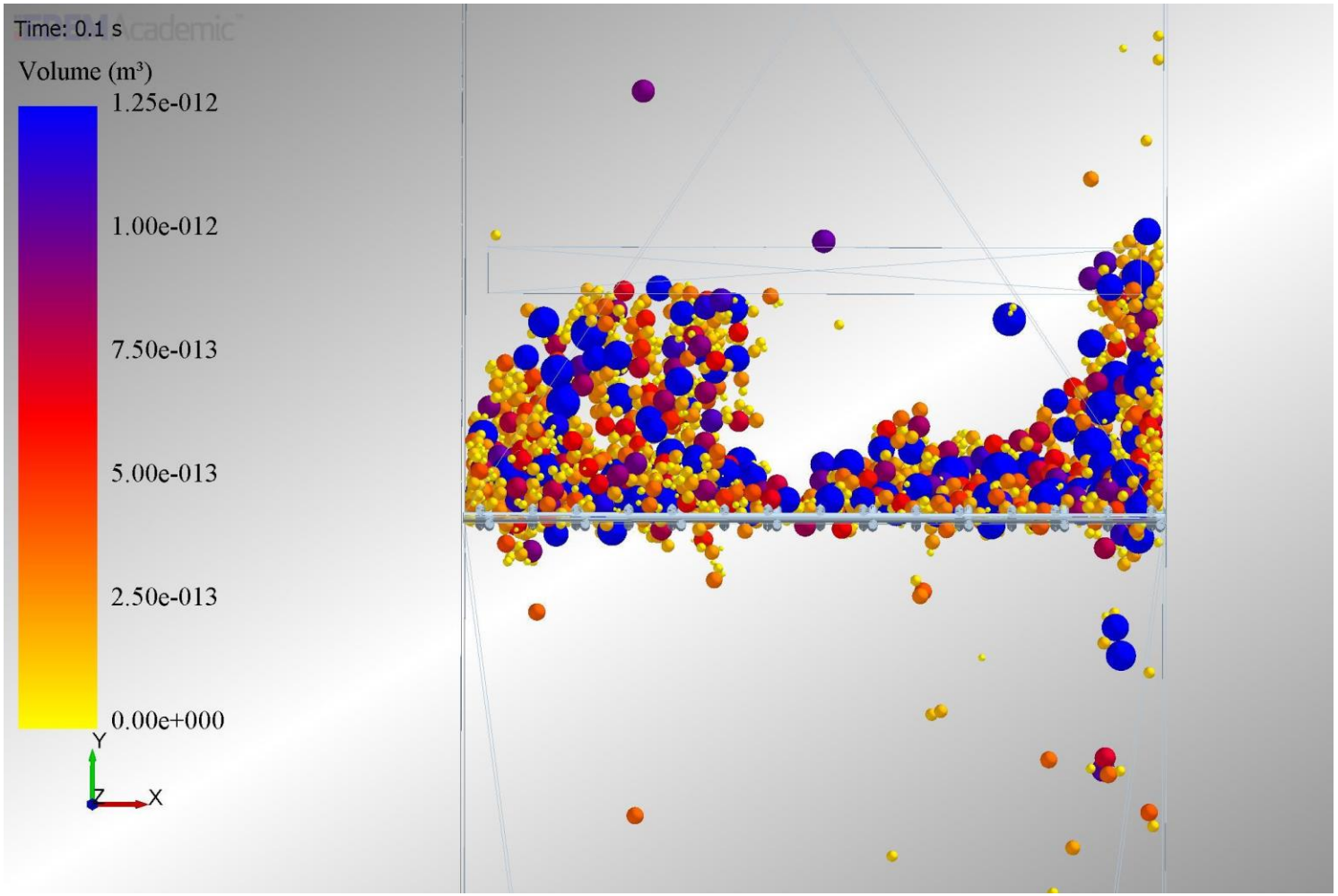

Figure 6-2: Wheat flour particles (HRW at 10% m.c) generation and segregation over 125 µm screen at simulation time = 0.1 s.

Table 6-4: Experimental and predicted particle size distribution of HRW flour at 14 % moisture content.

Screen size, µm	Sieving time								SEP
	At 5 s		At 10 s		At 15 s		At 20 s		
	Predicted	*Experimental*	*Predicted*	*Experimental*	*Predicted*	*Experimental*	*Predicted*	*Experimental*	
125	88.6	93.40 (0.14)	87.92	91.22 (0.78)	87.88	87.56 (0.42)	87.87	87.18 (0.49)	3.55
112	4.48	5.96 (0.28)	4.51	8.05 (0.42)	4.26	11.25 (0.14)	4.24	11.62 (0.38)	5.75
95	2.80	0.64 (0.07)	3.04	0.74 (0.07)	3.23	1.18 (0.71)	2.96	1.20 (0.02)	2.22
75	1.93	0.00	1.74	0.00	1.79	0.00	1.92	0.00	1.85
63	1.63	0.00	1.98	0.00	2.04	0.00	2.19	0.00	1.97
Pan	0.56	0.00	0.80	0.00	0.80	0.00	0.82	0.00	0.75

Based on the percentage mass retained (DEM predicted data) over the 125 µm screen after 15 s and 20 s simulation time, it was understood that there was no further separation of particles after 15 s due to the agglomeration of particles over the sieve surface (Table 6-3). A similar trend was observed during the lab scale validation, where the percentage mass retained over the 125 µm screen dropped only about by 0.5%, with increase in sieving time from 15 s to 20 s (Table 6-3). As can be seen in Figure 6-3, the agglomerates tend to block and lodge in the mesh, indicating the initiation of sieve blinding.

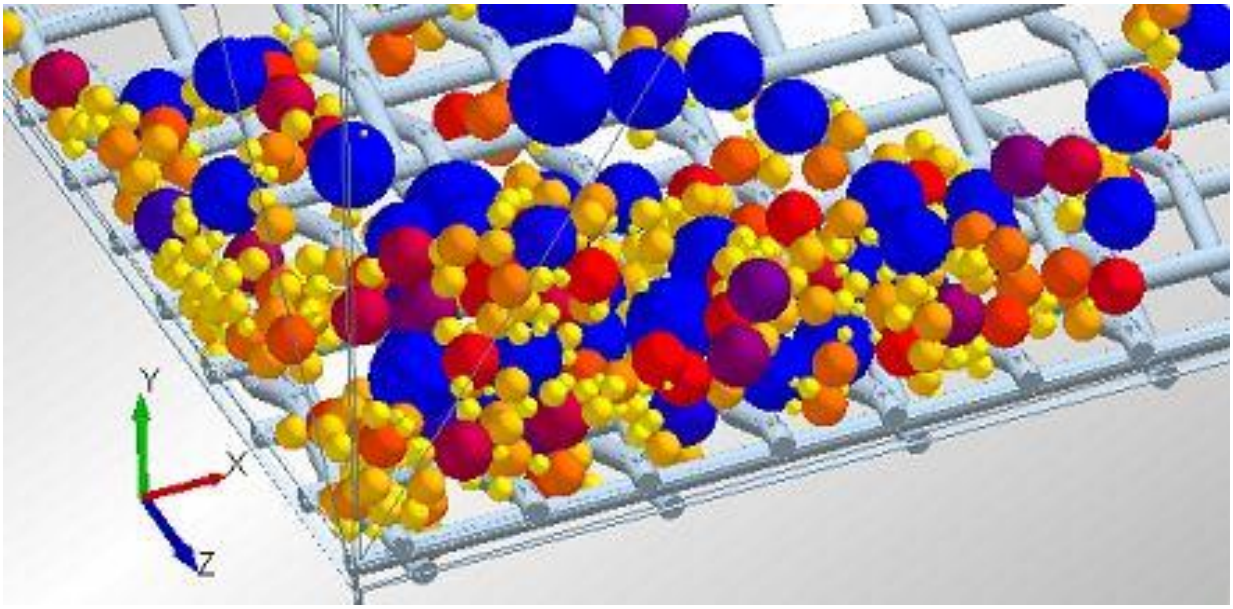

Figure 6-3: Flour particle agglomeration and initiation of sieve blinding over PA 10.5 XX (125 µm) screen at time = 15 s.

As expected, the increase in moisture content from 10 to 14 % w.b. reduced the sieving efficiency, due to the increase in inter-particle cohesion (Table 6-4). Teunou and Fitzpatrick (1999) and Iqbal and Fitzpatrick (2006) observed that with the increase in moisture content from 12 to 14 % w.b, cohesion between wheat flour particles increased due to the formation of liquid bridges . With the increase in flour moisture content, the percent mass retained on 125 µm sieve increased by 12 % (Table 6-3 and 6-4). This might be due to the formation of liquid bridges,

which in turn increased the inter-particle cohesion (Teunou and Fitzpatrick, 1999). As the SEP values indicate, the model was able to predict the sieving process at higher moisture content. The maximum SEP of 4.75% was recorded for 12 XX (112 μm) screen (Table 6-4). The reason for this deviation is that the particles that are smaller than 125 μm size passed through the 125 μm screen and retained on the 112 μm size screen, before the initiation of inter-particle cohesion by the model. By comparing the percentage mass retained from model and lab scale validation data over the 125 μm screen after 10 and 15 s sieve operation, it was understood that there was no further separation of particles after 10 s (Table 6-4). This was due to the formation of agglomerates over the 125 μm screen surface (Figure 6-3). From, this a conclusion can be put forward that, for HRW flour particles at 14 % m.c, the sieve blinding was initiated at 10 s. Based on the model and experimental validation of HRW 10 % and 14 % m.c flours, it could be concluded that increment in moisture level not only increased the percentage of mass at the screen with largest opening (i.e. 125 μm), but also led to the early initiation of sieve blinding by 5 s (Table 6-3 and 6-4).

Table 6-5 shows the percentage of mass retained over each screen obtained from model prediction and lab scale validation trials for SRW samples at 10 % m.c. The percentage of mass retained over top screen (i.e. 125 μm) for SRW particles is about 8 % greater (Table 6-5) than that of HRW samples at 10% m.c (Table 6-3), that followed the trend observed in lab scale experiments. Neel and Hoseney (1984) reported that the soft wheat flours sieving rate is 50% lower than that of hard wheat flours due to the differences in particle size and higher cohesion of soft wheat flours. It was initially expected that, as the particle size distribution of the SRW flours was less than HRW flours, there may be greater possibility of smaller sized particles to pass through the 125 μm screen. However, this was not observed in the prediction model as indicated

by the lower SEP value of 2.85% for 125 µm screen (Table 6-5). This indicates that, the Hertz-Mindlin JKR cohesion model used in this study is suitable for simulating the sieving process of wheat flours. Further investigation, based on the percentage mass retained over 125 µm from the model and the experiments reveal that after 10 s and 15 s sieve operation there was no further separation of particles after 10 s (Table 6-5). This was due to the formation of agglomerates over the 125 µm screen surface, which led to clogging of sieve apertures as shown in Figure 6-4. It could be concluded that, for SRW flour particles at 10% m.c, the sieve blinding could initiate at 10 s.

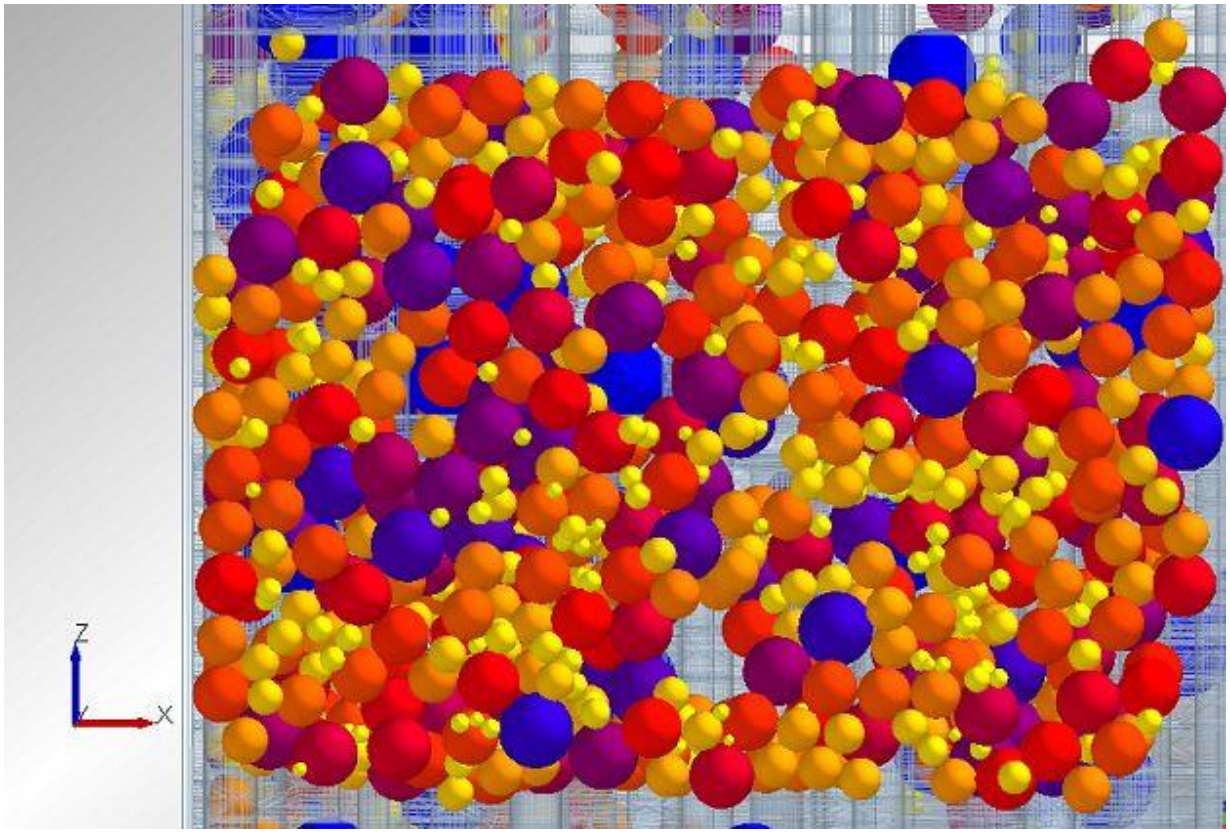

Figure 6-4: Flour particle agglomeration and initiation of sieve blinding over PA 10.5 XX (125 µm) screen at time = 10 sec.

Table 6-5: Experimental and predicted particle size distribution of SRW flour at 10 % moisture content.

Screen size, µm	Sieving time								SEP
	At 5 Sec		At 10 Sec		At 15 Sec		At 20 Sec		
	Predicted	*Experimental*	*Predicted*	*Experimental*	*Predicted*	*Experimental*	*Predicted*	*Experimental*	
125	80.46	84.81 (0.28)	78.93	76.28 (0.22)	78.86	73.59 (0.37)	78.84	73.27 (0.02)	4.61
112	16.47	13.66 (0.21)	17.65	21.82 (0.36)	17.71	24.36 (0.23)	17.72	24.14 (0.12)	5.28
95	1.90	1.13 (0.07)	2.12	1.44 (0.07)	2.13	1.59 (0.14)	2.14	2.04 (0.21)	0.59
75	0.76	0.00	0.82	0.45 (0.07)	0.83	0.45 (0.07)	0.83	0.55 (0.07)	0.37
63	0.30	0.00	0.35	0.00	0.35	0.00	0.35	0.00	0.34
Pan	0.11	0.00	0.13	0.00	0.13	0.00	0.13	0.00	0.13

6.4. Conclusions

The DEM modeling technique was used to understand the wheat flour sieving process. The Hertz-Mindlin JKR cohesion model was used in the model development to incorporate inter-particle cohesion between the flour particles. The prediction model was validated using a lab scale sifter. The prediction model under predicted the percentage of flour retained over 10.5 XX screen (125 µm size) irrespective of the wheat class and moisture level. This was because of the creation of individual flour particles over the screen surface and delay in the initiation of inter-particle cohesion through Hertz-Mindlin JKR cohesion model, which led to the passage of smaller particles from the 125 µm screen. The predicted percentage of mass retained over 125 µm screen increased with increase in moisture level and it also led to the early initiation of sieve blinding, as was observed during validation trials. The predicted percentage of mass retained over 125 µm screen was higher for soft wheat flours compared to hard wheat flours. Based on the acceptable standard error of prediction values, it could be concluded that DEM modeling with Hertz-Mindlin JKR cohesion model is suitable for predicting the particle separation during wheat flour sieving process, for flours from different wheat classes and at different moisture levels.

6.5. References

AACC International. (1988). Approved Methods of Analysis. (Method 26-21.02. Experimental Milling-Buhler Method for Hard Wheat. Method 26-31.01.Experimental Milling-Buhler Method for Soft Wheat Straight-Grade Flour, 11th ed.,). St. Paul, Minnesota.

AACC International. (1999). Approved Method of Analysis. (Methods 08-01.01; 30-25.01; 32-10.01; 46-30.01; 76-30.02, 11th ed.,). St. Paul, Minnesota.

AOAC International. (2006). Official Methods of Analysis. (17th ed.,). Gaithersburg Maryland.

Bian, Q., Sittipod, S., Garg, A., & Ambrose, R. P. K. (2015). Bulk flow properties of hard and soft wheat flours. *Journal of Cereal Science*, 63, 88–94.

Boac, J. M., Casada, M. E., Maghirang, R. G., & Harner, J. P., III. (2010). Material and interaction properties of selected grains and oilseeds for modeling discrete particles. *Transactions of ASABE*, 53, 1201–1216.

Campbell, G. M., Fang, C., & Muhamad, I. I. (2007). On predicting roller milling performance VI - Effect of kernel hardness and shape on the particle size distribution from first break milling of wheat. *Food and Bioproducts Processing*, 85, 7–23.

Chen, Y. H., & Tong, X. (2010). Modeling screening efficiency with vibrational parameters based on DEM 3D simulation. *Mineral Science Technology*, 20, 615–620.

Cleary, P. W. (2001). Recent advances in DEM modelling of tumbling mills. *Minerals Engineering*, 14, 1295–1319.

Coetzee, C. J., Basson, A. H., & Vermeer, P. A. (2007). Discrete and continuum modelling of excavator bucket filling. *Journal of Terramechanics*, 44, 177–186.

Cundall, P. A., & Strack, D. L. (1979). A discrete numerical model for granular assemblies. *Geotechnique*, 1, 47–65.

DEM Solutions. (2013). EDEM 2.5 User Guide. DEM Solutions, Ltd., Edinburgh, UK.

Dong, K. J., Yu, A. B., & Brake, I. (2009). DEM simulation of particle flow on a multi-deck banana screen. *Mineral Engineering*, 22, 910–920.

Gonzalez-Montellano, C., Fuentes, J. M., Ayuga-Tellez, E., & Ayuga, F. (2012). Determination of the mechanical properties of maize grains and olives required for use in DEM simulations. *Journal of Food Engineering*, 111, 553–562.

Iqbal, T., & Fitzpatrick, J. J. (2006). Effect of storage conditions on the wall friction characteristics of three food powders. *Journal of Food Engineering*, 72, 273–280.

Jansen, M. L., & Glastonbury, J. R. (1967). The size separation of particles by screening. *Powder Technology*, 1, 334–343.

Kozmin, P. A. (1917). Flour milling. D. Van Nostrand Company. New York. USA. pp. 387-388.

Markauskas, D., Kacianauskas, R., Dziugys, A., & Navakas, R. (2010). Investigation of adequacy of multi-sphere approximation of elliptical particles for DEM simulations. *Granular Matter*, 12, 107–123.

Metzger, M. J., & Glasser, B J. (2013). Simulation of the breakage of bonded agglomerates in a ball mill. *Powder Technology*, 237, 286–302.

Morrissey, J. P. (2013). *Discrete element modelling of iron ore pellets to include the effects of moisture and fines.* Unpublished PhD Thesis, The University of Edinburgh, Scotland.

Neel, D. V., & Hoseney, R. C. (1984). Sieving characteristics of soft and hard wheat flours. *Cereal Chemistry*, 61, 259–261.

Patwa, A., Malcolm, B., Wilson, J., & Ambrose, R. P. (2014). Wheat mill stream properties for discrete element method modeling. *Transactions of the ASABE*, 57, 891–899.

Ricklefs, R. (2002). New NOVA sieve applications and equipment. *Association of Operative Millers Technical Bulletin*, August, 7825.

Roberts, T. A., & Beddow, J. K. (1968). Some effects of particle shape and size upon blinding during sieving. *Powder Technology*, 2, 121–124.

Sarnavi, H. J., Mohammadi, A. N., Motlagh, A. M., & Didar, A. R. (2013). DEM model of wheat grains in storage considering the effect of moisture content in direct shear test. *Research Journal of Applied Sciences, Engineering and Technology*, 5, 829–841.

Schroeder, J. (2000). The evolution of sifting media and its effect on sifter performance and sieve frame design. *Association of Operative Millers Technical Bulletin*, May, 7451.

Siliveru, K., Kwek, J.W., Lau. G., & Ambrose, R.P.K. (2016). An image analysis approach to understand the differences in flour particle surface and shape characteristics. *Cereal Chemistry*, 93, 234–241.

Standish, N. (1985). The kinetics of batch sieving. *Powder Technology*, 41, 57–67.

Teunou, E., & Fitzpatrick, J. J. (1999). Effect of relative humidity and temperature on food powder flowability. *Journal of Food Engineering*, 42, 109–116.

Thakur, S. C. (2014). *Mesoscopic discrete element modelling of cohesive powders for bulk handling applications.* Unpublished PhD Thesis, The University of Edinburgh, Scotland.

Wang, L., & Flores, R. A. (2000). Effects of flour particle size on the textural properties of flour tortillas. *Cereal Chemistry*, 31, 263–272.

Weigler, F., Scaar, H., & Mellmann, J. (2012). Investigation of particle and air flows in a mixed flow dryer. *Drying Technology*, 30, 1730–1741.

Chapter 7 - Summary of Conclusions and Discussion

7.1. Restatement of Dissertation Goals

Wheat milling involves a series of grinding and sifting operations, where the bran and germ layers are separated from the endosperm and subsequently reducing the size of the endosperm into flour. To ensure the quality of end products made from flour, a miller aims to produce the flour at specific particle size without bran contamination in it. Sieving process is an important unit operation in the wheat milling process that influences the production of quality flour. There are different machine parameters and wheat flour characteristics that directly affect this process which have been discussed in Section 2.2 of this dissertation.

The aim of this dissertation work was to understand the flour particle properties that influence the inter-particle cohesion in order to improve the size based separation process. The specific objectives as stated in Chapter 1 were:

1. Determine the surface physical and chemical characteristics of hard and soft wheat flours.
2. Determine the significance of particle size, moisture content, sifter load, and chemical composition on bulk cohesion of wheat flours.
3. Develop a correlation to predict the flow behavior of wheat flours based on the particle physical and chemical characteristics.
4. Develop and validate a discrete element method (DEM) model to describe the wheat flour sieving process.

In this part of dissertation, a project overview is described in Section 7.2. In Section 7.3 the major findings from the experimentation and the modeling approaches are discussed. Suggestions on possible future work in this research area based on the questions evolved while carrying out this dissertation work are discussed in Section 7.4.

7.2. Project Overview

Chapter 1 includes a discussion on the rationale behind undertaking this study, the research hypothesis, objectives, and goals. The studies and results available in literature explaining the factors affecting cohesion of granular systems were reviewed in Chapter 2. The effects of moisture content, particle size distribution, morphology, surface characteristics, and type of wheat class on cohesion were discussed in detail. Modeling and experimental approaches developed by various researchers to predict the cohesive/flow behavior of fine powders were also detailed. In addition, the DEM modeling technique, its working principle, different cohesive contact models, and their applicability were also provided in Chapter 2.

Chapter 3 highlights the 1st research objective on determination of the surface physical and chemical characteristics of hard and soft wheat flours. The procedures used for the measurement of these properties namely surface lipid content, morphology of flour particles, surface topography measurements: fractal analysis (at macroscopic level) and surface roughness quantification (at microscopic level) were described. All the characteristics were measured for flour from five classes of wheat (hard red spring [HRS], hard red winter [HRW], hard white winter [HWW], soft red winter [SRW], and soft white winter [SWW]).

In Chapter 4, the significance of physical characteristics, chemical composition, and variation in sifter load on bulk cohesion of wheat flours were discussed. The experimentally measured bulk cohesion and flow function values of flours from five different wheat classes at various moisture contents, particle sizes, and sifter loads were presented. The effect of chemical composition of wheat flour on the bulk cohesion was also described.

A part of Chapter 5 included the procedures used for the calculation of particle physical properties, surface chemical composition, and flow function coefficient. Remaining part of this

Chapter discussed the development of mathematical model to predict the flow behavior of flour samples with narrow particle size ranges and flour blends. The model was found to predict the flow behavior of wheat flours within acceptable limits.

Chapter 6 focused on the development of the DEM model to understand the wheat flour sieving process. This chapter discussed the development of a DEM model by using the Hertz-Mindlin with Johnson-Kendall-Roberts (JKR) contact model for the implementation of inter-particle cohesion between the flour particles. The physical and surface properties needed as input parameters were measured and used in the model development and simulation. The model simulation results were validated with the lab scale sieving tests. The model was found to predict the sieving efficiency of wheat flours with acceptable standard error of prediction.

7.3. Discussion of Major Findings

Microscopic and macroscopic approaches were used to understand the inter-particle cohesion of wheat flours at particle and at bulk level. The effects of moisture content, particle size distribution, morphology, surface characteristics, type of wheat class, and sifter load on inter-particle cohesion were quantified and then mathematical models were developed to explain the flow behavior during size based separation process.

7.3.1. Surface characteristics of wheat flours

The objective of measuring different surface physico-chemical characteristics of wheat flours was to develop an understanding of particle cohesion as influenced by the surface properties. The surface lipid content increased with particle size in hard wheat flours but decreased in soft wheat flours. Surface lipid content increases the cohesion between flour particles and could limit the loading rate in sifters. The fractal dimension and surface roughness

results confirmed that the soft wheat flour particles have higher surface roughness compared with flour particles from hard wheats. The surface morphology results confirmed that flour particles were irregular in shape irrespective of their wheat class and particle size. The protein fragments attached to the spherical starch particles resulted in aspherical flour particles. The surface lipid and roughness data indicates that soft wheat flours will be more cohesive and could increase the stickiness and agglomeration, limiting the flowability characteristics. For example, during size-based separation processes, percolation of smaller particles through bigger particles is an important phenomenon. Higher surface roughness could hinder the percolation owing to interlocking of soft wheat flour particles.

7.3.2. Bulk cohesion of wheat flours

The aim of this study was to quantify the effects of moisture content, particle size, sifter load, and chemical composition on the shear flow properties of wheat flour. The physical independent variables (moisture content, particle size, and sifter load) and chemical composition (damaged starch, protein, and fat) were highly correlated with the shear flow properties (cohesion and flow function). This demonstrated that each parameter had a significant contribution on the cohesion and flowability of wheat flour. Increase in moisture content above 12% (wet basis) and reduction in particle size of flour below 45 μm shifted the flowability of wheat flour from ‘easy flowing’ to ‘very cohesive’. The sifter load of 1.0 kPa was found to be appropriate for wheat flour sieving process. Increase in sifter load above 1.0 kPa, leads to increase in inter-particle cohesion and thus reduces the flowability. The chemical components (protein and fat) had mixed effects on the cohesive properties of hard and soft wheat flours and needs further investigation to understand the effects of composition on the cohesive properties.

7.3.3. Prediction of flow behavior of wheat flours

Flour particle physical and surface chemical compositions were used to develop a model for predicting the wheat flour flow behavior using the granular Bond number. Based on the surface component measurements (% Raman intensity values), it was established through this study that, along with other physical characteristics the surface chemical composition is also significant contributor for cohesiveness of wheat flour. In the development of prediction model, to address the variation in the surface chemical composition, the dispersive surface energies (γ_d) were calculated and used as an input parameter. The granular Bond number, defined as the ratio of the vdW force of cohesion to particle weight was successfully used to predict the flow function coefficient, a metric used to assess the flow behavior of wheat flour samples with narrow particle size ranges and flour blends. The ability to predict the flour behavior based on particle properties can be very useful in sieving process. The multi-component granular Bond number concept developed could be extended to any blend of hard and soft wheat flours and provides guidance not only during their sieving but also in other processing operations. The model could be used to identify the right sifter load setting, blending of flour for quality purposes and the cut-off moisture content of flour to prevent the flour from blinding the screen surfaces.

7.3.4. Discrete Element Method (DEM) modeling of wheat flour sieving process

The DEM modeling technique was applied to understand the wheat flour sieving process. The Hertz-Mindlin JKR cohesion model was used to model the inter-particle cohesion between the flour particles. The developed DEM simulation model indicated that, the increase in moisture content from 10 to 14 % w.b. led to an increase in the mass held over on the 125 µm screen by 12 % and led to sieve blinding. The lab validation also indicated a similar trend. Through the developed simulation model it was also noted that the percentage of mass retained over 125 µm

screen for SRW particles was about 8 % greater than that of HRW samples at 10 % m.c, indicating the exact sieving pattern of hard and soft wheat flours as observed in lab validation. This simulation model will help the millers to predict the sieving efficiency and initiation of sieve blinding phenomena.

7.4. Future Work

Fundamental and applied studies were used to understand the inter-particle cohesion of wheat flours. Different shear flow properties of wheat flours were measured for five different wheat classes at different moisture levels, particle sizes and sifter loads. A mathematical model was developed to predict and understand the flow behavior of wheat flour during particle size separation process. The measured parameters and flow properties were used as inputs for the development of a DEM model to understand the wheat flour sieving process. In this section, three areas of advanced research are identified that could help develop a higher understanding on the inter-particle cohesion of wheat flours.

7.4.1. Establishing a relationship between surface chemical composition of flours and the breakage pattern of wheat

Presence of different chemical components in various proportions on the surface of wheat flours leads to variability in inter-particle cohesion. Understanding the surface chemical composition and their structures will not only give an insight into the role of these components during particle cohesion, but also explains the inherent difference in breakage patterns. The electron spectroscopy for chemical analysis (ESCA) and X-ray photoelectron spectroscopy are some of the techniques that could be used for evaluation of these differences in surface composition.

7.4.2. Determination of individual particle-particle cohesion between flour particles

The force of cohesion between single wheat flour particles will give an accurate measure of inter-particle forces. Atomic force microscopic (AFM) measurement technique could be used. The quantified force from AFM can then be used to simulate the sieving or other material handling process. For modeling purposes, the use of individual particle-particle cohesion data will be more appropriate than using bulk cohesion data.

7.4.3. Shape approximation of flour particles

In this study, one major assumption was that the particles are spherical in shape. But, flour particles contain a mix of spherical (starch particles) and non-spherical particles (endosperm, protein fragments, bran, etc). Simulating particles with effective shape approximation would help in developing an accurate model to predict the flour sieving process. But, then the major challenge would be the computational time. To simulate 20 s of sieving process, in this study, it took an average of 916.4 h to complete the simulation. So, developing prediction models using quasi-2D approach would save computational time.

Appendix

Table A - 1: Shear flow properties of hard red spring [HRS] wheat flour.

Moisture content, (% w.b)	Particle size, μm	Applied pressure, kPa	Cohesion, kPa	FF	AIF, °
10	<45	0.5	0.19 (0.01)	1.60 (0.03)	41.54 (3.82)
		1.0	0.39 (0.01)	1.35 (0.07)	33.58 (1.45)
		1.5	0.72 (0.01)	1.21 (0.04)	25.38 (2.90)
	45-75	0.5	0.08 (0.01)	4.14 (0.10)	33.60 (4.10)
		1.0	0.14 (0.01)	3.44 (0.03)	29.56 (4.08)
		1.5	0.26 (0.01)	3.01 (0.08)	28.52 (1.38)
	75-106	0.5	0.06 (0.01)	7.52 (0.16)	34.75 (0.82)
		1.0	0.10 (0.01)	5.92 (0.16)	28.85 (2.85)
		1.5	0.19 (0.01)	3.51 (0.09)	26.55 (1.74)
12	<45	0.5	0.23 (0.01)	1.32 (0.05)	38.55 (2.55)
		1.0	0.42 (0.01)	1.21 (0.04)	34.75 (1.50)
		1.5	0.84 (0.01)	1.12 (0.02)	21.46 (1.95)
	45-75	0.5	0.09 (0.02)	3.17 (0.07)	36.78 (0.34)
		1.0	0.22 (0.01)	2.47 (0.03)	28.45 (1.40)
		1.5	0.37 (0.01)	2.26 (0.09)	26.45 (0.65)
	75-106	0.5	0.06 (0.01)	6.22 (0.13)	30.70 (1.35)
		1.0	0.13 (0.01)	3.79 (0.07)	28.75 (1.40)
		1.5	0.23 (0.01)	3.37 (0.06)	26.15 (0.85)
14	<45	0.5	0.27 (0.01)	1.06 (0.02)	40.25 (2.30)
		1.0	0.47 (0.01)	1.02 (0.01)	38.26 (1.32)
		1.5	0.88 (0.01)	1.03 (0.01)	28.45 (1.75)
	45-75	0.5	0.12 (0.01)	2.07 (0.11)	33.45 (2.60)
		1.0	0.26 (0.02)	1.72 (0.12)	30.65 (1.65)
		1.5	0.50 (0.01)	1.51 (0.03)	25.80 (1.52)
	75-106	0.5	0.07 (0.01)	4.23 (0.06)	30.15 (2.05)
		1.0	0.16 (0.02)	3.29 (0.03)	28.52 (1.65)
		1.5	0.28 (0.01)	3.10 (0.06)	26.45 (0.85)

*Values in the parenthesis are standard deviations.

Table A - 2: Shear flow properties of hard white winter [HWW] wheat flour.

Moisture content, (% w.b)	Particle size, μm	Applied pressure, kPa	Cohesion, kPa	FF	AIF, °
10	<45	0.5	0.21 (0.01)	1.58 (0.06)	41.24 (4.16)
		1.0	0.37 (0.01)	1.32 (0.09)	35.54 (2.18)
		1.5	0.74 (0.01)	1.18 (0.11)	24.85 (1.94)
	45-75	0.5	0.11 (0.01)	4.26 (0.17)	32.84 (3.84)
		1.0	0.16 (0.01)	3.52 (0.08)	28.76 (4.24)
		1.5	0.24 (0.01)	2.97 (0.08)	26.34 (1.64)
	75-106	0.5	0.05 (0.01)	7.64 (0.28)	34.92 (1.28)
		1.0	0.12 (0.01)	5.84 (0.14)	29.54 (2.78)
		1.5	0.22 (0.01)	3.46 (0.18)	26.34 (1.62)
12	<45	0.5	0.26 (0.01)	1.32 (0.05)	36.32 (2.48)
		1.0	0.44 (0.01)	1.21 (0.07)	33.48 (2.08)
		1.5	0.82 (0.01)	1.14 (0.02)	22.82 (1.83)
	45-75	0.5	0.07 (0.02)	3.21 (0.07)	37.46 (0.36)
		1.0	0.24 (0.01)	2.52 (0.09)	29.39 (2.06)
		1.5	0.33 (0.01)	2.21 (0.11)	25.84 (1.28)
	75-106	0.5	0.08 (0.01)	6.34 (0.54)	30.70 (1.35)
		1.0	0.15 (0.01)	3.84 (0.12)	27.64 (2.05)
		1.5	0.25 (0.01)	3.32 (0.04)	26.15 (0.85)
14	<45	0.5	0.29 (0.01)	1.12 (0.03)	41.64 (2.18)
		1.0	0.49 (0.01)	1.04 (0.01)	37.20 (1.45)
		1.5	0.92 (0.01)	1.01 (0.01)	29.65 (1.94)
	45-75	0.5	0.13 (0.01)	2.10 (0.08)	34.30 (2.44)
		1.0	0.28 (0.02)	1.74 (0.14)	29.95 (1.86)
		1.5	0.48 (0.01)	1.48 (0.06)	25.07 (1.76)
	75-106	0.5	0.07 (0.01)	4.30 (0.08)	31.54 (2.42)
		1.0	0.18 (0.02)	3.34 (0.12)	26.50 (1.28)
		1.5	0.31 (0.01)	2.94 (0.08)	23.80 (1.52)

*Values in the parenthesis are standard deviations.

Table A - 3: Shear flow properties of soft white winter [SWW] wheat flour.

Moisture content, (% w.b)	Particle size, μm	Applied pressure, kPa	Cohesion, kPa	FF	AIF, °
10	<45	0.5	0.26 (0.01)	1.34 (0.03)	37.45 (5.20)
		1.0	0.46 (0.01)	1.24 (0.02)	31.74 (2.05)
		1.5	0.75 (0.01)	1.13 (0.02)	24.62 (1.85)
	45-75	0.5	0.12 (0.01)	3.25 (0.04)	35.80 (1.60)
		1.0	0.15 (0.01)	2.85 (0.10)	31.85 (2.55)
		1.5	0.41 (0.01)	2.38 (0.04)	27.65 (1.64)
	75-106	0.5	0.06 (0.01)	7.05 (0.11)	32.40 (2.74)
		1.0	0.11 (0.01)	5.68 (0.12)	30.86 (1.12)
		1.5	0.16 (0.01)	5.28 (0.04)	29.65 (0.35)
12	<45	0.5	0.26 (0.01)	1.28 (0.04)	33.52 (3.26)
		1.0	0.52 (0.02)	1.17 (0.01)	32.40 (0.95)
		1.5	0.78 (0.01)	1.09 (0.06)	24.36 (2.30)
	45-75	0.5	0.11 (0.01)	2.97 (0.08)	36.45 (1.20)
		1.0	0.21 (0.01)	2.54 (0.04)	32.80 (1.95)
		1.5	0.43 (0.02)	2.26 (0.05)	28.40 (1.05)
	75-106	0.5	0.07 (0.01)	3.98 (0.11)	31.85 (3.05)
		1.0	0.15 (0.01)	3.72 (0.07)	30.76 (2.35)
		1.5	0.23 (0.01)	3.46 (0.05)	28.25 (0.50)
14	<45	0.5	0.32 (0.02)	1.12 (0.06)	42.48 (5.36)
		1.0	0.54 (0.01)	1.06 (0.04)	39.30 (3.12)
		1.5	0.81 (0.02)	1.01 (0.04)	25.72 (4.15)
	45-75	0.5	0.12 (0.01)	2.68 (0.03)	34.93 (1.20)
		1.0	0.25 (0.01)	2.39 (0.04)	32.86 (0.84)
		1.5	0.45 (0.02)	1.87 (0.05)	28.44 (1.12)
	75-106	0.5	0.09 (0.01)	3.57 (0.04)	35.30 (1.84)
		1.0	0.16 (0.01)	3.26 (0.06)	30.26 (1.35)
		1.5	0.29 (0.01)	2.69 (0.08)	27.42 (2.14)

*Values in the parenthesis are standard deviations.

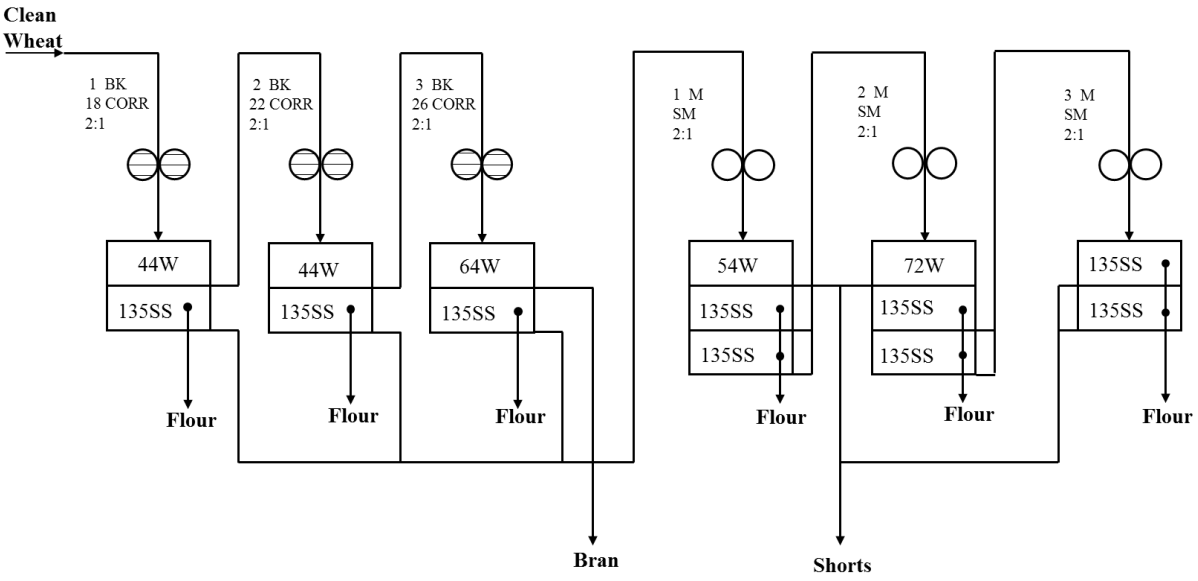

Figure A - 1: Flour flow diagram for the Bühler laboratory mill.

BK = break rolls, CORR = corrugated, M – middlings, SM – smooth, W – wire, SS – stainless steel.

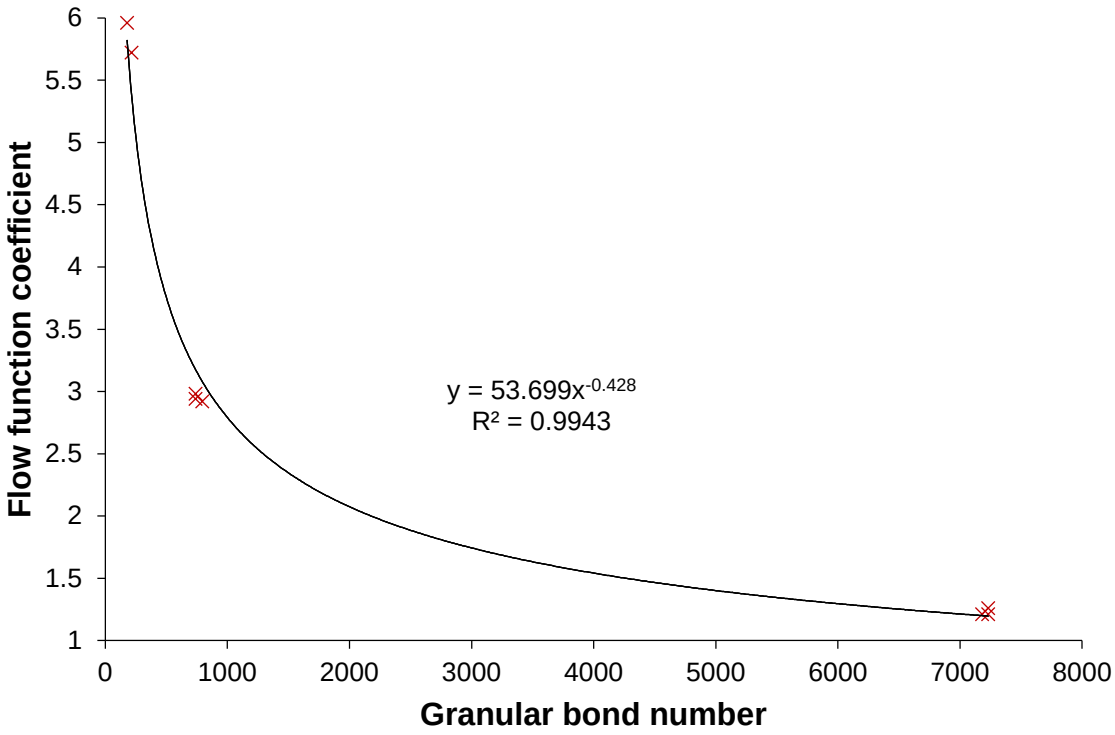

Figure A - 2: Relationship between granular Bond number and flow function coefficient (preliminary results).